# IMPROVEMENTS IN MICROFABRICATION OF INTEGRATED COLLAGEN SCAFFOLDS CONTAINING EMBEDDED MICROCHANNELS INSIDE 3D EXTRACELLULAR MATRIX WITH 2D BASEMENT MEMBRANE LININGS

**Ali Maghzian**

A THESIS SUBMITTED TO THE FACULTY OF GRADUATE STUDIES

IN PARTIAL FULFILLMENT OF THE REQUIREMENTS FOR THE DEGREE OF

MASTER OF APPLIED SCIENCE

GRADUATE PROGRAM IN MECHANICAL ENGINEERING

YORK UNIVERSITY

TORONTO, ONTARIO

April 2024

# Abstract

Collagen's biocompatibility, biodegradability, and cell-adhesive properties make it vital for developing biomimetic scaffolds in tissue engineering. This thesis enhances the microfabrication of collagen scaffolds with micro-conduits, mimicking the Extracellular Matrix (ECM). These scaffolds feature a 3D porous collagen sponge, mimicking the interstitial matrix, with embedded microchannels with varying widths (70-1000 μm) resembling veins and vessels and micropatterns, as well as a 2D collagen film lining the microchannel walls that mimic the basement membrane. Through soft lithography, freeze-drying, and contact printing, scaffolds with enclosed macrochannels in multiple layers were created and reinforced with composite effects of components and crosslinking. Characterization methods included microscopy, ImageJ analysis, optical profilometry, flow studies, and SEM imaging. Factors influencing scaffold flatness and achievable microchannel dimensions were investigated in a parametric study. Preliminary cultures evaluated scaffold viability for culturing mice brain tissue and studying various cell behaviors, including HEp2, HEp2D and HEK 293T cell lines. These scaffolds offer customizable physical characteristics for diverse tissue applications, facilitating blood vessel modeling, cell co-culture, and drug delivery studies.

# Acknowledgments

I am deeply grateful for the invaluable support, kindness, and guidance provided by Professor Rezai throughout my research journey. His mentorship has been instrumental in shaping my academic and professional growth, and I express my heartfelt appreciation for his commitment and encouragement.

*"In loving memory of dearest uncle ever,*

*My Daei Joon Hasan,*

*whose unwavering support and wisdom continue to inspire me"*

# Table of Contents

# List of Figures

# List of Tables

# 1 Introduction

## 1.1 Tissue Engineering

As we age, our tissues undergo damage, often due to disease, injury, or trauma. Traditional clinical therapy for such damage has relied on open transplants, involving the donation of organs from a donor to a recipient. However, the growing waiting list for organs highlights the urgent need for alternative approaches to tissue repair and regeneration [1] [2].

In cases of large tissue defects in bone, conventional repair methods often involve autografts or allografts. While these techniques have been used successfully, they come with limitations such as a limited supply, risk of infection transmission, and potential rejection by the recipient's immune system [3] [4].

To address these challenges, there has been a surge of interest in the application of artificial scaffolds in tissue regeneration. This approach, central to tissue engineering, involves cultivating relevant cells *in-vitro* to generate the desired tissue. The goal is to understand the structure and function of tissues and develop biological tools capable of restoring lost organ function [4] [5].

Figure 1-1 depicts the general steps of tissue engineering. Initially, cells are isolated from a specific organ. These cells are then expanded in two dimensions within a container or flask and cultivated. Subsequently, they are proliferated across multiple flasks before being seeded onto a porous scaffold with specific features. Additional components such as growth factors or stimuli may also be incorporated into the scaffold to facilitate growth. Once the tissue has matured, it is implanted back into the individual's body [2].

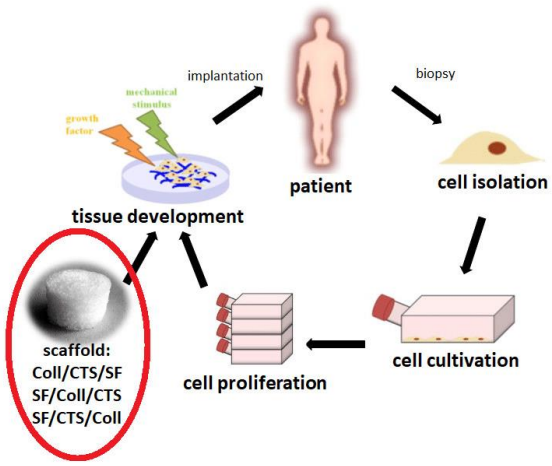


*Figure 1-1: Steps of tissue engineering. Figure reprinted from MDPI [5] from an open access article.*

## 1.2 A Brief Physiology of *in-vivo* Tissues

### 1.2.1 Extracellular matrix

The Extracellular Matrix (ECM) is a non-cellular component found in almost all tissues and organs. In addition to supplying the physical structure and pharmacological and biomechanical cues required for cellular activity, ECM acts as an essential framework. The ECM is a vast three-dimensional network of proteins and other molecules that envelops, supports, and organizes the body's tissues and cells. Facilitating cell adhesion, conducting cell-to-cell communication, and encouraging cellular differentiation are among the ECM's primary roles. These processes, which include cell growth, movement, and other physiological activities, depend heavily on these operations [6].

The composition, mechanical properties, structure, and topology of the ECM vary across different tissues. Animal ECM comprises both the interstitial matrix and the basement membrane. Figure 1-2 illustrates a schematic representation of the animal ECM and its components.

Epithelial tissues, characterized by a thin, continuous layer of densely packed cells, serve as a protective barrier lining the outer surfaces of organs and blood vessels throughout the body, as well as the inner surfaces of various internal organs [6]. Moreover, the ECM comprises two main distinct components, elucidated further below.

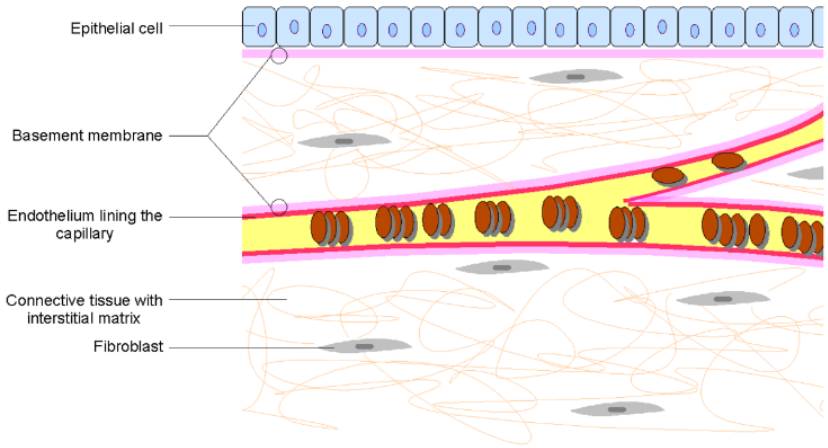


*Figure 1-2: Schematic of animal ECM and its components (released to the public domain by Wikimedia Commons [7])*

### 1.2.2 Interstitial matrix

The interstitial matrix (IM) is situated between animal cells, occupying the intercellular spaces. It forms a 3D porous network characterized by heterogeneous textures, serving both structural and signaling functions. Key determinants of the IM include pore size structure and mechanical properties, which significantly influence cellular behavior. Moreover, physical features of interstitial IM, such as fiber thickness, orientation, density, stiffness, and pore size influence cellular activities. It also acts as an important reservoir for growth factors, which promotes cell migration and proliferation [8] [9].

### 1.2.3 Basement membrane

Basement membranes (BM) serve as sheet-like depositions of the Extracellular Matrix (ECM) upon which various cells such as epithelial cells rest. Within these membranes, proteins fill the interstitial space, acting as a compression buffer against the stress exerted on the ECM. Basement membranes fulfill a range of crucial functions within tissues, including: i) providing a substrate for cell adhesion and migration, and ii) serving as a barrier that separates tissues and prevents the transmigration of most cells [6]. The BM gives the tissues mechanical strength in addition to sculpting them and acting as a surface for cell adhesion. Laminin and type IV collagen polymeric networks, which are connected by additional ECM proteins such nidogen and perlecan, give BM its sheet-like shape [10]. The thickness of the BM varies from 20 nm to 500 nm in different tissues [11] [12].

## 1.3 Scaffolds

As previously mentioned, our cells in the body are embedded within the ECM. In tissue engineering, substitutes called scaffolds are utilized to mimic this basal matrix. A porous scaffold serves as a template, enabling cells to grow and replicating the functions of the ECM. Once implanted and after guiding tissue regeneration, the scaffold is expected to degrade, allowing cells to deposit their own extracellular matrix [2] [13].

To ensure effective cellular attachment, the substrate scaffold must satisfy several essential criteria. Firstly, it should exhibit suitable surface chemistry conducive to cellular adhesion, fostering interactions between the scaffold and the cells. Additionally, the scaffold material should be biodegradable or bioresorbable, with a degradation rate tailored to match the tissue regeneration process, and without of any harmful byproducts that could impede cellular function. Moreover,

the scaffold must possess adequate mechanical properties to withstand the rigors of implantation and handling without compromising its structural integrity. Furthermore, versatility in fabrication is essential, allowing for the creation of scaffolds in diverse shapes and sizes to suit various tissue engineering applications. Lastly, the scaffold should feature interconnecting porosity, facilitating tissue integration and vascularization by promoting nutrient and oxygen diffusion throughout the scaffold's structure, thereby supporting the growth and vitality of the engineered tissue. Meeting these criteria ensures that the scaffold provides an optimal environment for cellular attachment and tissue regeneration in tissue engineering endeavors [13] [14].

### 1.3.1 Different materials and fabrication techniques of scaffolds

In tissue engineering, a variety of materials have been used [15] to fabricate via different techniques [16]. These materials used for fabrication of engineering tissues can be classified to natural-based materials (e.g., gelatin [17] [18], collagen [19] [20] [21] , chitosan [18] [22], alginate [17] [23], hyaluronan [24], chondroitin sulfate [25], and heparin sulfate [26]) and synthetic-based materials such as polymers (e.g., polycaprolactone [27], polyglycolic acid [28], poly lactic acid [29], and poly vinyl alcohol [30] ) and finally ceramics [31]).

Naturally derived materials have garnered significant attention due to their ability to promote cell growth. However, there are concerns regarding their structural properties and compatibility with fabrication methods. Obtained from various animal sources, these materials may elicit an immune response in the body. Additionally, certain natural materials, like collagen, contain proteins that are sensitive to high temperatures, rendering them incompatible with fabrication methods involving elevated temperatures. Therefore, careful consideration of fabrication techniques is essential when working with such materials [32] [33] [34].

When considering synthetic materials for tissue engineering, their physical properties can be conveniently adjusted to accommodate various fabrication methods, providing greater flexibility. Biodegradable polymers offer an attractive alternative in this regard. While synthetic polymers possess valuable properties, some may lack surface chemistry conducive to optimal cell adhesion. Moreover, many synthetic polymers are thermoplastic, raising concerns about the formation of potentially toxic byproducts during degradation [15]. On the other hand, ceramics, such as hydroxyapatite (HA), excel in applications involving hard tissue, such as bone regeneration. However, ceramics are unsuitable for soft tissue engineering due to their inherent rigidity [31].

The chemical composition of scaffolds significantly influences cellular responses, encompassing adhesion, differentiation, viability, proliferation, and signaling, thereby playing a crucial role in tissue regeneration and repair within tissue engineering. Modifying the scaffold's chemical composition, such as through the incorporation of hydroxyapatite [35], enables the manipulation of cell-ECM interactions.

### 1.3.2 Porous scaffolds

Porous scaffolds play a crucial role in tissue engineering by providing a supportive framework for cell attachment, proliferation, and differentiation. The porous structure allows for the infiltration of nutrients, oxygen, and waste products, facilitating cellular activity and tissue regeneration [22] [36] [37]. Moreover, the interconnected pores promote tissue ingrowth and vascularization, enabling the formation of functional and integrated tissue constructs. By mimicking the natural extracellular matrix, porous scaffolds create a conducive microenvironment for cells to organize and develop into mature tissues, ultimately leading to the successful repair or replacement of damaged or diseased tissues in the body [37] [38] [39].

Several techniques have been developed for fabricating porous structures from synthetic scaffold materials in tissue engineering. These include solvent casting-particulate leaching [40], phase separation [41], gas foaming [42], emulsion freeze drying [14] and fiber meshes [43].

The porogen leaching method offers control over pore size and porosity in scaffolds but often results in isolated pores, limiting its suitability for tissue engineering due to probable need of using toxic polymers [44].

Pre-prepared ice particulates have been utilized to enhance the pore structure and mechanical properties of collagen-based porous scaffolds, although this method requires sophisticated fabrication facilities and precise parameter control [45].

In the gas foaming method, a gas is dissolved into a polymer solution under high pressure, forming bubbles that expand upon release of pressure and solidification of the solution, resulting in a porous structure. This technique allows for the production of scaffolds with controlled porosity and pore size, facilitating cellular infiltration and tissue regeneration [42].

The fiber mesh method involves arranging biodegradable polymer fibers into a mesh-like structure, which is then shaped into the desired scaffold geometry. Then processes such as solvent casting, freeze drying, or thermal annealing stabilize the fibers, leaving behind interconnected pores within the scaffold [43].

Freeze drying, also known as lyophilization, is a widely used method for creating porous materials while preserving their structure and bioactivity. By removing water from a material under low temperature and pressure conditions, interconnected pores are formed, preserving the bioactivity of delicate biomolecules and ensuring long shelf stability [37]. Overall, freeze drying offers a

gentle and effective approach to tailor porous materials to specific needs, as further described and demonstrated in this study.

The mechanical properties of scaffolds must be carefully customized to meet the biomechanical demands of the target tissue and ensure optimal tissue regeneration and functional integration [22] [36]. This entails selecting appropriate biomaterials, scaffold architecture, fabrication techniques, and post-processing methods tailored to specific tissue engineering applications. However, there exists a trade-off between scaffold pore size and mechanical properties, representing an inverse relationship between these factors. Pore size dictates the scaffold's porosity and interconnectivity, crucial for cellular infiltration, nutrient diffusion, and waste removal. While larger pores promote better cell infiltration and tissue integration, increasing pore size often compromises the scaffold's mechanical strength and stability [34] [45].

## 1.4 Collagen Scaffolds

Collagen is one of the naturally based polymers used in scaffolds tissue engineering. Collagens are the building blocks of connective tissue. Rope-like proteins are found in high concentrations in load-bearing tissues such as tendon, bone, skin, and cartilage [46]. As Collagen is a natural polymer that is the main component of ECMs, it makes an appropriate candidate for fabricating tissues mimicking in-vivo environments for cells [47].

In most tissue engineering studies, collagen is proved to be a promising material because cells can adhere to the specific motifs on collagen [48], and also it has unique biological properties such as biocompatibility, biodegradation, high bioactivity, good integration of healing tissues, lowest immune and foreign-body responses, non-cytotoxicity and generally is more native for cellular

attachment [15] [46]. To date, collagen scaffolds have been fabricated in different shapes and forms which are depicted in Figure 1-3. All in all, these properties of collagen made it the commonly used biomaterial in tissue engineering.

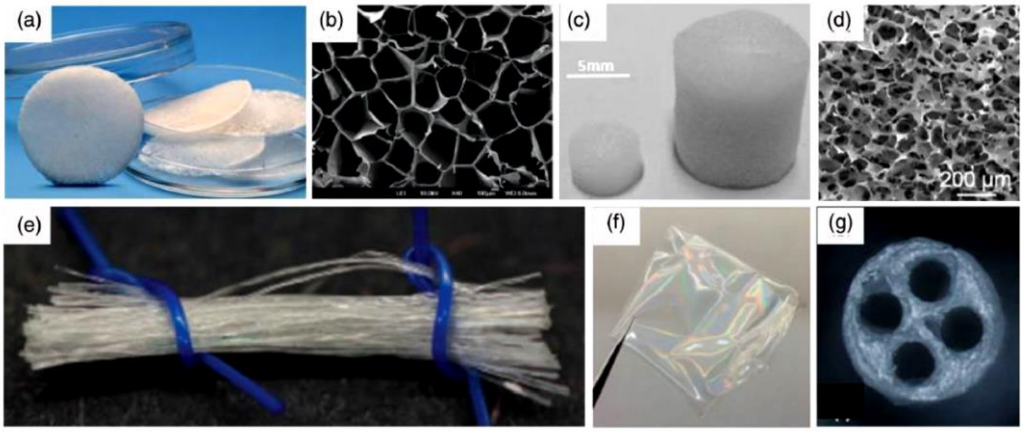


*Figure 1-3: Collagen-based biomaterials for biomedical applications: (a) Disk-shaped collagen sponge composed of type 1 collagen. (b) Magnified view displaying the porous network structure of the collagen sponge. (c) Versatile scaffolds with customizable dimensions (d)SEM images of jellyfish collagen scaffold (e) a cluster made by extrusion form type I collagen (f) a collagen type I transparent film (g) multichannel type I neural conduit. Image reprinted with permission from John Wiley and Sons [46]*

### 1.4.1 Fabrication methods of collagen scaffolds

Fabrication routes of collagen scaffolds offer various methods to tailor the pore sizes, structures, and mechanical properties to specific tissue engineering needs. Freeze drying, also known as lyophilization, involves freezing a collagen solution and sublimating it under vacuum to create a porous structure (described in next section). Solvent casting-particulate leaching entails dissolving collagen in a solvent, mixing it with porogen particles, casting it into a mold, and leaching out the porogen to form pores [49]. Electrospinning uses an electric field to draw collagen fibers from a solution, resulting in a fibrous scaffold with interconnected pores [50]. Phase separation involves mixing collagen with a solvent, leading to scaffold formation through phase separation [51].

Two-dimensional (2D) fabrication methods of collagen involve techniques that produce planar collagen-based structures. Solvent casting entails mixing collagen solution with a solvent and casting it onto a substrate, followed by solvent evaporation to form a thin collagen film [19]. Spin-coating applies a collagen solution onto a rotating substrate, spreading it evenly to create a thin film upon solvent evaporation [52]. These methods are suitable for creating thin collagen films or coatings for various applications such as cell culture substrates, biosensors, or wound dressings. However, they are limited to producing 2D structures and may not be suitable for complex tissue engineering scaffolds requiring three-dimensional (3D) architectures [53].

### 1.4.2 Freeze drying in fabrication of porous collagen scaffolds

Freeze drying, sometimes referred to as lyophilization, is a common method for extracting solvent or water from materials without damaging their structure. Sublimation is a process that occurs during freeze drying that result in the formation of a porous structure. The substance is first frozen at extremely low temperatures, usually below its triple point, in the freeze drying process. This causes the water or solvent within the material to freeze and create ice crystals. The surrounding pressure is then lowered by applying a vacuum to the frozen substance. In these circumstances, the solvent or frozen water sublimates, converting straight from the solid to the gas phase without changing into a liquid [37] [54].

A porous structure is created when the ice crystals sublimate and leave holes or pores in the material. The secret to forming these holes is sublimation, or the elimination of ice. The size, form, and distribution of the pores can be affected by a number of variables during the freeze drying process, including the freezing rate, material composition, and processing parameters [36] [37].

Changes in the freezing procedure employed during the freeze drying process can efficiently influence the configuration of the pores since the resulting scaffold's porous structure resembles the ice crystal structure formed during freezing. Therefore, tweaking this procedure is essential to producing a variety of scaffolds with distinct pore structures. The parameters that affect the porosity and pore diameters of the scaffolds that are fabricated include collagen concentration, final freezing temperature, cooling rate, heating step, directional freezing, and pH [14] [36] [37] [54].

### 1.4.3 Challenges of using collagen for scaffolds

Using collagen as a scaffold in tissue engineering holds significant promise [55], yet it comes with several challenges that need to be addressed for optimal performance.

The mechanical properties of native collagen are often insufficient for certain tissue engineering applications, necessitating modifications or reinforcements to enhance its strength and stability [34] [35] [36] [37]. Therefore, improving the mechanical properties of collagen scaffolds is crucial depending on the intended application.

The rapid degradation rate of collagen scaffolds may not align with the desired tissue regeneration timeline, leading to inadequate support for cell growth and tissue formation [37]. Various approaches, including crosslinking techniques, have been explored to regulate degradation rates [34].

Achieving precise control over the pore size, structure, and degradation rate of collagen scaffolds can be challenging, impacting their ability to effectively support tissue regeneration. Addressing these challenges requires innovative approaches in scaffold design and fabrication techniques [22] [34] [35] [36] [37].

Furthermore, the cost and scalability of obtaining collagen from natural sources or producing it through recombinant methods can be limiting factors in large-scale tissue engineering applications. However, ongoing research efforts aim to overcome these limitations, recognizing the promising benefits of collagen scaffolds in tissue regeneration [33] [56]. Overall, addressing these challenges necessitates innovative approaches in scaffold design, fabrication techniques, and biomaterial engineering to optimize the performance and effectiveness of collagen-based scaffolds in tissue regeneration [33] [56].

### 1.4.4 Cross-linking of collagen scaffolds

Type I collagen serves as a cornerstone in tissue engineering due to its widespread availability. Nonetheless, its inherent weaknesses in mechanical properties and stability pose limitations to its broader application. To overcome these challenges, various cross-linking methods have been explored to enhance the properties of biomaterials, particularly collagen scaffolds, by reinforcing chemical and physical interactions among polymers. These methods include chemical, physical, and biological approaches. Chemical cross-linking emerges as the most potent method, despite concerns regarding cytotoxicity and cost [5] [34]. Glutaraldehyde is a well-established reagent for cross-linking and stabilizing collagens and other protein-based materials, such as gelatin [38] [53] [57]. However, it is associated with undesirable side effects like calcification, local cytotoxicity, and induction of inflammatory responses. Alternatively, cross-linking with ethanol offers a simpler and more cost-effective option [18]. Physical cross-linking methods, such as de-hydrothermal treatment (DHT), have also been explored, although they are generally less effective [21] [22] [36]. Despite the effectiveness of individual cross-linking methods, it is important to acknowledge

that they may not fully meet scaffold fabrication requirements, underscoring the necessity for comprehensive strategies [34].

### 1.4.5 Vascularization of Scaffolds

Porous scaffolds serve as superior models for tissue engineering due to their ability to facilitate cellular growth in a three-dimensional environment, enabling interstitial flow and various cellular activities such as migration, cell-cell interactions, and interactions with the extracellular matrix [35] [53]. Initially, engineered tissues were created without pre-vascularization and then implanted directly into patients' bodies, relying on the natural invasion of vascular networks within the tissues. However, research has shown that natural invasion post-implantation occurs at a very low rate per day [23] [58], leading to insufficient blood supplies from the generated vascular networks and resulting in cell death in regions distant (>200μm) from capillaries [20] [35]. Furthermore, different tissue types necessitate varying rates of nutrient and oxygen transfer at the scaffold surface, which can promote mineralization and impede diffusion, further limiting the mass transfer of essential components to the scaffold interior [14].

Scaffold vascularization may be necessary to support the growth of thick tissue cross-sections, ensuring adequate nutrient and oxygen supply for cell survival [35]. One approach to address this has been pre-vascularization, where pre-defined channel networks were embedded within engineered tissues, followed by their invasion to mimic *in-vivo* vascularization processes [14] [35] [59].

A variety of microfabrication techniques have been used for the microfabrication of embedded pre-vascularized networks. These microfabrication techniques are injection moulding [60], laser

patterning [61], subtractive moulding [62], sacrificial moulding [14] [63], micropatterning [64], and bioprinting [65] [66].

### 1.4.6 Small size microchannels for tissue engineering scaffolds

The idea of controlling cell orientation through topographical cues has long been integrated into tissue engineering scaffold design. For instance, planar substrates with contact-printed extracellular matrix or cell adhesion protein patterns have been utilized to regulate the proliferation of various cell types, including vascular smooth muscle cells [67], cardiomyocytes [68], and neurons [69].

One method described in literature involves the production of porous hydrogel scaffolds with 3D undulating microtopographies resembling dermal papillae geometries. Utilizing microfabrication techniques and the natural scaffold material Gel-CS6-HA, accurate tissue scaffolds were created using mechanical micromilling. The microtopographies were then transferred via elastomer molding, and the porous microstructure of the hydrogel scaffolds was accurately formed through lyophilization. These dermal papillae mimic scaffolds demonstrated effectiveness for in-vitro cell culture for up to seven days [70].

In a study micromodeling and lyophilization were employed to produce porous chitosan micropatterns with surface ridge/groove and inner porosity structures. As depicted at Figure 1-4(a), evaluation of the micropatterns revealed stable stripe-like structures, with the 30/30 μm sample exhibiting superior stability. Schwann cells cultured on these micropatterns displayed oriented adhesion and directional growth, particularly on the 30/30 μm pattern, indicating effective cell orientation. Furthermore, the secretion of nerve growth factor (NGF) remained unaffected, suggesting no negative impact on Schwann cell function [71].

Micron-scale topographical cues have also shown promise *in-vitro* by mimicking native vascular smooth muscle cell (VSMC) behavior. Sarkar et al. [39] fabricated such cues using PLGA-leached scaffolds through soft lithography, melt molding, and particulate leaching of polylactic-co-glycolic acid (PLGA) micro/nanoparticles. These scaffolds shown in Figure 1-4(b) provided a platform for studying VSMC responses to specific topographical features in the context of vascular tissue engineering and regenerative medicine.

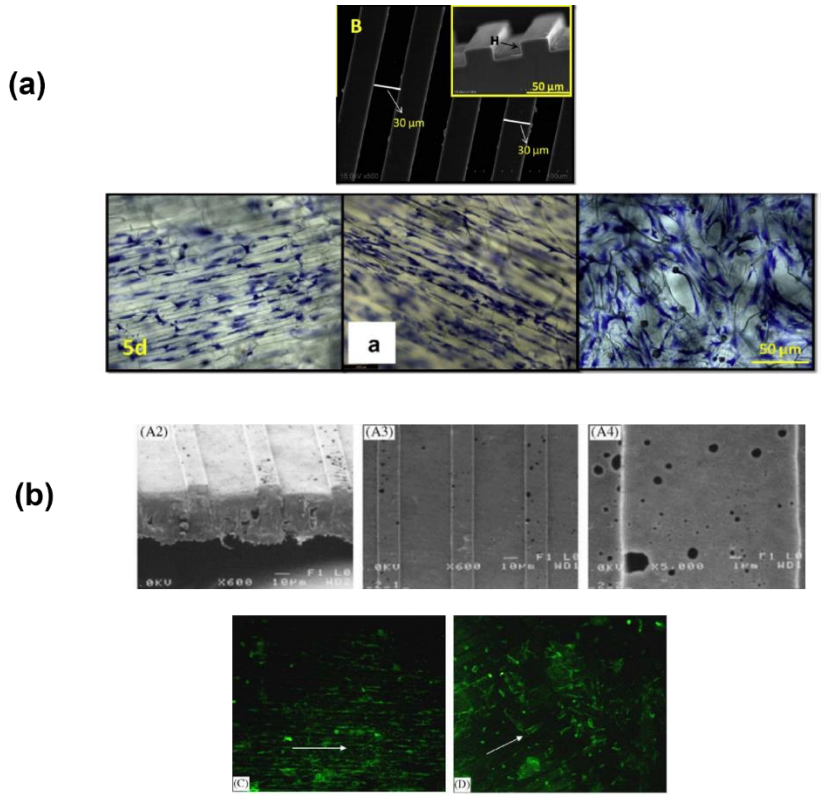


*Figure 1-4: Examples of controlling of surface topography for tissue engineering applications. (a) Porous chitosan micropatterns fabricated via lyophilization with dimensions of 30/30 µm demonstrate alignment guidance for Schwann cells. Figure reprinted with permission from Elsevier [71]. (b) Tissue scaffold microtopography, specifically microchannels with a width of approximately 50 µm, enables control over vascular smooth muscle cell (VSMC) response and extracellular matrix (ECM) remodeling. This effect was observed in poly(caprolactone) (PCL) scaffolds embedded with poly (lactic-co-glycolic acid) (PLGA) micro/nanospheres. Figure reprinted with permission from Elsevier [39].*

Additionally, in various research endeavors, oriented or aligned migration of glial cells [72] and fibroblasts on Titanium [73] has been achieved using micro-channeled surfaces.

### 1.4.7 Microchannels on collagen scaffolds in literature

Several studies have been conducted on producing scaffolds with different features and the effect of the microchannels on the surface of the collagen scaffolds have been investigated. Different sizes of microchannel with different scaffold components have been tried for several purposes.

Micropatterning of bioactive substances on two-dimensional substrates including collagen has been vastly studied for investigating adhesion, spreading, proliferation and differentiation of cells [50] [74] [75]. However, three-dimensional *in-vivo* microenvironments differ from two-dimensional substrates since they imitate the biological and physiochemical cues seen in the surrounding *in-vivo* microenvironments of [38] [75]. As mentioned before, porous scaffolds offer a three-dimensional framework for cell adhesion, proliferation, differentiation, and extracellular matrix secretion to direct the development of new tissue and regeneration. We hereinafter look into some previous works on collagen with microchannels.

Bush et al. investigated the impact of a 3D nonporous cellular microenvironment on epithelialization and basal keratinocyte interaction. Their study focused on developing a matrix fabricated of collagen resembling features at the dermal-epidermal junction and its effect on epithelialization, proliferation, and keratinocyte localization. Photolithography, collagen processing, and biochemical conjugation techniques were combined to create microfabricated dermal epidermal regeneration matrices. Narrow channels (50-100 µm) showed enhanced epithelialization, analogous to cultures on decellularized dermis, suggesting potential benefits in

mimicking rete ridges to improve epithelialization rates and dermis-epidermis cohesion after mechanical stress [19] [21].

A collagen fibril membrane with a papillary shape was developed in a work by Lammers et al. [76] in an effort to replicate the three-dimensional structure of the human papillary dermis. This membrane was made of a double-layered collagen construct that replicated the lower layer of the reticular dermis and the upper layer of the papillary dermis. A micro-structured collagen membrane was also created and assessed in order to mimic the papillary dermis of human skin's natural 3D architecture. Compared to flat membranes, these collagen membranes dramatically affected the cellular shape, gene expression profiles, and protein expression of cultured keratinocytes. They represented the natural architecture of dermal papillae. Physical modification may be the cause of these effects.

In a study by Suzuki et al [77] aimed at developing a non-porous oral mucosa equivalent, types I tilapia scale collagen scaffold with microstructures mimicking the dermal-epidermal junction was utilized. Micropattern prototypes were designed and fabricated using soft lithography with polydimethylsiloxane and silicon substrates. Despite sparse internal fibril networks, micropattern configurations were well preserved. Histologic examinations revealed fully differentiated and stratified epithelial layers on all scaffolds, indicating potential for clinical use. Enhancing mechanical properties is necessary for further improvement.

In another study micropatterned collagen scaffolds were fabricated with pores, utilizing micropatterned ice particulates or ice lines as templates. The micropatterns were controlled by adjusting ejection pressure, distance, and nozzle caliber of water creating ice lines having a diameter of 507 ± 10 μm. These ice particles can be easily removed through freeze drying and are

biocompatible. However, creating features on the surface requires specialized equipment and facilities and achieving smaller features were not tried [38].

Collagen gels have been used in variety of studies in microfluidic devices [50]. One of these devices has been applied to demonstrate the potential applications of skin equivalents in dermatological studies and for drug testing. For example, one study involved the creation of perfusable vascular channels in a skin equivalent model. These channels were coated with endothelial cells on a collagen gel layer to provide nutrition to the skin equivalent. Both edges of the vascular channels were fixed to connectors of a culture device attached to a perfusion system consisting of a peristaltic pump and silicone tubes. Cultures were conducted, followed by histological analysis [78].

In another method, it has been reported to organize cells and collagen gel within microfabricated PDMS channels, resulting in the formation of endothelial tubes. When human umbilical vein endothelial cells (HUVECs) are cultured within microscale channels coated with collagen gel, cells can organize into tubes with lumens within 24–48 hours. Furthermore, the tube diameter can be controlled by varying the channel width, with cells forming larger tubes as the channel width is increased from 70 to 194 and 244 μm [79]. Figure 1-5 provides more details.

In another work, the use of collagen porous scaffolds with parallel and concave microgrooves to engineer anisotropic tissues like muscle and nerve, which have well-aligned cells, blood vessels, and ECM was investigated. By employing micropatterned ice templates and freeze drying, the researchers developed collagen scaffolds. Co-culturing vascular endothelial cells and skeletal muscle myoblasts on these scaffolds with microchannels led to spontaneous cell assembly into anisotropic muscle bundles with well-aligned tubule-like structures. The muscle cells exhibited high alignment within the tissue bundles, expressed myosin heavy chain abundantly, and

incorporated the aligned tubule structures of vascular endothelial cells. This micropatterning approach facilitated the engineering of anisotropic tissue with well-ordered tubules, offering a platform for studying cell assembly in micropatterned material environments [80].

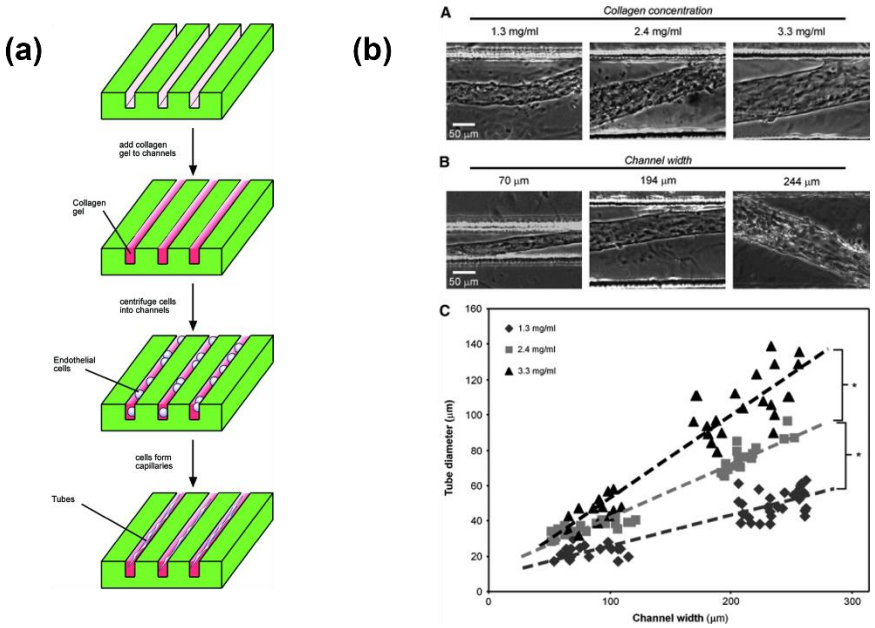


*Figure 1-5: (a) Schematics illustrate how collagen gel and cells are arranged inside of microfabricated channels. (b) Methods for regulating the diameter of endothelial tubes. (A) Exemplary phase-contrast images illustrating variations in tube diameters resulting from adjustments in collagen concentration. Human umbilical vein endothelial cells (HUVECs) were cultured in collagen gels of specific concentrations within channels measuring 100 μm in height and 200 μm in width for 24–36 h before fixation. (B) Illustrative phase-contrast images depicting modifications in tube diameters due to alterations in channel width. HUVECs were cultured in 2.4 mg/mL collagen gels within 100 μm tall channels of different widths for 24–36 h before fixation. (C) Graph presenting the average tube diameter relative to channel width and collagen concentration. Figure reprinted with permission from Elsevier [79].*

In a continuation work of abovementioned by Chen et al. aimed for Dexamethasone-loaded biphasic calcium phosphate nanoparticles/collagen composite scaffolds with various concave microgrooves were developed to simultaneously enhance angiogenesis and osteogenesis.

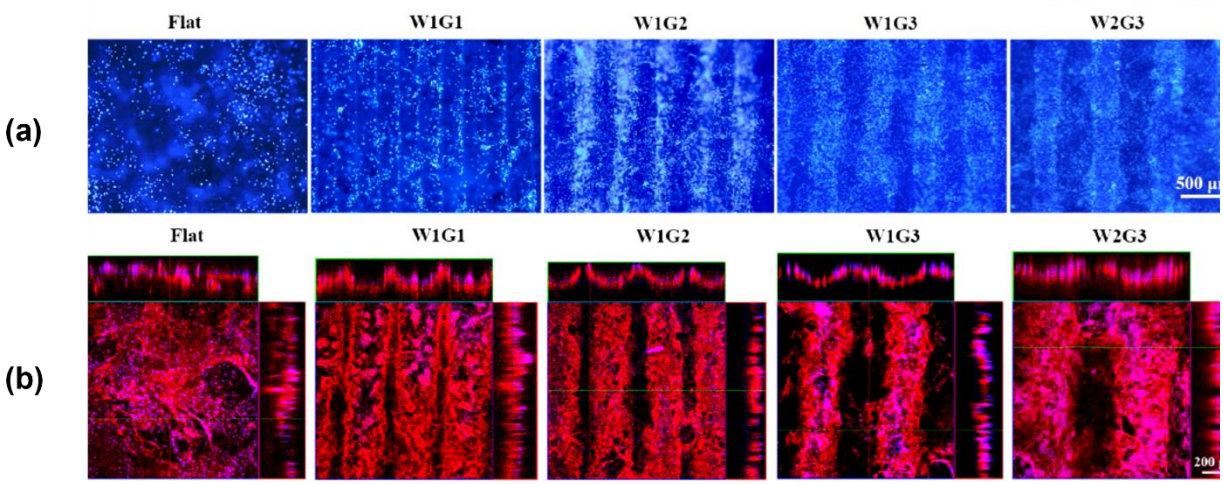


*Figure 1-6: (a) Distribution of HUVECs after 3 days of in-vitro culture. (cell nuclei stained by DAPI). (b) Assembly of HUVECs in the microchannels after 3 days of in-vitro culture (stained with human-CD 31). The scaffolds facilitated cell attachment and expansion. While the flat composite scaffold exhibited a dispersed arrangement, the scaffolds with microchannels displayed a predominant distribution of HUVECs within the concave microgrooves, with fewer cells observed on the convex ridges. Image reprinted from an open access article published by Springer Nature [53].*

These microgrooves were designed to guide the alignment of human umbilical vascular endothelial cells (HUVECs) into well-structured tubules, facilitating rapid angiogenesis. The scaffolds were utilized for co-culturing HUVECs and human bone marrow-derived mesenchymal stem cells. Subcutaneous implantation in mice revealed increased blood vessel formation and new bone growth in the composite scaffolds with microchannels compared to control scaffolds. Among the scaffolds with parallel microchannels, those with a concave width of 290 µm and a convex ridge width of 352 µm exhibited the most significant promotion of angiogenesis and osteogenesis. These findings suggest that microgrooves within the composite scaffolds facilitate angiogenesis and stimulate new bone formation, making them promising for repairing large bone defects [53]. Figure 1-6 depicts the distribution of HUVECs after 1 and 3 days of in-vitro culture.

Previous studies have also explored the use of larger macrochannels to facilitate scaffold perfusion, aiming to enhance the transport of oxygen and vital metabolic components and the elimination of

waste products within scaffolds (in deeper areas). These channels are typically larger than the microchannels reported in the abovementioned studies. Figure 1-7 shows some examples [3] [14] [36] [81].

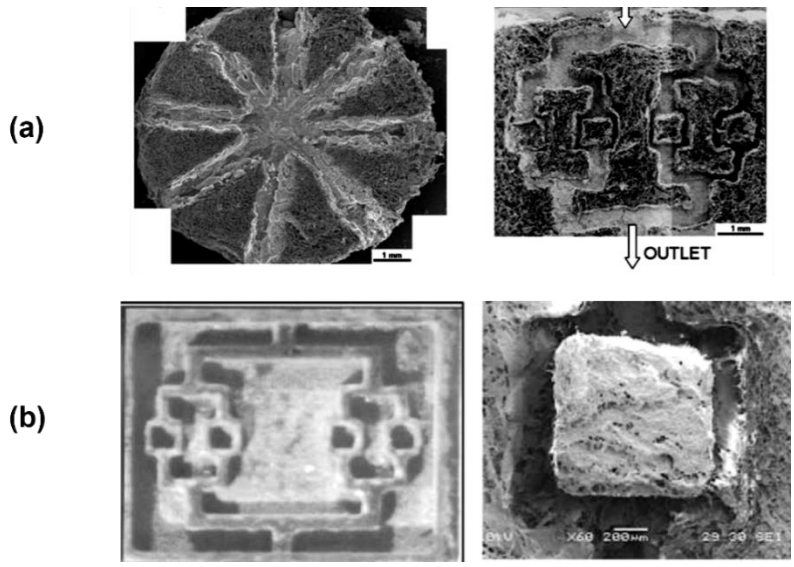


*Figure 1-7:(a) a design of a collagen-hydroxyapatite scaffold aimed at creating pathways for internal vascularization (image reprinted with permission from Springer Nature [36]) (b) Similar design on collagen type I (image reprinted with permission from Emerald Publishing Limited [81]*

### 1.4.8 Collagen scaffolds with different components

As previously discussed, three-dimensional (3D) scaffold models offer greater advantages compared to their two-dimensional (2D) counterparts. Some studies have been so far focused on fabrication of basement membrane on collagen and laminin [69] [26] while many of others have explored porous and nonporous structures resembling the interstitial matrix [53] [77]. However, natural tissues typically comprise multiple components, including an interstitial matrix and a basement membrane covering them. Therefore, in a scaffold, if a 2D membrane is added to a 3D structure, the 3D portion can be likened to the interstitial matrix, while the 2D membrane component can be likened to the basement membrane. While many collagen-based tissue-engineered scaffolds have been developed, fewer works have focused on incorporating both a 3D

interstitial matrix and a 2D basement membrane component [19] [21] [77] [82]. Addition of microchannels resembling vesicles to these 2D-3D scaffolds is another complexity for biomimicking that is less intensely studied.

Basement membranes are integral components of various tissues (e.g., skin, muscle), and microfabricated 2D membranes may find applications in tissue engineering and developmental biology [19] [29]. Some studies have been so far focused on fabrication of basement membrane on spider protein [27] or polymers [29]. Therefore, incorporating basement membranes into collagen scaffolds and engineering their properties can make the corresponding tissues more physiologically relevant to *in-vivo* tissues and organs [21] [65] [83] [84].

For *in-vitro* investigations, the co-culture of cells may provide another incentive for developing scaffolds with barriers on surfaces. Previous studies have utilized sophisticated microfabrication techniques to develop synthetic polymer-based co-culturing systems, allowing cells to communicate through microchannels while physically apart [65] [78] [83] [85].

Micropatterning has been shown to promote cell orientation and growth, and larger channels have been designed to improve the mass transportation of nutrients and oxygen, as well as allowing the removal of cell metabolic waste during *in-vitro* culturing processes. Moreover, microchannels consisting of collagen in all parts can serve as models of blood vessels. While significant progress has been made towards creating functional blood vessel substitutes, the fabrication of vascular grafts with mechanical, structural, and functional properties similar to native vessels remains an ongoing challenge [39] [79].

In continuation of previous work conducted in the labs of Professors P. Rezai and T. Sachlos [82], in an attempt to produce a multilayered more biologically relevant scaffold, a method was developed to create porous collagen scaffolds with enclosed microchannels, including basement

membrane. This technique involved integrating photolithography, freeze drying, and contact printing processes. The preliminary goal of this study was first to address the absence of collagen-based scaffolds in the existing literature that encompassed all the essential elements found in corresponding in-vivo tissues. Thus, this research represented a valuable advancement in the field by aiming to produce scaffolds incorporating three biologically relevant components including a 3-dimensional porous collagen structure (3D collagen sponge) resembling the interstitial matrix (IM) and a thin 2-dimenstional collagen membrane (2D collagen membrane) similar to the basement membrane (BM), plus integrating single microchannels embedded through the scaffold. In this work, single channels sizing from 300 -1500 µm were fabricated by casting collagen slurry on a negative microfabricated made with the aid of 3D printing molds on PDMS via soft lithography. Figure 1-9 depict the schematic 2D-3D integrated scaffold introduced previously.

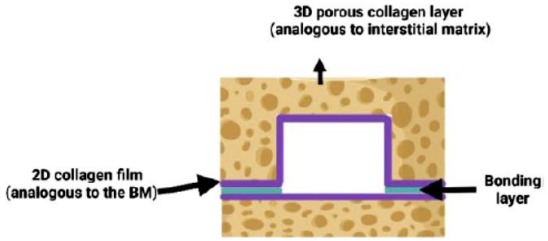


*Figure 1-8: Schematic of pre-vascularized collagen model with 3D porous sponge and a channel lined with a 2D collagen membrane (image reprinted by permission from thesis author [82])*

# 1.5 Research Gaps

## 1.5.1 Benefits of our previously developed method for collagen scaffolds

Various fabrication methods for scaffolds were discussed in detail in section 1.4.1. Our technique, as explained in Figure 1-8, offers distinct advantages over other methods. For instance, unlike bioprinting, this method does not necessitate specific material viscosities, enabling the fabrication of a wide range of materials with this approach [65] [66] Additionally, our microfabrication

technique does not subject materials to high temperatures [86] or harsh solvents like in sacrificial molding [87] [88]. This makes our technique particularly suitable for natural polymers such as collagen or laminin, which are susceptible to denaturation in relative high temperatures. While alternative methods like 3D printing have been explored, they often struggle to achieve smaller channel sizes. Further, it is important to acknowledge that this process may expose scaffolds to potential contamination and residual toxic byproducts, which could be detrimental to cell culture or subsequent *in-vivo* experiments and must be carefully managed [14] [36] [81]. Furthermore, creating patterns with ice templates has also been attempted for larger channel sizes, necessitating additional facilities and design considerations for creating patterns using ice templates [53] [80].

PDMS known for its exceptional mechanical properties, is extensively utilized in various engineering applications. In this thesis, PDMS has been used as material for molding collagen layers against. Its biocompatibility has made PDMS a popular choice for biomedical purposes. This widespread adoption has also led to the proliferation of the soft-lithography technique, primarily used for rapid prototyping of micro and nanostructures using elastomeric materials, particularly PDMS. In our method, PDMS serves as a biocompatible substance, combined with photolithography, both of which are cost-effective and straightforward methods suitable for laboratory settings. Therefore, this microfabrication technique offers a simple and gentle process, serving as a valuable reference for designing tissue engineering scaffolds [89]. Moreover, the layer-by-layer fabrication technique allows for the incorporation of multiple substrates into the scaffold, bonded together using suitable bonding methods like contact printing [82] [90]. This enables the embedding of enclosed microchannels within tissue-engineered scaffolds. By employing efficient bonding techniques, these patterning methods can be utilized to create models

of blood vessels and vasculatures, facilitating co-culture studies involving different cell types distributed throughout the scaffold, as depicted above in Figure 1-8.

Various bonding techniques, including contact printing with collagen gel [90], or collagen slurry [19] [76] [82], adhesive medical sealants [82], and high-temperature bonding [86] have been developed. However, methods like hot embossing at high temperatures can denature the substrate, potentially impacting scaffold integrity. While collagen as a bonder offers the benefit of native collagen's cell adhesion motifs, it may lack strength and precision in layer thickness control.

All in all, investing effort into refining the fabrication process, optimizing its parameters, and thoroughly evaluating its strengths and weaknesses is crucial for driving innovation and progress in collagen scaffolds tissue engineering.

### 1.5.2 Improvement of our collagen scaffold fabrication method

There are several areas that require attention for the characterization and development of 2D-3D integrated scaffolds. It is essential to thoroughly characterize each component of the scaffold. Identifying and addressing shortcomings and areas for improvement is crucial for further applications of the scaffold in tissue engineering, including cell studies, tissue regeneration, and blood vasculatures. Figure 1-9 illustrates the forthcoming areas of further development for the 2D-3D integrated collagen scaffolds, which are described below.

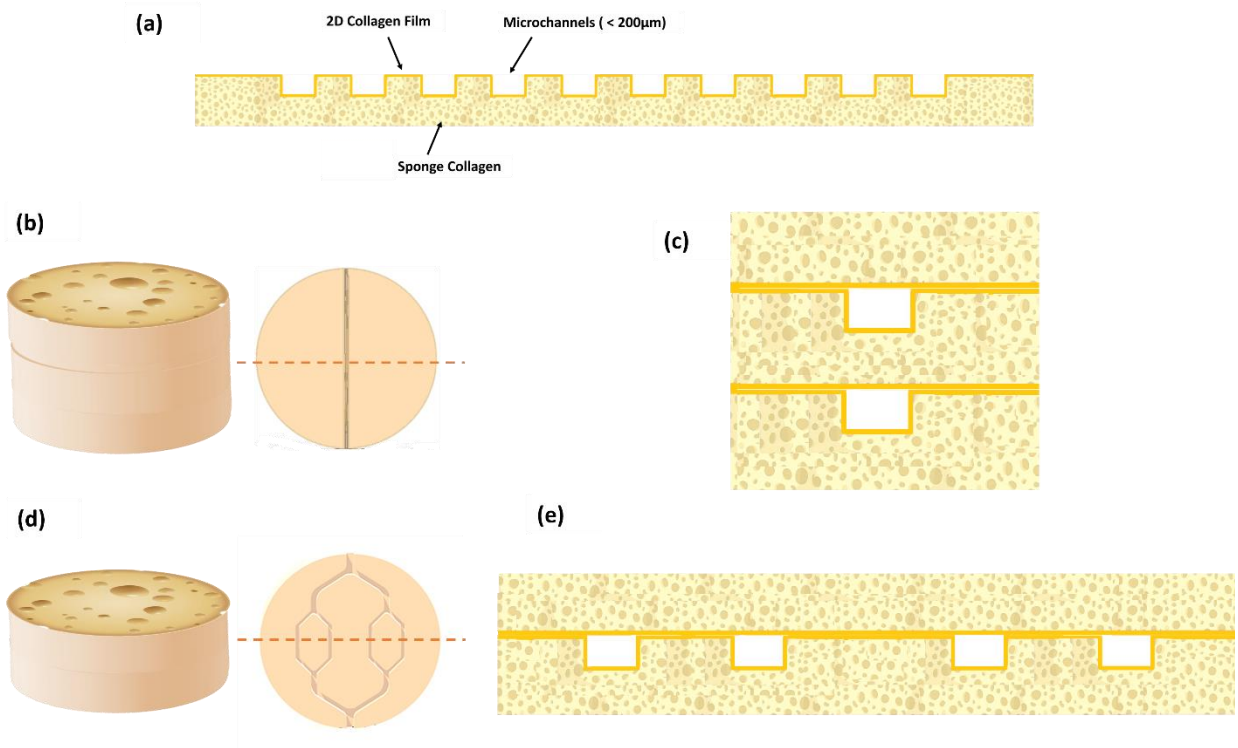


*Figure 1-9: Areas of further development for integrated 2D-3D collagen scaffolds. (a) Investigation model of achievable microchannels (<200 µm) after fabrication process. (b) Scaffold schematic with enclosed microchannels in different layers. (c) Cross-sectional schematic of microchannels in the middle of a multilayer scaffold. (d) Scaffold schematic featuring branch-shaped enclosed microchannels resembling simplified blood vessel design in a single layer. (e) Cross-sectional schematic of channels in the middle of the branched scaffold.*

***Small size microchannels on 2D-3D scaffolds***

Different studies have demonstrated the importance of incorporating microchannels or micropatterns on scaffold surfaces to enhance cell organization and alignment across various tissue types as described in the previous sections (1.4.6 and 1.4.7). In both *in-vitro* and *in-vivo* [53] cell culture studies, different sizes of microchannels have been shown to be most suitable for promoting cell viability, alignment, and proliferation.

For instance, Li et al. [22] found that porous chitosan micropatterning effectively regulates Schwann cell growth, particularly on the 30/30 µm pattern, indicating successful cell orientation.

Sarkar et al. [91] demonstrated that control over vascular smooth muscle cell (VSMC) behaviors, such as alignment and extracellular matrix (ECM) remodeling, was diminished with increasing pattern size beyond 80 μm on PDMS molds with microchannels. Furthermore, Bush et al. [21] investigated the impact of nonporous collagen cellular microenvironments on epithelialization and basal keratinocyte interaction, with narrow channels (50-100 μm) showing enhanced epithelialization. Similarly, micropatterned PLGA-leached porous scaffolds sized 50 μm have provided an effective platform for studying VSMC responses to specific topographical features as demonstrated by Sarkar et al [39]. Additionally, collagen scaffolds with curvy microchannel with an average width of 200 μm facilitated more ordered muscle tissue formation compared to scaffolds with narrower or wider ones [80]. However, in a similar work, calcium phosphate nanoparticles/collagen composite scaffolds with various concave microchannels promoted angiogenesis and osteogenesis while co-culturing HUVECs and human bone marrow-derived mesenchymal stem cells, with optimal results observed in scaffolds with a concave width of 290 μm and a convex ridge width of 352 μm microgroove dimensions [53].

These studies underscore the importance of tailoring scaffold microchannel dimensions for specific cell culturing applications. The possibility of fabricating a more biologically relevant collagen scaffolds with microchannels smaller than 200 μm of desired width and depth using our method (encompassing photolithography and freeze drying) warrants further investigation. Such an approach is not only biocompatible for culturing cells but also avoids the production of chemical toxic byproducts, making it suitable for a wide range of applications in tissue engineering and regenerative medicine. Figure 1-9(a) show the schematic model of 2D-3D integrated scaffolds with parallel microchannels smaller than 200 μm on the surface.

***Adjusting porous structure***

Porous scaffolds play a crucial role in engineering 3D tissues for repairing or restoring diseased tissues [37]. It is widely acknowledged that the size of pores significantly influences scaffold design, as successful scaffolds must facilitate vascularization and allow cells to access essential nutrients and oxygen for their survival. While researchers have differing opinions on the ideal pore size for tissue growth *in-vitro* and *in-vivo* [14] [38], it is recognized that optimal pore sizes vary depending on the tissue and cell types involved; for instance, skin tissue engineering often requires pores of around 100 μm [36]. Freeze drying enables the adjustment of pore size by modifying factors like collagen dispersion concentration, freezing rate which influence ice crystal nucleation and growth rates. Ice crystal formation during freezing creates porosity, forcing collagen to aggregate into interstitial spaces and form an interconnected network of collagen fibrils [36] [37]. Further in-depth research is needed in our approach to investigate and fine-tune pore size, particularly to assess diffusion and transport of nutrients and perhaps cells through the scaffold.

***Minimizing surface deformations***

Our previous fabrication process is conducted by placing the collagen film with microchannels on the collagen slurry and then it undergoes freeze-drying. The membrane will absorb water since the patterns are now soaked with collagen slurry. Thus, there was a significant deformation seen during the freeze-drying step, as reported before [14] [22] [82]. It can influence the dimension of the microchannels as well as the overall surface of the scaffolds. This needs to be addressed when layers or scaffolds are aimed, specifically during bonding. The surface deformation reversely affects the bonding process.

***Enhancement of scaffold properties***

The integration of a 2D thin membrane into the current scaffold design offers several advantages. Firstly, it may improve the integrity and stability of the microchannels, enhancing the overall structure of the scaffold during cell culture studies. Additionally, the membrane can serve as a physical barrier at the interface between the channel and the 3D collagen scaffold [82], preventing excessive leakage while potentially allowing for the diffusion of gases, cells, or signaling molecules in future applications if it contains pores on its surface. This pore size can be controlled to be smaller than the target cells, facilitating selective permeability. The fabrication of the 2D membrane in a porous structure presents an intriguing possibility for achieving these objectives. This porous membrane can either cover the entire scaffold surface or be selectively porous in specific areas, with the option to manipulate pore sizes accordingly.

Previous studies have demonstrated the potential of collagen tissues for co-culturing vascular endothelial cells and target tissue cells within porous scaffolds, offering promise for engineering vascularized tissue [53] [80]. Cultivating different cell types within the microchannels of collagen scaffolds represents a valuable approach for engineering anisotropic vascularized tissue and exploring cell-cell interactions within a 3D micropatterned material environment. Moreover, these developed models can be further expanded for applications on the vasculature-related biological processes such as bone marrow models, angiogenesis [53]. Therefore, preparing better scaffolds for co-cultures in different cells, medium and condition should be taken into account in our research. Technically our scaffold can be improved to fit these applications. Figure 1-9 (b,c) shows schematic models of such scaffolds.

The potential of microfabrication techniques to create pre-vascularized collagen-based scaffolds capable of accommodating flow has garnered significant attention. Cells cultured within the

microchannels has been exposed to mechanical stress from the flowing media [23] [81] [92]. Our scaffold can mimic a blood vessel model with minimal leakage from the 2D membrane acting as a barrier [82]**.** Figure 1-9 (d,e) shows a schematic model of the blood vessel. The integration and enclosure of microchannels emulate the structure of arteries and veins, minimizing convective leakage and ensuring fluid velocity, akin to natural vasculature. Further investigations can delve into flow rates in the blood model and assess their influence on cell behavior within the scaffolds while allowing for material exchange through the channel walls. This collagen-based microfluidic system holds promise for evaluating cells under dynamic conditions, simulating blood flow within vessels. Moreover, these scaffolds can serve for examining fundamental cellular processes and studying the effects of medications on specific cell types.

Another benefit of our fabrication approach offers the advantage of layer-by-layer construction, enabling the integration of various biomaterials into the scaffold. For instance, a secondary membrane consisting of different bioactive materials such as laminin and fibronectin [69] [91] can be positioned on the inner microchannel face, while collagen forms the porous side.

With thorough research and improved testing and characterization, these scaffolds can be instrumental in exploring tissue biology, conducting chemical and drug screening on multicellular tissues, and potentially integrating them into the human body for long-term tissue repair applications.

***Evaluation of new applications for collagen scaffolds***

Permeability is a crucial feature of scaffolds, serving as a platform for tissue growth while regulating the passage of media. Collagen scaffolds offer versatility by allowing adjustment of

pore size and permeability to control media flow and interaction with the substrate texture. It is essential for scaffolds to maintain integrity and properties when exposed to culture media.

Emerging applications for collagen scaffolds are continually expanding. One promising area is their use in brain studies. Investigating the feasibility of culturing brain slices, such as hippocampal-entorhinal cortical slices from mice, on these scaffolds can be explored. This involves assessing viability, tissue recovery, and neuronal maturation of brain slices on 3D collagen sponges. Currently, artificial polymers stands are employed for such studies on mouse brain slices to evaluate viability in contact with specific factors. The pore size and permeability of these filters play a critical role, underscoring the need to investigate the advantages of collagen scaffolds in influencing cultured tissue. Also, the integrity and stability of scaffolds are of essence while they are exposed to biological media and further implantation. This should be addressed separately. Especially, after scaffolds as contacted with cell culture media, they can deform and lose their surface micropatterns and structural stability.

## 1.6 Research Objectives

Previously, our group developed a model comprising a closed channel by bonding an integrated 3D sponge-2D membrane collagen scaffold to another similar collagen scaffold (Figure 1-8). However, further investigation is required in various areas as described in the previous section. Therefore, building on this work, my thesis aims to progress through the following steps:

Objective 1: Develop 2D-3D integrated collagen scaffolds with minimal deformation, including microchannels smaller than 200 μm, and investigate the impact of fabrication factors on scaffold characteristics through a parametric study.

Objective 2: Fabricate and characterize multi-layered 2D-3D integrated collagen scaffolds with enclosed microchannels in different layers.

Objective 3: Fabricate and characterize integrated 2D-3D collagen scaffolds with enclosed branch-shaped microchannels in a layer with descending sizes from 1000-500 μm and conduct fluid tests on the scaffold.

In the first step, I fabricated 2D-3D integrated scaffolds and identified factors influencing surface deformation. Crucial parameters affecting this were adjusted, and a parametric study assessed the effect of different factors on microchannel formation, such as freezing temperature and collagen slurry concentration. These results can guide the selection of fabrication parameters to manipulate scaffold properties for specific cell applications and are complied in Chapter 3.

In the second step, I fabricated multi-layered 2D-3D integrated collagen scaffolds with enclosed microchannels. This model is suitable for investigating the effects of microchannels on different cell types, as co-culture of cells inside and outside the microchannels in a porous scaffold mimics the interstitial matrix. In the third step, I aimed to develop a scaffold suitable for thick tissue by creating integrated 2D-3D collagen scaffolds with enclosed branch-shaped microchannels in a single layer. Fluid tests were conducted to ensure the scaffold's ability to accommodate fluid and investigate fluid characteristics, which can aid in modeling simplified blood vessels. Both results are presented in Chapter 4.

By adjusting fabrication parameters, I successfully fabricated 2D-3D integrated scaffolds with porous 2D membranes, facilitating media exchange. These scaffolds can be used to study cellular mechanisms or the effects of drugs on specific cells.

Lastly, we started to test the scaffolds in some biological applications. In collaboration with Dr. Andreas Velasco lab in Germany, we initiated tests to assess the biocompatibility of the fabricated collagen scaffold with mice brain slices. Also, in another collaboration to test the behavior of different cells on the surface of 2D collagen membranes, some cell culture studies were conducted in Dr Mark Bayfield lab at York University. Preliminary results of both cultures are presented in Chapter 4.

# 2 Designs and Experimental Methodologies

This chapter explains the designs and experimental methodologies, encompassing a range of topics including the design principles of collagen scaffolds, utilization of different replication molds in scaffold fabrication, materials selection, scaffolds fabrication processes, various types of fabricated scaffolds, test structures investigated, and the characterization techniques utilized such as image studies and flow tests.

## 2.1 Design of Collagen Scaffolds

In this thesis, we fabricated and characterized collagen scaffolds featuring embedded microchannels as shown in Figure 2-1. The scaffold comprised three primary elements: (1) a 3D porous collagen sponge resembling the interstitial matrix (IM), (2) a 2D collagen membrane mimicking the basement membrane (BM), and (3) microchannels serving as vascular structures or surface patterns within the scaffold to facilitate cell proliferation or resemble blood vessels. From here on, we call this the integrated 2D-3D collagen scaffold.

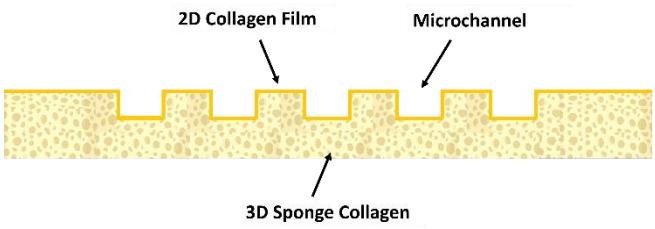


*Figure 2-1: Integrated 2D-3D collagen scaffolds with embedded microchannels. The scaffold contains main components of 3D porous collagen sponge resembling the IM, 2D collagen film resembling the BM, and a microchannel embedded within the scaffold*

The integrated 2D-3D scaffold was composed entirely of pure collagen across all its components. We opted for collagen due to its biological relevance and suitability for cell attachment, as

discussed in Chapter 1. Our fabrication method involved casting collagen slurry over various patterned replication molds containing desired channels, then freeze drying the assembly to form the 3D porous collagen sponge with the embedded channels. Incorporation of the 2D collagen film into the scaffold's design was achieved by drying collagen slurry at room temperature on the molds prior to casting and freeze drying of the porous sponge. Throughout the fabrication process, our aim was to integrate microchannels characterized by square-shaped cross-sections, exhibiting diverse dimensions. This encompassed microchannels sizing from 1000 μm in width down to 10 μm. The choice of square shape microchannels was due to simplicity in fabricating the corresponding replication molds as discussed later.

## 2.2 Materials and Consumables

All materials and consumable chemicals for fabrication of collagen scaffolds in this thesis are listed in Table 2-1.

*Table 2-1: Materials and consumables used in this thesis for scaffolds fabrication.*

| Description | Vendor | Country |
|---|---|---|
| Acetic acid | Sigma-Aldrich | USA |
| Acetone | Sigma-Aldrich | USA |
| Ethanol | Sigma-Aldrich | USA |
| Sylgard 184 PDMS kit | Dow Corning | USA |
| Silicon (Si) wafer | Wafer World Inc | USA |
| SU8 Photoresists | MicroChem Corporation | USA |
| M154 Reusable Plastic Molds | MetLab corporation | USA |
| Fibrillar collagen type I from bovine Achilles tendon | Sigma Aldrich | USA |

## 2.3 Master and Replication Molds

PDMS replication molds, in which collagen was cast and cured, played a crucial role in every stage of our fabrication process. These PDMS replication molds were fabricated by soft lithography, i.e., casting of PDMS over negative master molds. We employed two distinct types of master molds, each serving specific size ranges of channels as outlined in the sections 2.3.1 and 2.3.2. Then, the PDMS replication molds were used to cast collagen against them as described in section 2.3.3.

### 2.3.1 Silicon wafer master molds with patterned photoresist

For smaller channel sizes of 10-200 μm, requiring greater precision, SU8-patterned silicon (Si) molds were microfabricated through photolithography (Fig. 2-2 (a)). Si wafers, with a diameter of 4 inches and a thickness of 500-550 μm, were procured from Wafer World Inc., USA, for mold creation. As different channel depths were targeted, various SU8 photoresists (MicroChem Corporation, USA) and corresponding recipes were employed.

Initially, a layer of SU8 photoresist was spin-coated onto the Si substrate. For molds requiring shallower and more precise channels, a ~50 μm thick layer of SU8 2025 was applied via spin coating. Conversely, for molds with deeper channels, a layer of SU8 2075 with thicknesses of ~100 μm and ~150 μm was spin-coated on the Si wafer. This layer underwent baking at 65 and 95 °C to eliminate residual solvents and enhance substrate adhesion.

Subsequently, a photomask containing the desired pattern of the microchannel(s) was aligned on the Si substrate, and the photoresist layer was exposed to UV light through the mask. Following exposure, the photoresist was baked again at 65 and 95 °C before proceeding to the chemical bath based development step. During development, the unexposed regions of the photoresist were

selectively removed. Finally, the substrate underwent a final hard bake at 150 °C to ensure the stability of the SU8 properties.

### 2.3.2 3D printed master mold

For the fabrication of larger microchannels in both width and depth (500-1000 μm), a negative 3D-printed master mold containing the microchannels was fabricated. The 3D-printed mold was designed in SolidWorks in a single channel and also a branching shape resembling the distribution pattern found in blood vessels. A Projet MJP 3600 resin 3D printer (USA) was then used to manufacture the master mold as depicted in Figure 2-2(b).

### 2.3.3 Polydimethylsiloxane (PDMS) replication mold

PDMS replica molds were utilized to construct various microchannel test structures in collagen due to the biocompatibility and non-adhesive nature of PDMS to collagen. This allowed for easy fabrication of multiple collagen scaffolds [89]. For this, a mixture of PDMS elastomer and curing agent (Sylgard 184 kit from Dow Corning, USA) was prepared at a ratio of 10:1 and degassed in a vacuum chamber. This mixture was then poured onto the above-mentioned Si or 3D printed master negative molds (placed inside cylindrical mold holders of Figure 2-2(e)) to generate the positive PDMS replica. After degassing, the PDMS mixture was cured on a hot plate for 3 hours at 85°C before being carefully peeled off from the negative mold. Subsequently, the positive PDMS replica underwent thorough washing with water in preparation for further use (Figures 2-2(c-d)).

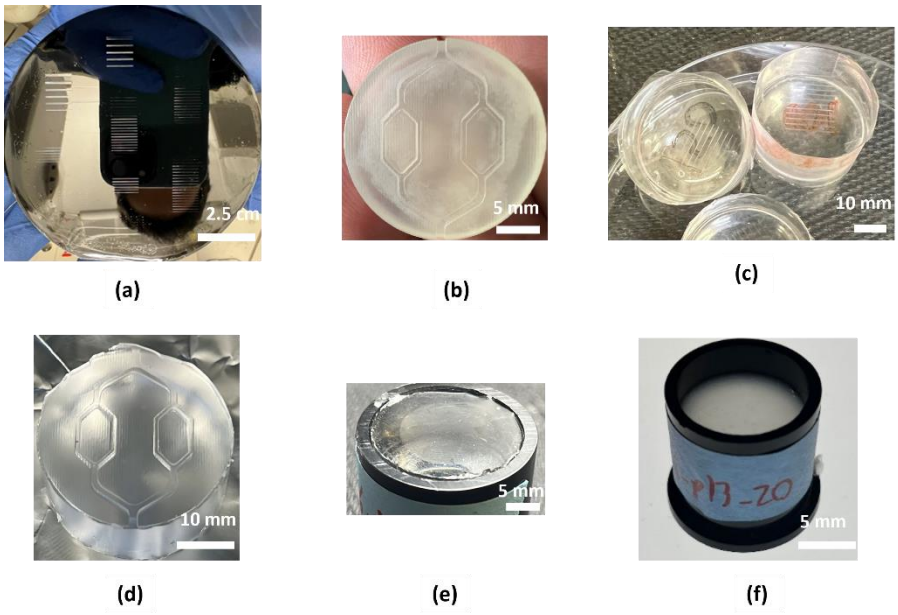


*Figure 2-2: Various molds utilized in the collagen scaffolds fabrication process. (a) SU8 patterned Si wafer molds for small microchannels. (b) 3D-printed branched-channel master mold for large channels. (c-d) PDMS replicas of master molds a and b. (e) Plastic cylindrical mold holders. PDMS replica molds were inserted inside the cylindrical molds, offering space on top of the molds for casting the collagen slurry (f).*

Reusable plastic cylindrical molds with a diameter of 1 inch (MetLab corporation, USA) were purchased, acting as a container to cast various volumes of collagen slurry on top of the PDMS molds for fabricating both 2D membrane and 3D sponge collagen layers. Their design let better handling of collagen slurry to manipulate the height of these layers and allowed further treatment of casted collagens to obtain surface flatness. Figure 2-2(e) and (f) show these reusable plastic holders with PDMS mold and collagen slurry inside.

## 2.4 Microchannel Test Structure Designs

To investigate the possibility of fabricating small-sized microchannels under 200 µm in collagen scaffolds, a series of parallel microchannels were CAD designed and tested. The widths of the microchannels ranged from 10 µm to 200 µm, with a consistent distance of 500 µm between each

channel, as illustrated in Figure 2-3(a). Subsequently, the CAD model was utilized to generate a photomask required for photolithography of SU8 on Si wafer as described above. The depths of the microchannels were varied at 50, 100, and 150 µm. These structures were instrumental in evaluating the efficacy of this approach in fabricating microchannels with specific dimensions for future scaffold designs. For instance, Figure 2-3(b) presents a sample featuring both single and branched microchannels on the surface with small sizes, fabricated with the aforementioned steps.

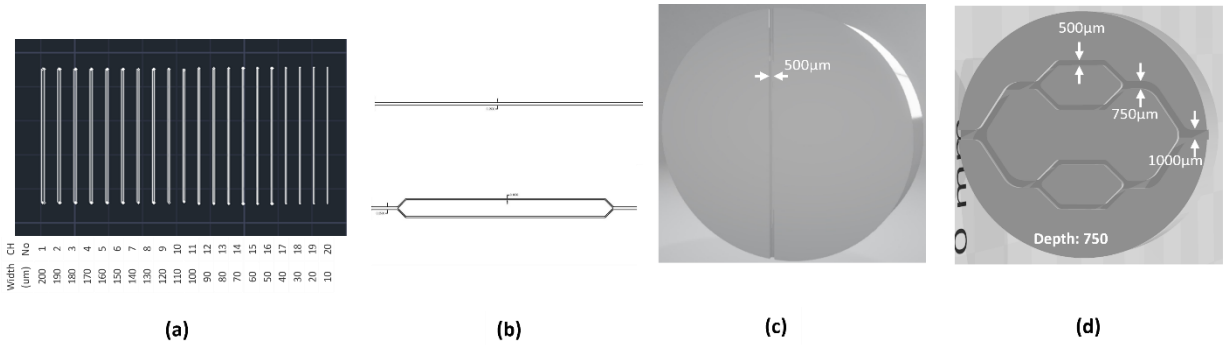


*Figure 2-3: (a) CAD model displaying a series of parallel microchannels, ranging in widths from 10 to 200 µm, with a consistent spacing of 500 µm. (b) Sample showcasing both single and branched microchannels on the surface, each with a width of 100 µm. (c) SolidWorks model with a single microchannel with width of 500 (d) SolidWorks model with a branched structure with widths ranging from 1000 µm to 500 µm and a depth of 750 µm.*

For the investigation of larger macrochannels, a SolidWorks model was created with single channel with width of 500 µm (Figure 2-3(c)) and a branched structure spanning widths of 1000 µm, 750 µm, and 500 µm, as shown in Figure 2-3(d). These sizes correspond to smaller arteries and veins in the body [93]. Subsequently, this design was utilized to generate a 3D-printed negative mold, which was then used to create the positive PDMS replica, following the procedures outlined in the previous section.

## 2.5 Fabrication of 2D Film, 3D Sponge, and 2D-3D Integrated Collagen Scaffolds

The fabrication steps for various collagen scaffolds are depicted in Figure 2-4. First, a suspension of collagen was prepared by mixing 0.5, 1, or 1.5 g of fibrillar collagen type I from bovine Achilles tendon (Sigma Aldrich, USA) with 0.05 mol/L acetic acid, resulting in collagen slurries of 0.5%, 1%, and 1.5% w/v concentration, respectively. The resulting collagen slurries were then incubated overnight at 4°C and agitated using a conventional blender on an ice bath to maintain a low temperature and ensure homogeneity. To eliminate any bubbles in the collagen slurry, centrifugation was carried out at a relative centrifugal force of 400 ×g.

As shown in panel A of Figure 2-4, the collagen slurry, at the desired concentration, was poured over the patterned PDMS replica mold inside the cylindrical holder (Figure 2-4(a,b)). Then it was left at room temperature to allow for evaporation of water, resulting in the formation of a 2D collagen film on the PDMS mold as shown in Figure 2-4(c). Then, a freshly prepared collagen slurry was cast at the desired concentration on top of the 2D collagen film while it was still supported by the mold holder (Figure 2-4(d)). The assembly was then frozen at a designated temperature (i.e., -10, -20, -40, or -80 °C). The frozen collagen was freeze dried (see section 2.6), leading to the formation of an integrated 3D porous collagen scaffold layer attached to the dense 2D collagen membrane (Figure 2-4A(e)). We call this type of integrated 2D-3D collagen scaffold "substrate" hereinafter.

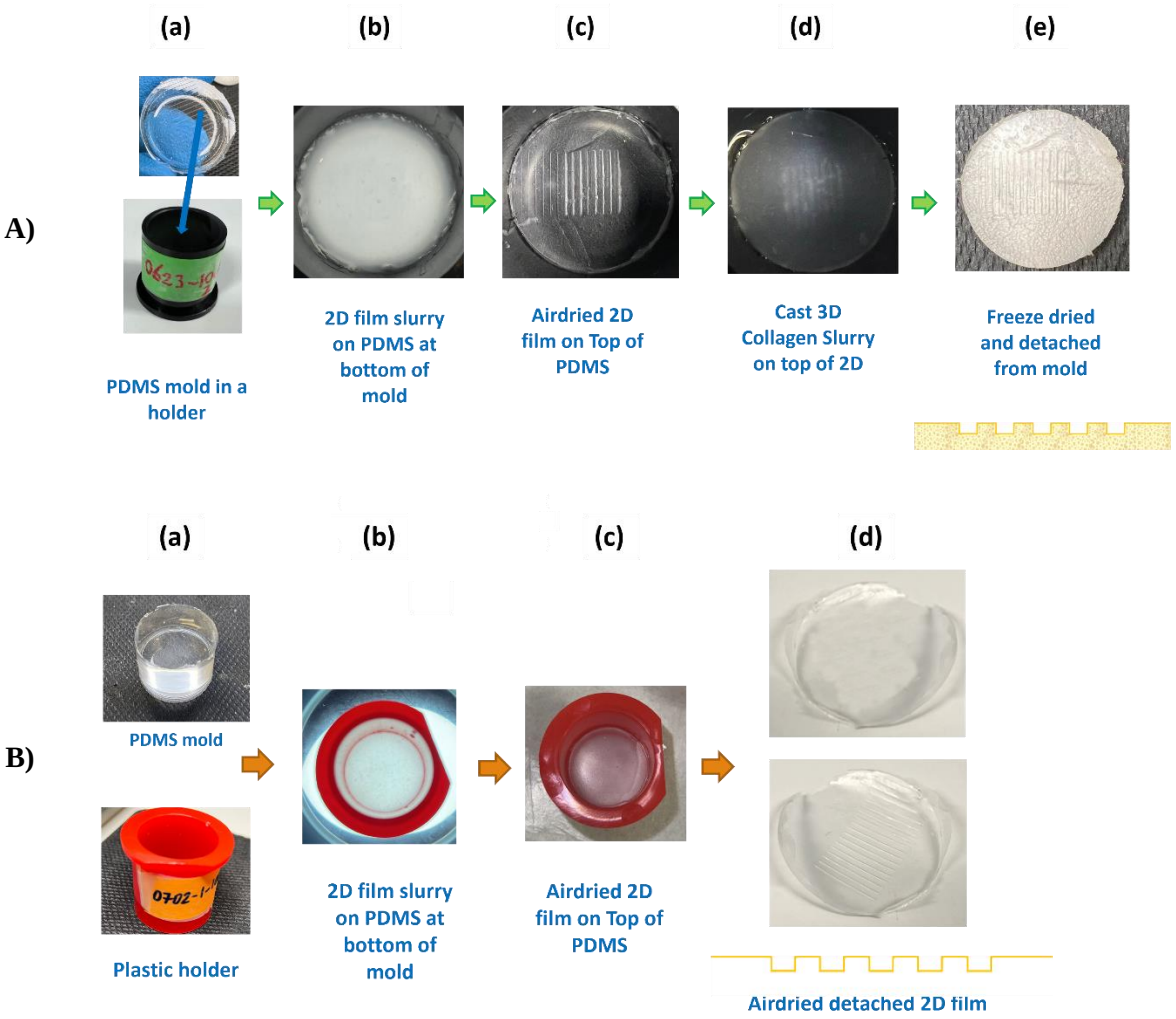


*Figure 2-4: Fabrication steps of (A) integrated 2D-3D collagen scaffolds and (B) 2D collagen films*

For the fabrication of sole 2D collagen membranes as depicted in the panel B of Figure 2-4, steps (a) to (c) were identically followed, after which the 2D film was gently detached from the PDMS replication mold for further experiments. Similarly, for the fabrication of sole 3D collagen sponges (see Figure 2-4(A)), steps (a) to (e) were performed, but step (b) and (c) were skipped, and the collagen slurry in the mold was frozen immediately in step (d). Finally, the 3D collagen sponge was detached from the mold for further characterization.

A comparison of the fabrication process for different sizes of microchannels can be observed in Figures 2-5 and 2-6.

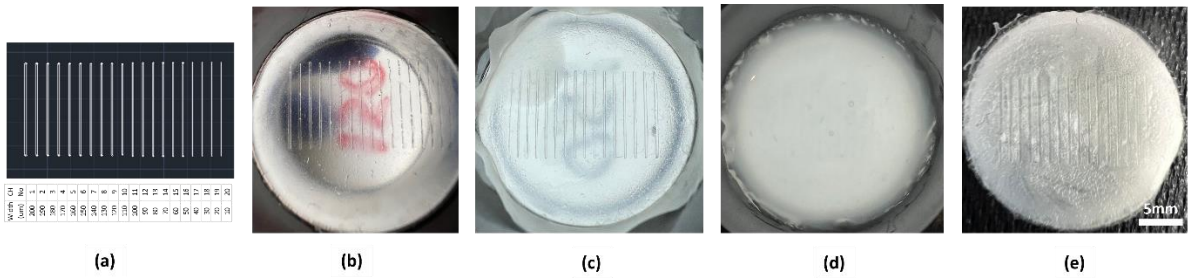


*Figure 2-5: Fabrication steps for samples with microchannels smaller than 200 µm. (a) CAD design of series of microchannels with widths from 10- 200 µm. (b) PDMS microfabricated mold with replica of microchannels. (c) 2D collagen film casted and air dried over the PDMS microchannels. (d) Casted 3D sponge collagen on top of 2D collagen film before freeze-drying. (e) Freeze-dried collagen scaffolds with 2D membrane and 3D sponge with embedded microchannels*

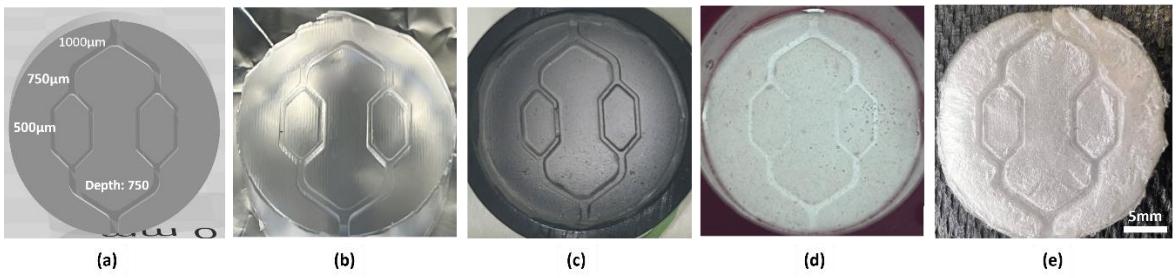


*Figure 2-6: Fabrication steps for samples with larger microchannels. (a) SolidWorks design of branched microchannels with descending size of 1000, 750 and 500 µm and the depth of 750 µm. (b) PDMS microfabricated mold with replica of microchannels. (c) 2D collagen film casted and air dried over the PDMS microchannels. (d) Casted 3D sponge collagen on top of 2D collagen film before freeze-drying. (e) Freeze-dried collagen scaffold with 2D membrane and 3D sponge with embedded microchannels*

## 2.6 Freeze Drying of Scaffolds

For the freeze-drying of the scaffolds, a scientific Freeze Dryer (Harvest Right Scientific, Canada) was employed. This apparatus consists of a freezer, a heater, and a vacuum pump, providing adjustable functions during different steps of the process. The freeze drying procedure entails the following steps [94]:

1. Freezing: This initial step involves freezing the product before activating the vacuum pump. The freezer is turned on, while the vacuum and heater remain off. The freezing duration was set to 2 hours to ensure complete freezing.

2. Vacuum-Freeze: During this step, the pressure is reduced further to lower the core temperature of the product before applying heat to the shelving unit. The freezer remains on, and the vacuum is activated to reach a predefined low-pressure level, termed the "target pressure," with a controlled rate of pressure reduction per minute. The heater remains off, and the target pressure was set to 450 mT.

3. Drying with temperature ramp up: In this stage, the temperature is gradually increased to reach the target temperature. The shelf temperature is regulated by the vacuum pressure. The “ramp up” adjust level controls the speed at which the heater ramps up, with lower values indicating a slower rate. Both the freezer and vacuum remain on, while the heater is activated. ramp up was set to 1 mT/hr to ensure staying near equilibrium.

4. Dry Process: During this step, the shelf temperature is regulated by the vacuum pressure. A target temperature and pressure range are set. Once the vacuum pressure reaches the target pressure, the heater is activated. The “heat off” pressure determines the pressure at which the heater will deactivate, regulating the rise in vacuum pressure due to sublimation. The heater attempts to maintain the target temperature while the pressure is below the heat off pressure. The target pressure was set to 500 mT, with a ramp up of 1 mT/hr to maintain proximity to equilibrium for 6 hours.

5. Dry Final: This final step serves as a secondary drying phase to measure the rate of pressure change and determine if the product is completely freeze dried. Throughout this step, the freezer,

vacuum, and heater remain operational. The target pressure was set to 400 mT, with a ramp up of 1 mT/hr to maintain proximity to equilibrium for 6 hours.

## 2.7 Factors Causing Non-flat Collagen Scaffolds

Achieving a flat integrated 2D-3D collagen layer was pivotal in this study as the channels replicated in this layer were aimed to be enclosed via bonding to another flat collagen layer. Any defects and waviness in these layers will hinder their bonding and enclosure of the channels. Accordingly, we identified influencing factors and pinpointed parameters that could serve as the primary contributors to defects. Subsequently, the effects of each parameter were investigated. To facilitate a more comprehensive assessment, factors were categorized as causes and effects. we delved into the identification of root causes for each defect by classifying and evaluating influencing factors. This precise process allowed us to prioritize the significant influencing causes for a more targeted understanding of the issues at hand.

To identify the root causes of defects, we employed the "root cause analysis" technique utilizing the "Ishikawa" or "fishbone" conceptual diagram. Factors or causes associated with various issues were classified into groups, and their effects were systematically examined through a series of tests. The main branches of the diagram (presented in the results chapter) represented the type or origin of each cause of defect. The defect itself is mentioned in the head of the fish bone conceptual diagram. Subsequently, each cause underwent in-depth scrutiny, and its impact was thoroughly investigated. Appropriate actions were proposed as solutions. These solutions were then tested, and their impact was carefully checked. This iterative process ensured that the desired properties of the scaffold were progressively achieved with our facilities and method. Furthermore, other

influencing factors and potential sources of each defect were managed and maintained at controlled levels.

## 2.8 Parametric Studies

Microchannels play a pivotal role in augmenting the functionality of scaffolds as described in Chapter 1. In this study, a parametric investigation was carried out to explore the factors influencing the properties of 2D-3D integrated collagen scaffolds with embedded microchannels smaller than 200 µm. The effects of factors such as 2D slurry concentrations, 2D slurry casting volume, 3D slurry concentration, and freezing temperatures on scaffold microchannels were examined. Each factor pertains to a domain in the fabrication process, such as slurry, process, mold, etc., and can impact individual scaffold components as well as the overall structure of the 2D-3D scaffold. The influential parameters studied in this work have been compiled in Table 2-2, specifying each factor, its domain, testing values, and units.

*Table 2-2: Parameters impacting microchannels in 2D-3D integrated collagen scaffolds. Underlined values were kept constant in testing of other factors.*

| **Parameters** | **Domain** | **Unit** | **Tested Values** | | | |
|---|---|---|---|---|---|---|
| 2D concentration | Slurry | % | 0.5 | *1* | 1.5 | |
| 2D Volume | Process | mL | *1* | 2 | 3 | |
| 3D Concentration | Slurry | % | 0.5 | *1* | 1.5 | |
| Freezing Temperature | Process | °C | -10 | *-20* | -40 | -80 |
| Channel Width (designed) | Mold | µm | 10 to 200 | | | |
| Channel Depth (designed) | Mold | µm | 50 | 100 | *150* | |

The impact of each factor on the scaffold was examined individually by keeping all other variables constant while varying the target parameter. The constant value for each factor was selected based on its promise for our intended application, denoted in italic underlined font in the table. For instance, when evaluating the impact of 2D slurry concentration on the scaffold, all other factors were maintained at the promising values identified in our preliminary experiment (i.e., 2D volume = 1 mL, 3D concentration = 1%, and freezing temperature = -20 °C, using the same mold with 10-200 µm microchannels and depth of 150 µm).

After fabricating the collagen layers, the width and height of the microchannels on collagen scaffolds were measured and compared to the design values via optical microscopy and optical profilometry. Three replications were fabricated for each sample, and the mean results were reported along with the corresponding standard deviation. These findings offer valuable insights for tailoring scaffolds with specific microchannels to suit various applications.

As examples of fabricated collagen layers, Figure 2-7 illustrates samples prepared with variable freezing temperatures and 2D film thicknesses, while maintaining a constant collagen slurry concentration of 1% for both 2D and 3D components. As the microfabrication molds were the same, the depth of channels was maintained at 150 µm. For each sample, three replicates were investigated to ensure reliability. The mean width and depth of microchannels on scaffolds were measured and the data were analyzed to assess the effect of each factor. The presence of each microchannel was considered as proof for capability of creating microchannels of that size level, while quantitative channel size measurements were used to determine the accuracy of channel replication. This approach facilitated an investigation into how each changing parameter influenced the final characteristics of the scaffold.

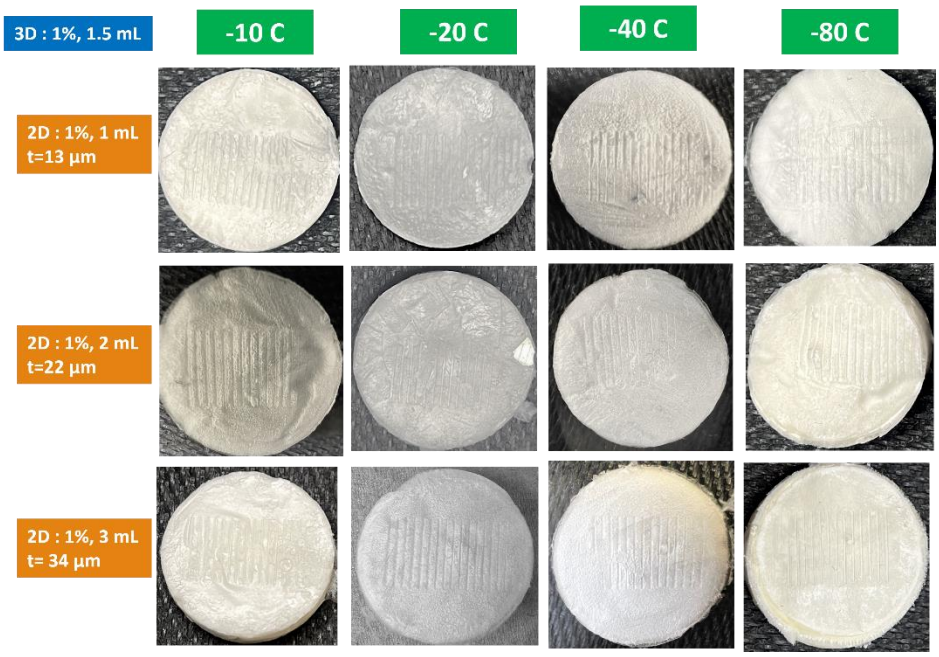


*Figure 2-7: Samples prepared with variable freezing temperatures (-10, -20, -40, -80°C) and 2D average film thicknesses (13, 22 and 34 µm), while the 2D and 3D collagen slurry concentrations were constant at 1%. The same PDMS mold (channels' widths of 10-200 µm and depth of 150 µm) was used for all collagen layers shown.*

## 2.9 Fabrication and Flow Testing of Enclosed Microchannels Within Collagen Scaffolds

The fabrication process of enclosed channels within two or more layers of collagen is described here.

### 2.9.1 Fabrication of double layer enclosed channels

For developing an enclosed channel, two layers of collagen substrate were utilized. Figure 2-8 shows the schematic of fabricating the enclosed channel. Once the collagen-based microchannels with 2D-3D substrate were fabricated as the first layer, a second substrate without any patterns was used to cover it and seal the patterned channels (Figure 2-8(a)). For this, similar steps to Figure 2-4 were followed to fabricate a non-patterned 3D scaffold over a flat 2D collagen layer on a flat

PDMS mold. Then, the patterned collagen substrate 1 was bonded to the non-patterned collagen substrate 2 using the method of contact printing as described below [82].

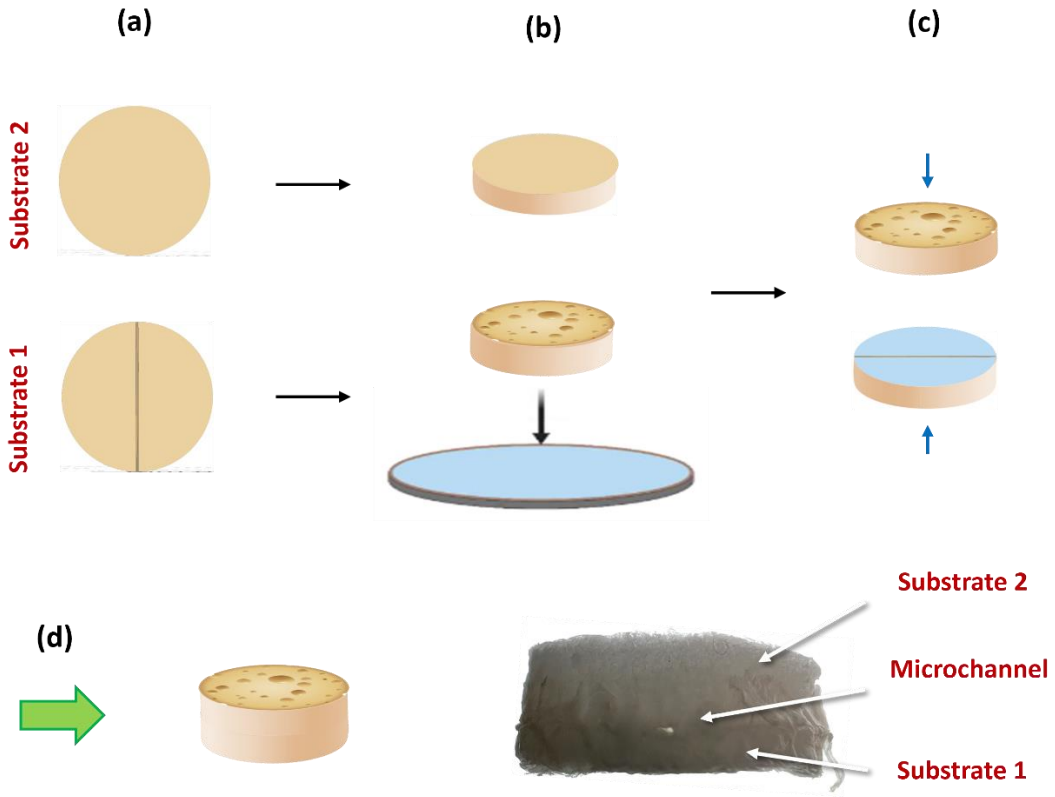


*Figure 2-8: Schematic of fabricating an enclosed channel by bonding patterned and non-patterned substrates. (a) Substrate 1 represents a 2D-3D scaffold with microchannels while substrate 2 is a 2D-3D scaffold without microchannels. (b) collagen slurry is spread over the glass substrate, then collagen slurry is applied onto the patterned substrate, with the substrate contacting the surface of the slurry-covered glass while the other substrate is unchanged. (c) Subsequently, substrates 1 and 2 are brought into contact and bonded. (d) The final achieved scaffold shown schematically and in real.*

For contact printing, a layer of collagen slurry was applied over a piece of glass to serve as a bonder. Various concentrations of collagen slurry, including 0.5%, 1%, and 1.5%, were tested. Also, two methods were employed for spreading the collagen slurry on the glass substrate. For thinner collagen slurries (0.5% and 1%), spin coating was utilized. Specifically, 0.5 mL of slurry was spin-coated at 1500 rpm for 30 seconds with a ramp of 100 rpm/s to achieve a uniform layer of collagen on the glass substrate. The other method involved sliding two glass substrates to create

a thin layer of collagen. This approach yielded better results with 1.5% collagen slurry, as the viscous jelly-like consistency of the slurry impeded spin coating. However, this method lacked precise control over the thickness of the bonding layer. Thicker bonding layers were found to be more effective but could potentially obstruct the channels depending on their size. Next, the scaffold containing microchannels was brought into contact with the layer of collagen slurry on a piece of glass (depicted in Figure 2-8(b)). Subsequently, it was bonded to the non-patterned collagen layer to seal the channel (as shown in Figure 2-8(c)). Finally, the bonded assembly was left at room temperature to allow for water evaporation. The final fabricated scaffold with the enclosed channel is illustrated in Figure 2-8(d).

### 2.9.2 Fabrication of multi-layer enclosed channels

Our steps for fabricating channels within collagen at different layers are outlined in Figure 2-9. This method can be utilized to fabricate multiple layers with enclosed channels in different collagen layers. This feature holds potential for future applications of the enclosed channels, such as studying co-cultures in two distinct channels with different flow or exposure to media in different layers but on a single scaffold. It can also pave the way for fabricating thicker and more biomimetic vascularized tissues in the future.

For the development of 2D-3D integrated scaffolds with two sets of microchannels at different layers, three distinct substrates are required. As depicted in Figure 2-9, in Step 1, substrate 1 constitutes a typical 2D-3D scaffold. Substrate 2 necessitates both a sole 2D film without microchannels and a 2D-3D substrate with embedded microchannels, both fabricated using the method outlined before. Similarly, for substrate 3, a plain 2D film and a 2D-3D substrate without channels are needed.

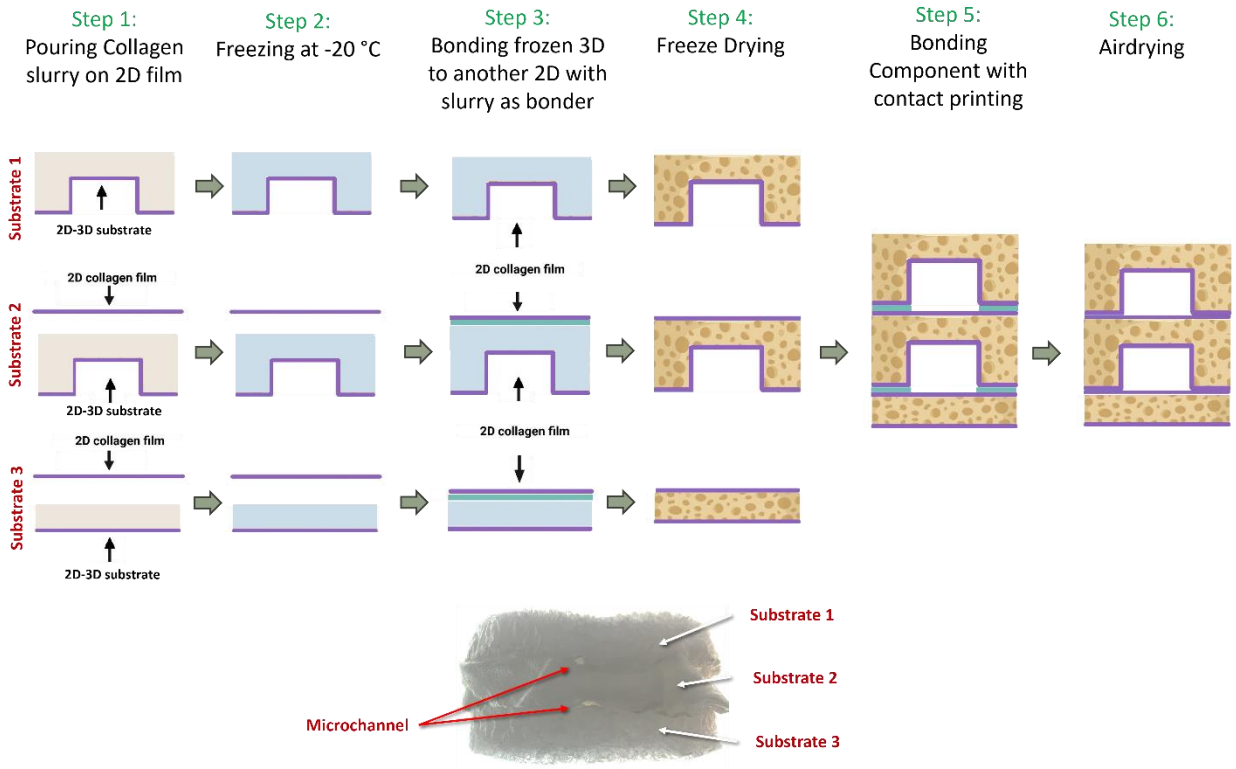


*Figure 2-9: Schematic depicting the steps for fabricating 2D-3D integrated scaffolds with double parallel microchannels at different layers, along with an illustration of a real fabricated scaffold.*

In Step 2, the three substrates (1, 2, and 3) described above were frozen at a temperature of -20°C. In Step 3, while substrate 1 remained unchanged, a sole 2D film was bonded to the surface of each of substrates 2 and 3. This process involved applying a droplet of 1% collagen slurry as a bonder onto the surface of the frozen 2D-3D substrate from the top, covering its frozen 3D sponge part. The cylindrical shape of the mold and the sliding PDMS design facilitated bringing the frozen substrates (2 and 3) to the top of the holder mold. The top surface of the substrate was then trimmed with a glass at the top of the plastic mold to ensure a flat and smooth top frozen surface for efficient bonding with the 2D film. Subsequently, a droplet of 1% collagen slurry was placed on top of each frozen substrate as a bonder, and the sole 2D film was gently laid on top of substrates 2 and 3, capturing them uniformly like a cap. Since the 2D film was prepared using the same mold, its base

area matched that of the substrates, allowing it to completely hold and cover the substrates. Prompt action is needed before melting of frozen substrate.

In Step 4, all the 2D-3D substrates were frozen at -20°C and freeze-dried, resulting in one normal 2D-3D substrate (substrate 1) and two disk-like substrates with 2D bases (substrates 2 and 3), facilitating further bonding. In Step 5, substrate 2 was bonded with contact printing from its both 2D bases to substrates 1 and 3, following the previously explained method. In Step 6, the scaffold was left to dry at room temperature, resulting in enclosed channels in two different layers.

### 2.9.3 Flow study of enclosed channels in collagen

A water flow test was conducted to assess the performance of the fabricated enclosed channels in the collagen scaffold. The effectiveness of this approach in developing scaffolds capable of accommodating a branched channel structure simulating veins was evaluated. In this evaluation,

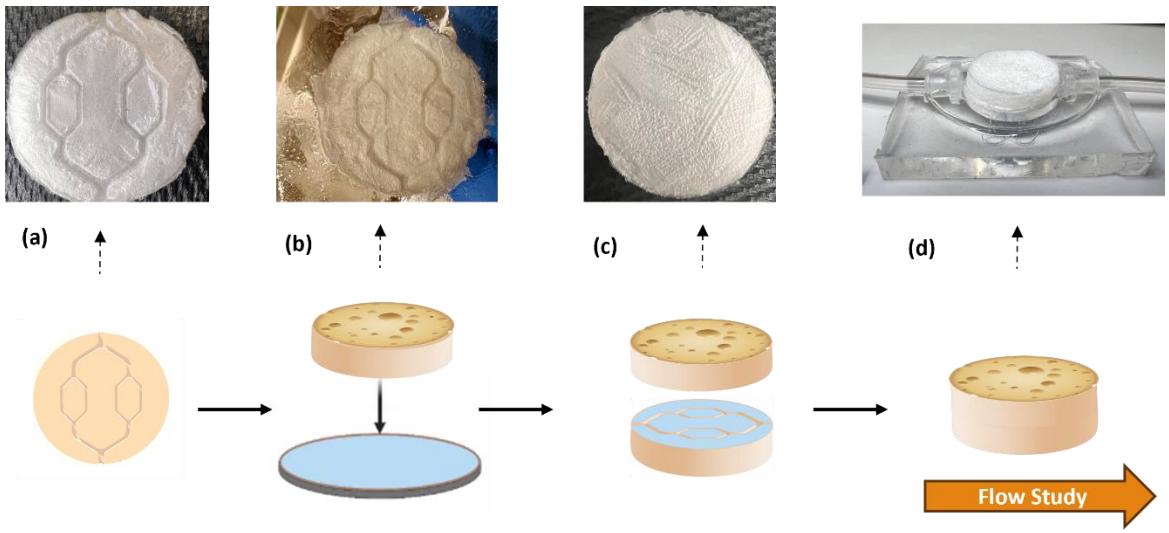


*Figure 2-10: Schematic and real photographs illustrating the fabrication process of an enclosed 2D-3D scaffold with branched microchannel structures resembling blood veins. (a) Substrate with branched microchannels. (b) Application of collagen slurry as a bonder on the substrate with branched microchannels. (c) Flat substrate without microchannels being brought into contact with the other half. (d) Final 2D-3D scaffold with branched structure in a PDMS holder with inlet and outlet, prepared for flow study.*

microchannels with descending widths of 1000 µm, 750 µm, and 500 µm, with a depth of 750 µm were utilized to investigate the scaffold's ability to transfer media. Figure 2-10 illustrates the steps involved in scaffold preparation which were described thoroughly in the previous section.

Figure 2-11 depicts the schematic of the test conducted to measure flow on collagen scaffolds. The flow delivery system utilized in the experiment comprised a dual syringe pump (KD Scientific - Legato® Syringe Pumps) and a device consisting of a PDMS holder with two plastic parts serving as inlet and outlet, connected to tubes for media flow through the scaffolds, as illustrated in Figure 2-10(d). A flow test was conducted to transfer media through the microchannels and evaluate the performance. Figure 2-11 depicts the schematic of the test conducted to measure flow on collagen scaffolds.

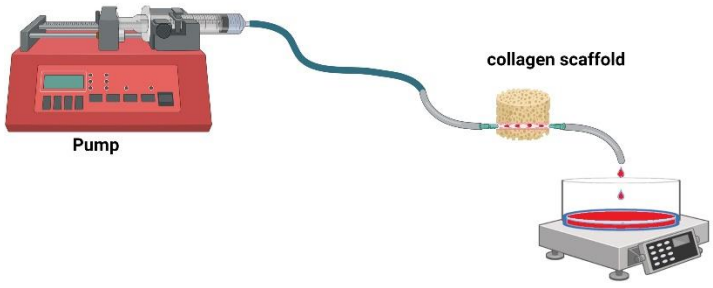


*Figure 2-11: The schematic of flow test set up to examine water transfer within the channels of collagen scaffolds*

To conduct the flow test, we passed dyed water through the microchannels at a flow rate of 50 µL/min, repeating the test for three different samples. The weight of the fluid collected at the outlet were measured with a Mettler Toledo ME54E lab scale (0.0001g accuracy, USA) over a set period of 5 minutes, allowing us to calculate the flow rate of water through the channel, and penetrating into the collagen scaffold, if any. The density of the dyed water was assumed to be 1 $g/cm^3$. The capability of various fabricated samples to pass the fluid was assessed. To quantify any

potential media leakage through the scaffold, we compared the volumetric flow rate of water at the inlet with the corresponding volumetric flow rates at the outlet.

## 2.10 Characterization of Collagen Scaffolds

Characterization of collagen scaffold components involved the use of various microscopy and image analysis methods discussed in this section. The effect of influencing factors on each component of the scaffold, including the 2D collagen film, 3D collagen sponge, and the final 2D-3D scaffold with embedded microchannels, was investigated separately. To obtain a cross-sectional view of the fabricated test structures, the collagen scaffolds containing the test structures were cut using a diamond wire saw (DWS 100, Diamond Wire Tec, Weinheim).

### 2.10.1 Optical microscopy

To assess the structure of the collagen scaffold, optical images of the scaffolds were captured using an upright Leica microscope equipped with a CMOS monochrome camera (GS3-U3-51S5M-C, Point Grey, Canada) or a TE300 Inverted Fluorescence Microscope (Nikon, Japan) equipped with the same camera. Figure 2-12 displays optical microscopy images of some collagen samples fabricated with casting 1% collagen slurry for both 2D film and 3D sponge on PDMS molds with 10-200 µm microchannels and frozen at variable temperatures (-10 to -80 °C) and freeze dried. These images were then utilized for qualitative macroscopic assessment of the scaffolds and to measure the channel widths and heights as discussed later.

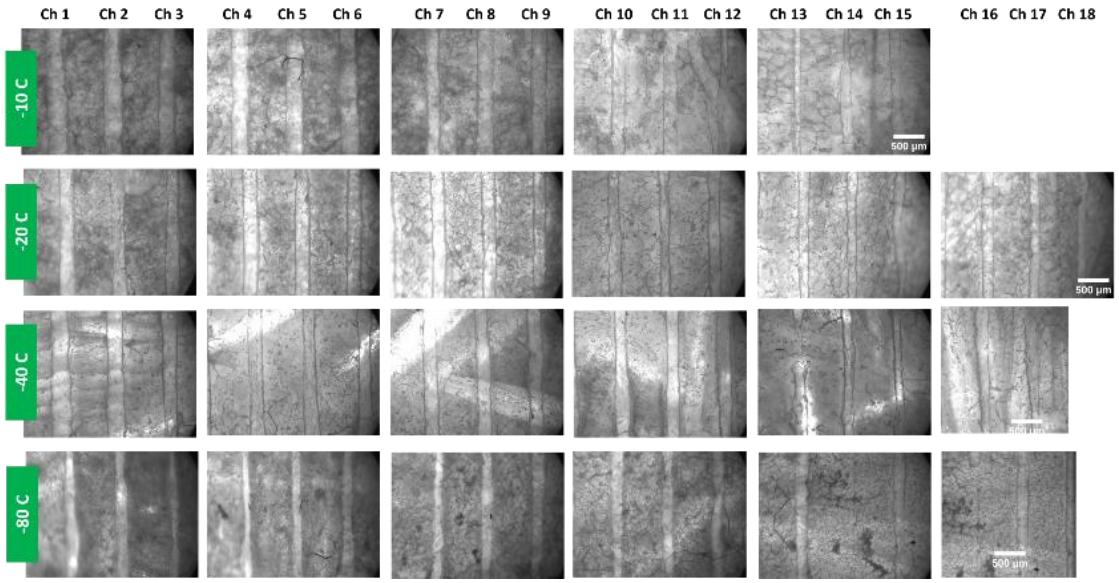


*Figure 2-12: Optical microscopy for inspection of collagen scaffolds fabricated with casting 1% collagen slurry for both 2D film and 3D collagen sponge on PDMS molds with 10-200 µm microchannels and frozen at variable temperatures (-10 to -80 °C) and freeze-dried (showing microchannels in different freezing temperatures while other parameters are constant).*

### 2.10.2 Scanning Electron Microscopy (SEM)

The microscopic structure of scaffolds was investigated using SEM. It provided an overall assessment of the microstructure, collagen layers' bonding, and porous structure including pore size measurements. The sample was mounted onto double-sided Carbon tape and subsequently coated with a 10-nanometer thick Platinum film using a sputter coater. The coated sample was then analyzed using a Thermofisher Quanta 3D (USA) SEM with an electron acceleration voltage of 30 kiloelectron volts (KeV).

### 2.10.3 Image processing

Measurements on the acquired images were conducted utilizing the ImageJ software, a publicly available image-processing tool developed by the National Institutes of Health (NIH) for a range

of image analysis applications. For measuring the microchannel widths, three images were captured for each channel with optical microscopy, and measurements were repeated across three distinct samples. Similarly, the thickness of the bare 2D film, produced using a PDMS plain mold as outlined in Section 2.3, was determined. Samples were precisely cut with sharp blades, and the cross-sectional area was utilized for thickness measurement, with readings taken from three separate samples.

To assess pore sizes, SEM images were employed initially. The methodology outlined by Hojat et al. [95] was adopted and tailored for our scaffold to ascertain the average pore size. The Particle Measurement features of ImageJ were then utilized to report average results and associated errors. The algorithm depicted in Figure 2-13 was specifically employed for statistical analysis of pore size distribution from the SEM images.

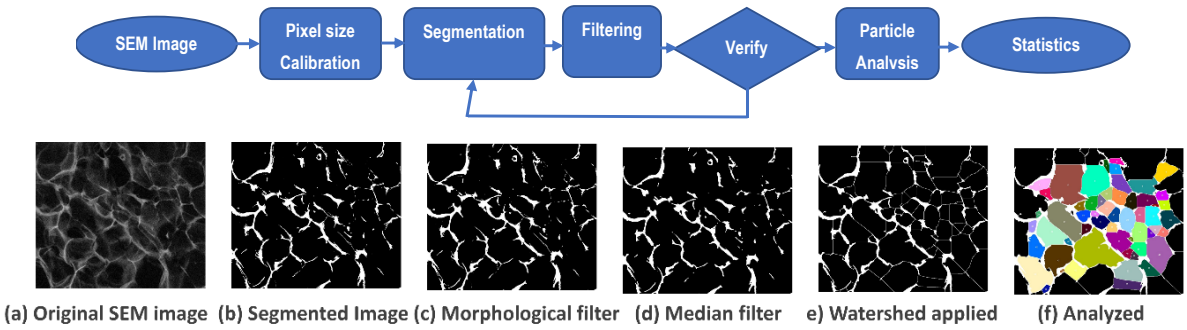


*Figure 2-13: Top row: Proposed algorithm steps as shown in the flowchart for pore size analysis using SEM images and ImageJ. Bottom row: Main steps from left to right, (a) Original SEM image of 3D sponge collagen scaffold with 1% concentration of collagen slurry frozen at -20 °C and freeze-dried, (b) Segmented image with thresholding and (c) morphological filter applied (erosion and dilation). (d) Median filter applied to omit unimportant pixels. (e) Watershed applied to close open pores. (f) Boundaries are detected representing each pore as a color island*

The proposed algorithm is presented in below main steps as shown in the flowchart of Figure 2-13:

(a) Receiving SEM image of porous structure and conduct pixel size unit conversion to metric units.

(b) Image segmentation (to 2 groups of pixels, scaffold material as bright and pores as dark pixels)

(c) Morphological filter to separate background from front pores

(d) Noise reduction filter to omit unimportant pixels with Median filter

(e) Watershed binary filter to close open pores

(f) Verification and pore size analysis and extract statistics from the detected pores using ImageJ features

A variety of information can be extracted from the "Particle Analysis" feature in ImageJ. The number of detected pores, with their areas, disposition of each pore in the frame, average area (or size), porosity and other statistical data can be achieved.

### 2.10.4 Optical profilometry

The depth of the microchannels was measured using an Optical Profilometer (ContourGT-K 3D Optical Profiler, BRUKER, USA). Micrograph maps of the channels were generated, and the software feature was utilized to extract error data. Measurements were conducted on three distinct samples to ensure accuracy and reliability. Figure 2-14 illustrates three separate measurements of microchannels with designed depths of 50 µm, 100 µm, and 150 µm.

The main benefits of using this measurement tool include high precision and minimal stress exerted on the sample during the measurement process. Unlike other techniques that involve cutting the sample, which can introduce stress and deformation, especially in small microchannels,

this approach is non-destructive. Additionally, samples can be reused after characterization, further enhancing its practicality and efficiency.

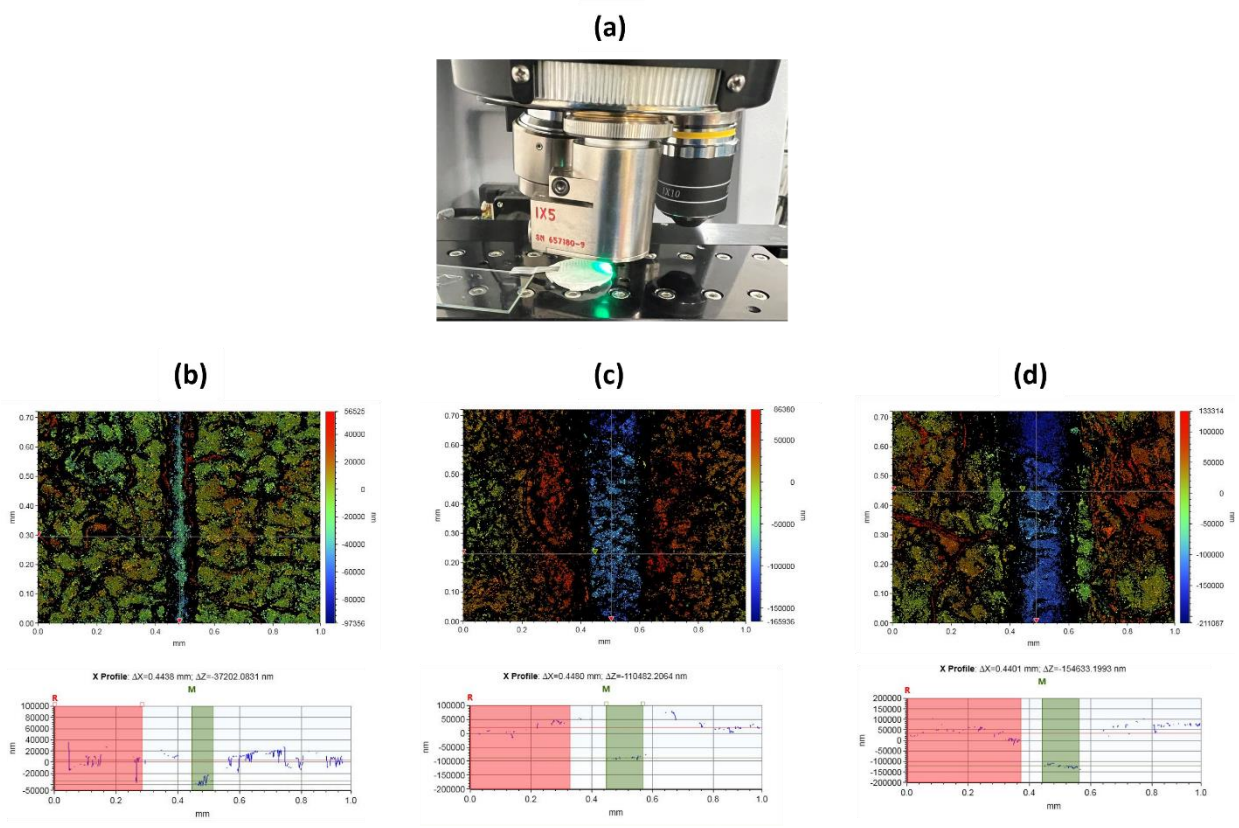


*Figure 2-14: Non-destructive depth measurements of microchannels with optical profilometry (a) the apparatus (b) sample with designed channel depth of 50 µm, (c) sample with designed channel depth of 100 µm and (d) sample with designed channel depth of 150 µm. ΔZ value is the depth of channel according to diagram profile*

For the validation of measurements conducted by the optical profilometer, cross-sections of channels were examined using optical microscopy images, and the depth of the channels was measured. Subsequently, the depths values obtained from the optical profilometer were compared with those obtained through optical measurements. Figure 2-15 illustrates this validation process, including a graph demonstrating the validated data obtained from the optical profilometer for a

PDMS replica mold of a channel. This validation procedure was also repeated for the collagen scaffold, yielding promising results (shown in Figure 2-16).

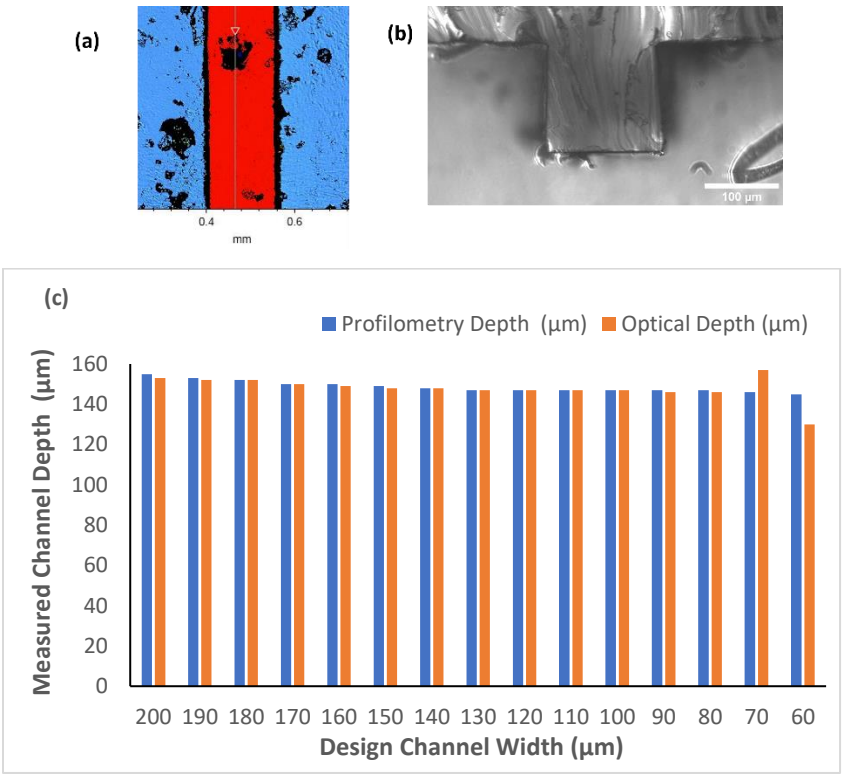


*Figure 2-15: Comparison of measurement of average depth of channels obtained by (a) optical profilometry and (b) optical image processing and on PDMS microchannels (c) Graph demonstrating the validated data obtained from the optical profilometer for a PDMS replica mold*

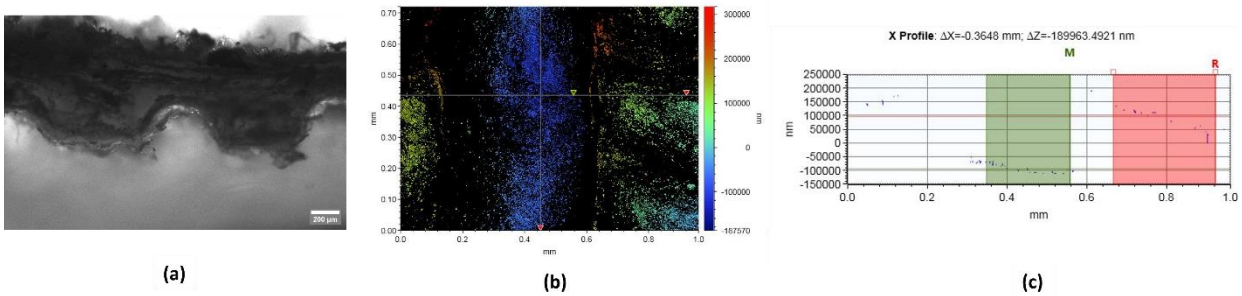


*Figure 2-16: Comparison of measurement of depth of microchannels measured by optical image processing and optical profilometry on collagen microchannels. (a) Optical microscope image of a microchannel of cross section of a 2D-3D integrated scaffold cut by wire saw. (b) Microchannel model from optical profilometer (c) Channel depth profile diagram. The green area marks the bottom of the channel and red area marks the surface of the scaffold. The depth of channel was estimated 190 µm with optical imaging and measured as ΔZ value equal to 189 µm with optical profilometry.*

## 2.11 Cross-Linking of Collagen Scaffolds

The collagen scaffolds discussed in the above sections are extremely hydrophilic and upon contact with water, we observed that they collapse very rapidly. For future applications of the collagen scaffolds such as cell culturing or biocompatibility assessments with brain slices (see next section), it was deemed important to strengthen the mechanical properties of the collagen layers via improving their cross-linking. Two distinct categories of scaffolds were studied: 3D sponge collagen and 2D-3D integrated scaffolds (with and without channels). These scaffolds were prepared with 1% collagen concentration for both 2D and 3D structures, and the fabrication process involved freezing at -20°C.

To stabilize the scaffolds, they were immersed in pure ethanol for approximately 1 hour, followed by sequential immersion in 70% (v/v) ethanol and then 50% ethanol, each for 30-minute intervals [18]. The behavior of these cross-linked scaffolds was investigated over time while exposed to water, the main component of culturing media. The changes in scaffold heights and percentage of scaffold shrinkage were measured as an indicator of stability in culturing media.

## 2.12 Biological Applications

### 2.12.1: Brian slice tissue culture on collagen scaffolds

The study explored the possibility of using collagen scaffolds as a substrate to culture brain slices of mice, particularly hippocampal-entorhinal cortical slices. The main aim was to assess the viability and support provided by these scaffolds during tissue recovery and neuronal maturation. This part of the research is being conducted in a collaboration with Prof. Andreas Vlachos' lab at the University of Freiburg, Germany.

Collagen disk shape scaffolds were fabricated as discussed in above and then shipped to Germany for co-culturing with mice brain tissues. For the initial step, four types of 3D collagen sponges frozen at different temperatures of -10, -20, -40 and -80 °C and subsequently freeze dried were tested. To assemble the collagen pieces and brain slices, we used a Culture Plate Insert (Millicell-CM, Ireland) with a polyester body and a BioporeM CM hydrophilized PTFE to put the scaffold on top as shown in Figure 2-17.

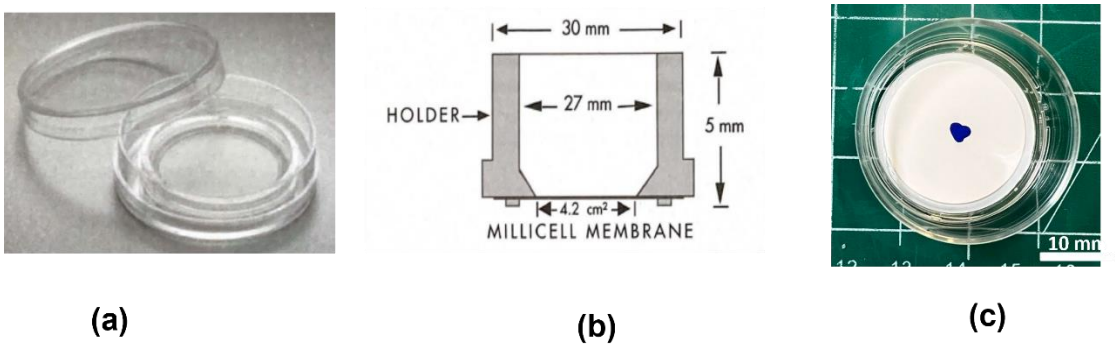


*Figure 2-17: (a) Millicell-CM culture plate insert, (b) The dimensional details of the plate insert. (c) Top view of real culture plate with a white PTFE filter. The blue area represents the size of the brain slice to be placed on top of the filter.*

Collagen scaffolds were first sterilized using UV light at a wavelength of 254 nm for 15 minutes. Then they were placed on top of the culture plate's PTFE filter. This setup allowed the scaffold to sit atop the filter with the medium below, limited to a volume of only 1 ml, making it impossible to reach from the lateral sides of the collagen scaffold as depicted in Figure 2-17. The medium traveled upwards through the PTFE filter and then through collagen scaffold. Figure 2-18(a) shows the collagen scaffold on top of the filters being wet by medium. Then small pieces of brain slices were prepared and put on the surface of the scaffold in a process known as brain slice implantation (via the method described by Galanis et. al [96]) and incubated. Eventually, the brain slice is exposed to the media. Incubated scaffolds carrying brain slice samples are shown in Figure 2-18(b).

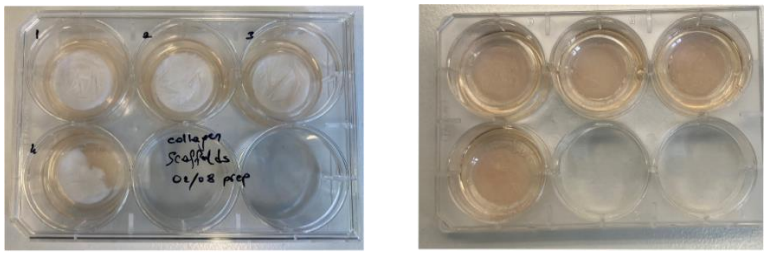


(a) (b)

*Figure 2-18: (a) Collagen samples are placed on the culture plate inserts and exposed to the medium. (b) Brain slices added on collagen scaffolds and incubated.*

The medium composition included MEM (Gibco 21575-022) with Hank's Salts, L-glutamine, 100mg/l glucose, without HEPES; BME (Gibco 41010-026) without L-glutamine and HEPES, 1000mg/l glucose; NHS heat-inactivated (Gibco 26050-088); HEPES (Invitrogen 15630-056); Sodium Bicarbonate (Invitrogen 25080-060); Penicillin/Streptomycin (Sigma P0781), Glutamax, and Glucose 45%.

The pH of the medium was carefully maintained at 7.3, ensuring optimal conditions for cell viability. The samples were incubated for 18 days. Throughout the culture period, the pH was monitored three times per week during medium changes, and adjustments were made as necessary to maintain a pH of exactly 7.30.

To evaluate the impact of the scaffold on the brain slice, propidium iodide (PI) and 4',6-diamidino-2-phenylindole (DAPI) staining were employed through the protocol described by Lenz et al [97] after finishing incubation. In this protocol for PI staining, a positive control using NMDA administration prior to PI staining was incorporated. Half of the samples were treated with NMDA before staining with PI, while the other half were stained with PI alone without prior NMDA treatment.

For staining without removing the media, 50μM NMDA was added into the media containing the positive control slices, followed by a 4-hour incubation in the cell culture incubator. Subsequently,

5µg/ml of PI was directly added into the media without changing it, and the samples were incubated for 2 hours in the cell culture incubator. It was crucial to note that PI is light-sensitive, so all pipetting steps were performed in the dark.

After staining, the samples were prepared for fixation. The media was discarded, and the slices were washed with PBS for 5 minutes at room temperature. Following this, a solution of 4% sucrose and 4% paraformaldehyde (PFA) was added into each well, and the samples were incubated for 1 hour at room temperature. The slices were then washed again with PBS three times for 5 minutes each at room temperature.

Next, the samples were counterstained with DAPI by incubating them in a 1:5000 dilution of DAPI solution for 20 minutes at room temperature. Afterward, the slices were washed with PBS three times for 5 minutes each at room temperature. Finally, the samples were mounted in an aqua mount for analysis.

### 2.12.2. Cell culture studies

To start evaluating the application of collagen scaffolds, cell culture studies were conducted on 2D collagen films in collaboration with Prof. Mark Bayfield lab at York University, Canada. As opposed to standard cell growth in a uniform monolayer, such as that which generally occurs when using a coated petri dish, cell growth and differentiation on a collagen scaffold more mirrors that which is executed in organisms. This investigation aims to delineate the subset of cell types that are viable, and the culture conditions that are necessary and sufficient, to support cell growth. The study by this lab involved the utilization of various cell lines, each with specific characteristics and roles. Notably, HEp2D cells were genetically modified through lentiviral transduction to incorporate an expression cassette encoding a non-targeting shRNA upstream of an RFP-encoding

gene, rendering them DOX (doxycycline)-inducible. This system allowed for precise control over gene expression, complemented by a puromycin selection marker downstream. Furthermore, the inclusion of HEp2 cells and HEK 293T cells added breadth to the experimental framework, encompassing cervical carcinoma and human embryonic kidney cells, respectively. This diverse cell lineup facilitated a comprehensive exploration of preliminary cellular responses within the scaffold environment.

Two dimensional films were prepared by us from 1% collagen slurry by casting and coated on small petri dishes similar to method described before in section 2.5. This helped mimicking the 2D collagen membranes in our integrated 2D-3D scaffolds.

Human cervical carcinoma epithelial cells (HEp2) and human embryonic kidney cells (HEK 293T) were graciously provided by Ultan Power (Queen's University, Belfast). Cell lines were cryopreserved in a liquid nitrogen storage container (-150 °C) until the point of thawing. Cells were rapidly thawed in a water bath (37 °C) for 90 – 120 s. Cells were then suspended in high glucose Dulbecco's modified eagle medium (DMEM 4.5 g/L glucose – Gibco Cat #11965092) and centrifuged at 300 g for 5 min. All cell lines were maintained in a humidified incubator (5% $CO_2$, 37 °C) until the point of manipulation or freezing. Cells were seeded at a density of $1.19 \times 10^5$ cells per well on Day 0 using Dulbecco's Modified Eagle Medium (DMEM) supplemented with either 5% fetal bovine serum (FBS) for HEp2 cells or 10% FBS for HEK 293T cells. Media swaps were conducted every 2 days post-seeding to ensure optimal cellular health. To prevent contamination, a 1X Penicillin/Streptomycin mix was introduced on Day 0 and with each subsequent media change.

At Day 7 post-seeding, cells underwent specific treatment and fixation processes according to the Immunofluorescence (IF) protocol. This involved fixation with 4% Paraformaldehyde for 20

minutes at room temperature, followed by permeabilization with 0.1% Triton in phosphate-buffered saline (PBS) for 10 minutes. Subsequent to each incubation step, cells were washed twice with room temperature PBS for approximately 30 seconds each, ensuring the integrity of the samples throughout the procedure.

After fixation and permeabilization, cells were subjected to counterstaining with DAPI (4',6-diamidino-2-phenylindole) for a duration of 2-5 minutes, followed by thorough washing steps. Utilizing an EVOS M5000 fluorescence microscope (Thermo Fisher Scientific, USA), imaging was performed. The GFP and RFP channels were engaged to observe fluorescent components of the collagen scaffold, while brightfield microscopy facilitated imaging of the scaffold itself. DAPI staining served to visualize cell nuclei, providing insights into cellular morphology and distribution within the scaffold. Imaging software used for analysis was that included as the software suite associated with the EVOS M5000 microscope, namely Celeste Image Analysis Software (Invitrogen).

# 3 Fabrication and Characterization of Collagen Scaffolds with Embedded Microchannels and Membrane Lining

In this thesis, our objective was to fabricate and enhance the characteristics and properties of an integrated 2D-3D collagen scaffold, incorporating the essential components found in *in-vivo* tissues. These tissues consisted of a noncellular extracellular matrix (ECM), comprising a 3D porous interstitial matrix (IM) for future cell proliferation, basement membrane (BM) linings on IMs, and microchannels serving as vesicles for nutrition and waste exchange, as well as aiding in cell proliferation, growth, and alignment. The structure and mechanical properties of the IM play a crucial role in influencing cell behavior, while the BM provides a substrate for cell attachment and acts as a selective barrier to cell transmigration.

Building upon this understanding, the objectives of the thesis were delineated into three main areas. Firstly, to develop 2D-3D integrated collagen scaffolds with minimal deformation, incorporating microchannels smaller than 200 μm, and investigating the impact of fabrication factors through a parametric study. Secondly, to fabricate and characterize multi-layered 2D-3D integrated collagen scaffolds with enclosed microchannels in different layers. Lastly, to fabricate and characterize integrated 2D-3D collagen scaffolds with enclosed branch-shaped microchannels, with sizes descending from 1000 to 500 μm, followed by conducting fluid tests on the scaffold.

This chapter provides a comprehensive exploration of the results obtained from characterizing various components integral to the fabrication of the engineered tissue, with a detailed analysis of the factors influencing these properties. Key considerations include the efforts to achieve flat scaffolds, analysis of pore size distribution, variations in thickness under different collagen

amounts, comparison of dimensions of microchannels between resulting collagen scaffolds and corresponding values in designed test structure molds, and evaluation of design and fabrication modifications and their subsequent impact on microchannel characteristics.

## 3.1 Preliminary Qualitative Assessment of Fabrication Factors to Prevent Major Defects on the 2D-3D Integrated Scaffolds

In this section, our focus was on conducting a comprehensive study to investigate the impact of various fabrication factors on the flatness of the integrated 2D-3D collagen scaffolds. Flatness is an essential characteristic for the scaffolds in order to be able to bond two collagen layers (one flat and one containing microchannels) to obtain enclosed channels as one of the objectives aimed for in this thesis. As described in Chapter 2, preliminary tests were conducted before the main tests to identify and comprehend the factors contributing to defects within the system. In the initial rounds of exploratory experiments, certain undesired characteristics and defects were observed in the scaffolds, potentially limiting their intended applications. Figure 3-1 illustrates some of these


*Figure 3-1: Examples of defects encountered in the fabrication of 2D-3D integrated collagen scaffolds: (a) Deformed structure with prominent wrinkles due to inappropriate freezing temperatures, (b) Loss of microchannels and the presence of a beveled edge due to poor mold preparation, and (c) Occurrence of bubbles and unintended deformations on the surface due to lack of degassing.*

defects that are discussed in this section. Examples of defects include bubbles on the surface, separation of 2D membrane and 3D sponge components, crack lines on the surface, and notably, both large and small wrinkles that were predominant and prevented the scaffolds' alignment and fabrication.

The primary issues identified included the presence of both small and large wrinkles, along with surface deformations (Figure 3-1(a)). This was caused mostly due to the use of inappropriate freezing temperature (-5 °C). Additionally, some of the initially designed microchannels were not fully realized, experiencing deformation in their dimensions due to issues associated with mold preparation (Figure 3-1(b)). Furthermore, certain scaffolds exhibited the emergence of bubbles, predominantly on the surface or at the interface of the 2D-3D scaffold (Figure 3-1(c)). They were placed mainly near the microchannels necessitating the need for degassing the collagen slurries.

Various approaches were implemented as solutions to address each identified defect. For instance, to combat overall dimensional deformation and deviation from the designed structure, cylindrical plastic mold housings were employed (Figure 2-2(f)), providing enhanced control throughout the fabrication process. Introducing microchannels onto the scaffold surface involved the use of PDMS molds, which could be cured inside the plastic cylinder housings that eliminated sharp corners in the mold and offered control over scaffold height by adjusting the volume of collagen casted into the cylinder. The cylindrical design facilitated the handling of scaffolds within the holder mold, allowing for additional adjustments in microfabrication. This technique proved valuable in producing collagen disks with parallel and flat surfaces. Achieving this involved smoothing the scaffold during the frozen stage of fabrication, eliminating solidification expansions, and yielding well-defined flat parallel sides of the scaffolds. Figure 3-2 shows the improvement of 2D-3D integrated scaffolds fabricated with cylinder molds.

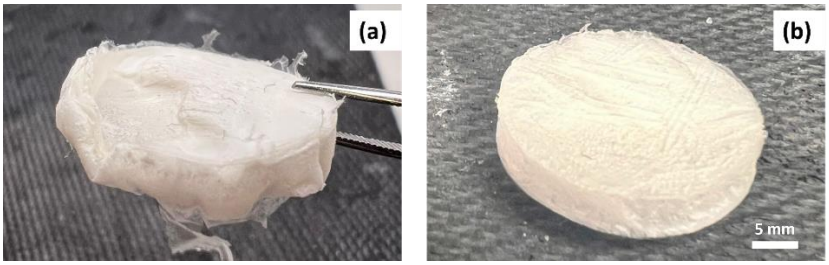


*Figure 3-2: The improvement of 2D-3D integrated scaffolds fabricated (a) without and (b) with cylinder mold housings.*

The parameters influencing the abovementioned defects were identified and classified as causes and effects. Root cause analysis, employing techniques such as the Ishikawa or fishbone diagram, was utilized to systematically categorize and evaluate these factors. The main branches of the diagram represented the type or origin of each cause of defect and the defect itself is mentioned in the head of the fish bone conceptual diagram. Each potential cause was meticulously examined,

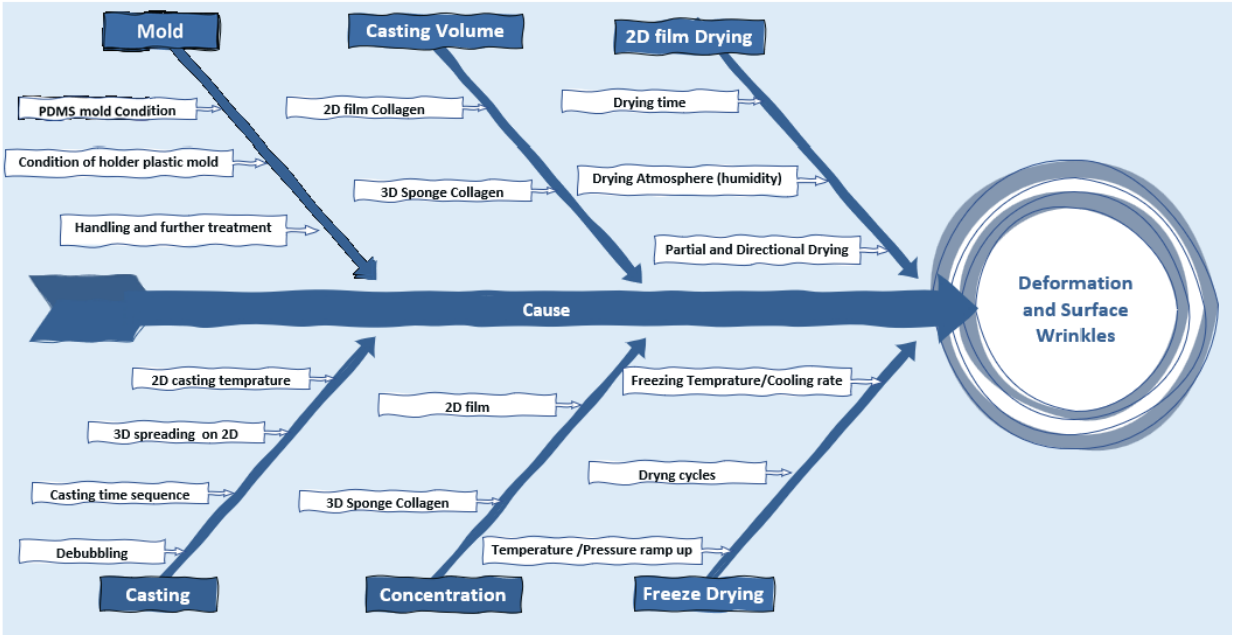


*Figure 3-3: Ishikawa fishbone conceptual diagram illustrating the identification of root causes leading to deformation and wrinkles defects on the collagen layer surface.*

and iterative testing was conducted to propose and validate solutions aimed at enhancing the system's performance. Furthermore, other influencing factors were carefully managed and regulated to mitigate their impact on defect occurrence. This methodology is elaborated upon to illustrate the improvement process, as depicted in Figure 3-3, which showcases the root cause analysis technique through an Ishikawa fishbone conceptual diagram. This diagram serves to pinpoint the root causes underlying deformation and wrinkles on the surface, thereby addressing them as critical defects within the system.

As pointed out earlier, considering the impact of each factor, various solutions were proposed and tested to rectify the fabrication process. Solutions for influencing factors include adjusting freeze drying parameters, controlling 2D film over-drying before casting the 3D sponge collagen, employing directional drying, and more. Table 3-1 provides a comprehensive breakdown of the types, causes, effects, and solution actions associated with the identified factors presented in the fishbone diagram in Figure 3-3.

Factors such as molds, casting methods, concentration selection, and freeze drying parameters were thoroughly examined to address the challenge of achieving flat scaffolds. After a comprehensive assessment of the causal factors and their effects, it was discovered that "Drying of 2D collagen film" stood out as the primary root cause behind the majority of surface wrinkles a revelation not readily anticipated prior to the evaluation. Figure 3-4(a-d) illustrates microfabricated collagen scaffolds with embedded microchannels, showcasing the difficulty in attaining flat structures. For instance, in scaffold in Figure 3-4(a), the freezing temperature was -5 °C and interactions cause wrinkles after pouring of 3D collagen slurry. Furthermore, the 2D collagen film was overdried and that led to deformation as wrinkles on the surface. In another sample depicted in Figure 3-4(b), the volume of 3D collagen slurry was not sufficient (1 mL), and the lower freezing

*Table 3-1: Causes, effects, and solutions for recognized factors contributing to scaffold deformation*

| Type | Cause (Factor) | Effect | Solution Action |
|---|---|---|---|
| **Mold** | PDMS mold Condition | PDMS samples with deformed or dented edges will cause deformation and improper surface | Lower temperature of curing PDMS (below -80 °C) and letting more time to cure (at least 3 hours) |
| | Holder Mold | Using cylinder plastic mold with smoother surface | Prepare more control of fabrication and facilitate for multi layers with microchannels |
| | Handling and further treatment | Highly affecting final quality | Should be performed gently and carefully, with proper time, tools, and sequences |
| **Casting Volume** | 2D membrane Collagen Volume | Has no significant effect on wrinkles but affects deformation of channels | Should be selected according to design |
| | 3D Sponge Collagen Volume | Has no significant effect on wrinkles on the surface and deformation of channels | Should be selected according to design |
| **Drying** | 2D Film Drying Time | Highly affecting both surface wrinkles and morphology | In normal condition can be adjusted according to design for desired results |
| | Drying Atmosphere (humidity) | Highly affecting both surface wrinkles and morphology | Should be controlled for less deformation |
| | Partial and Directional Drying | Can be applied by locally heating and affect drying of samples (in oven or on hot plate) | Should be selected according to design |
| **Casting** | 2D Film Casting Temperature | Warmed 2D film or frozen wet 2D film before pouring 3D slurry will cause solidification crack-lines and deformation on final product. | 2D membrane temperature should be around 4 °C |
| | 3D slurry Spreading on 2D film | Uniform and gentle pouring and spreading of slurry affects uniformity of final product | Optimum practical casting of 3D slurry on dried 2D film is pouring gently from sides to center of the mold |
| | De-bubbling (degassing) | Can cause bubble in final scaffold in both 2D film and 3D sponge collagen | Should be performed at least for 4 minutes at 400 xg |
| | Casting Time Sequence | Can have critical effect on flatness of scaffold | Should be casted right after the aimed drying time according to design |
| **Concentration** | 2D Film Collagen | Lower concentrations can cause 2D membrane to be detached from 3D sponge | Should be selected according to application |
| | 3D Sponge Collagen | Higher concentrations can cause surfaces to deform significantly to jelly character | Should be selected according to application |
| **Freeze Drying** | Freezing Temperature / Cooling rate | Lower temperature causes higher cooling rates and affect deformation | Should be selected according to application |
| | Drying cycles | Affect final scaffold properties | Choose enough time to dry completely (described in section 2.6) |
| | Temperature /Pressure ramp up | Affect final scaffold properties | Closer to equilibrium to suppress sudden and intensive change (described in section 2.6) |

temperature for this volume (-40 °C) caused appearance of solidification crack like lines on the surface which also deformed the microchannels. In the scaffold shown in Figure 3-4(c), the 2D collagen film was not sufficiently dried and some of the microchannel on excessively wet areas

were not realized. However, through strategic adjustments in fabrication parameters such as drying time and freezing temperature, structural deformations were successfully minimized. This optimization effort led to the attainment of planar scaffolds with smooth surfaces, as depicted in Figure 3-4(d).

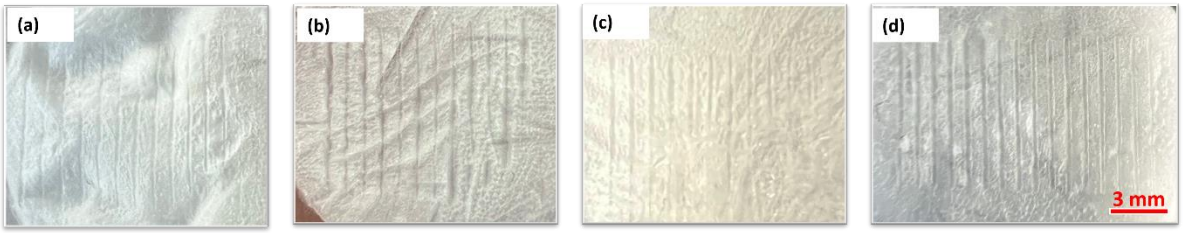


*Figure 3-4: 2D-3D collagen scaffolds with embedded microchannels, demonstrating (a-c) undesired uneven and (d) desired flat scaffold fabricated with 1 mL of 1% collagen slurry for 2D film dried for 48 hours, and 2 mL of 1% collagen slurry for 3D sponge frozen at -20°C and then freeze dried.*

A combination of the aforementioned effective actions in Table 3-1 was implemented in the subsequent round of the parametric study on the scaffolds, to identify the effect of different factors on the presence and characteristics of the replicated microchannels into the collagen scaffold.

## 3.2 Structural Analysis of 2D-3D Integrated Scaffolds

The structure and characteristics of various components of 2D-3D integrated scaffolds, as well as the impact of different parameters on them, are detailed in the subsequent sub-sections.

### 3.2.1 Structural analysis of porous 3D collagen

The 3D segment of the scaffold exhibits a sponge-shaped collagen structure with inherent porosity similar the Interstitial Matrix (IM). As explained in Chapter 1, such porous formations are characteristic of lyophilized fabricated materials, featuring interconnected pores that prove

advantageous in cell culture and tissue growth [37]. The interconnected pores can facilitate media transfer, nourishing the surrounding tissues or cells.

Fabrication of the 3D collagen sponge involves various factors influencing the shape and structure of collagen micropores. These factors encompass collagen slurry concentration, freezing temperature (freezing rates) and pH [14] [36] [37]. In this study, we specifically focused on investigating the impact of two primary parameters: collagen concentration and freezing temperature, while maintaining other variables constant at the optimal values mentioned in each section.

***Effect of freezing temperature on 3D sponge collagen micropores***

Figure 3-5 illustrates the visual macroscopic examination of samples fabricated with varying freezing temperatures, accompanied by their optical microscopic images. The collagen slurry concentration was maintained at 1%, and casted on a flat PDMS mold, with scaffolds subjected to freezing temperatures of -10 °C, -20 °C, -40 °C, and -80 °C and then freeze dried.

Moving from left to right in Figure 3-5, it is evident that lower freezing temperatures result in finer pore sizes, contributing to denser scaffolds. A visual comparison of the sample surfaces suggests a transition from a rough and coarse morphology to a smoother and more robust structure. The transition from a rougher surface to finer pore sizes and a smoother surface at lower freezing temperatures is attributed to the accelerated cooling rates experienced during the freezing step of process at these lower temperatures.

The temperature and temperature rate dependent phenomenon observed in Figure 3-5 follows a nucleation and growth mechanism [37], a characteristic of solidification. During the freeze-drying process, ice forms within the spaces between the collagen fibrils and solidifies. As the ice finds its

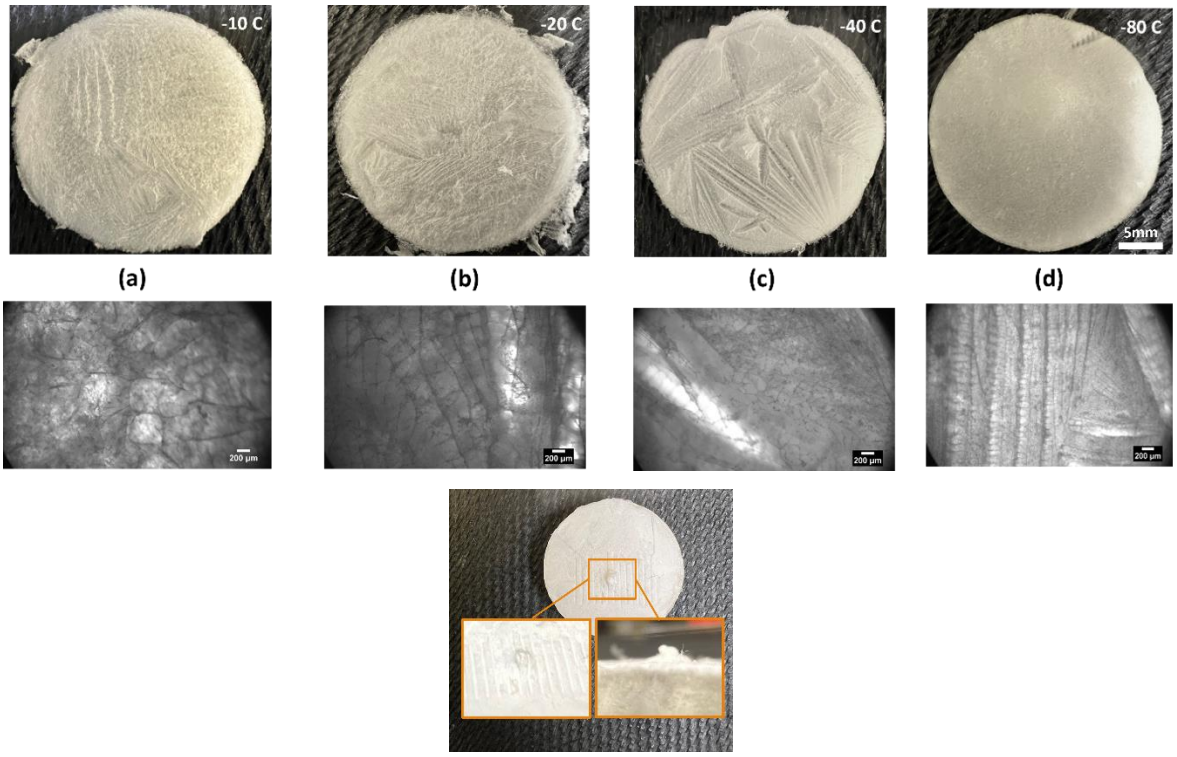


*Figure 3-5: Photograph and microscope images of 1% collagen scaffolds frozen at (a) -10 °C, (b) -20 °C, (c) -40 °C and (d) -80 °C, and then freeze dried. (e) A small peak arisen on the back surface of the -80 °C sample.*

way out of the structure due to vacuum pressure, it leaves behind empty spaces, forming pores. The higher cooling rate contributes to a more pronounced temperature gradient, which is called "undercooling", a known concept in solidification [37], acting as a driving force. Consequently, there is more nuclei and a more rapid and efficient formation and growth of collagen sheets, allowing them to reach each other and complete the structural framework earlier in the process. This ultimately results in finer pore sizes and a smoother surface in the final scaffold.

Distinct crack-like surface lines are observed on samples freeze dried at -10 °C, -20 °C, and -40°C, albeit rarely on those freeze dried at -80 °C. That may be caused by different directions of solidification. These lines are particularly prominent in samples subjected to -40 °C freeze drying

condition (Figure 3-5(c)). The reproducibility of these results in multiple experiments, which we have observed and not shown here due to repetition, underscores their significance. These lines may be attributed to the initial formation of coarse collagen sheets from the mold wall during the freeze drying process due to high undercooling and rapid solidification. However, in the case of -40 °C samples (Figure 3-5(c)), these lines become more recognizable and are likely the solidification crack-like formations resulting from higher cooling rates and temperature gradients. Similar disturbance in arrangement of the porous microstructure have been also reported at -40 °C freezing temperature elsewhere [37]. The accelerated cooling forces the initial collagen sheets to expand rapidly and collide with other forming collagen sheets. In instances where there is insufficient space for sheet expansion due to occupancy of mold space with frozen collagen, they exert pressure on each other, leading to small deformations manifested as lines on the surface of the scaffolds.

An intriguing observation involves the emergence of small peaks on the surface of samples (facing the PDMS mold) undergoing freeze drying at -80 °C. Figure 3-5(e) visually captures the presence of such peaks. The appearance of these elevated protrusions is also explained with the rapid cooling of the slurry and the resulting high temperature gradient. The slurry in close proximity to the walls of the plastic molds and the base face exposed to cold air rapidly solidifies and hardens, while the slurry adjacent to the PDMS remains in a liquid state. The presence of high cooling rates continues to contribute to a finer overall structure. Consequently, the expansion force exerted by the forming ice potentially deforms the flexible PDMS, resulting in the formation of these peaks on the sample's surface with fine pore size structures. Notably, the pore sizes associated with these peaks are significantly smaller than the dimensions of the peaks themselves. When creating scaffolds

with stacking layers, these peaks can interfere with the stacking process and should be addressed to ensure a uniform and well-structured scaffold.

***Effect of collagen slurry concentration on 3D sponge collagen micropores***

To delve more deeply into the influence of each parameter, it is crucial to consider the impact of collagen slurry concentration as a key factor in controlling the microstructure and, consequently, the overall properties of the scaffold. To establish suitable concentration values, preliminary tests were conducted to determine the applicable range of collagen slurries. Various concentrations have been reported in previous studies ranging from less than 0.5% to 5 % [14] [3] [35] [36] [82]. Accordingly. In this research, a parametric study was conducted using collagen concentrations of 0.5%, 1%, and 1.5%, as determined through initial assessments.

To analyze the microscopic structure of the collagen scaffolds fabricated at different freezing temperatures and slurry concentrations, sections were cut, and SEM images were acquired from the cross-sections of the collagen scaffolds. Figure 3-6 presents SEM micrographs of 3D sponge collagens with concentrations of 0.5%, 1%, and 1.5%, freeze dried at temperatures of -10 °C, -20 °C, -40 °C, and -80 °C on flat PDMS molds. The images reveal that both collagen concentration and temperature exert notable effects on the structure of 3D sponge collagen.

Each freezing temperature applied during the fabrication process of the 3D sponge collagen imparts a distinct structure. However, the resulting structure is also influenced by variations in the concentration of the collagen slurry. As illustrated in Figure 3-6, SEM micrographs reveal diverse microstructures with a range of typical appearances.

The 3D collagen sponges subjected to freezing at -10 °C (depicted in Figure 3-6(a-c)) exhibit a

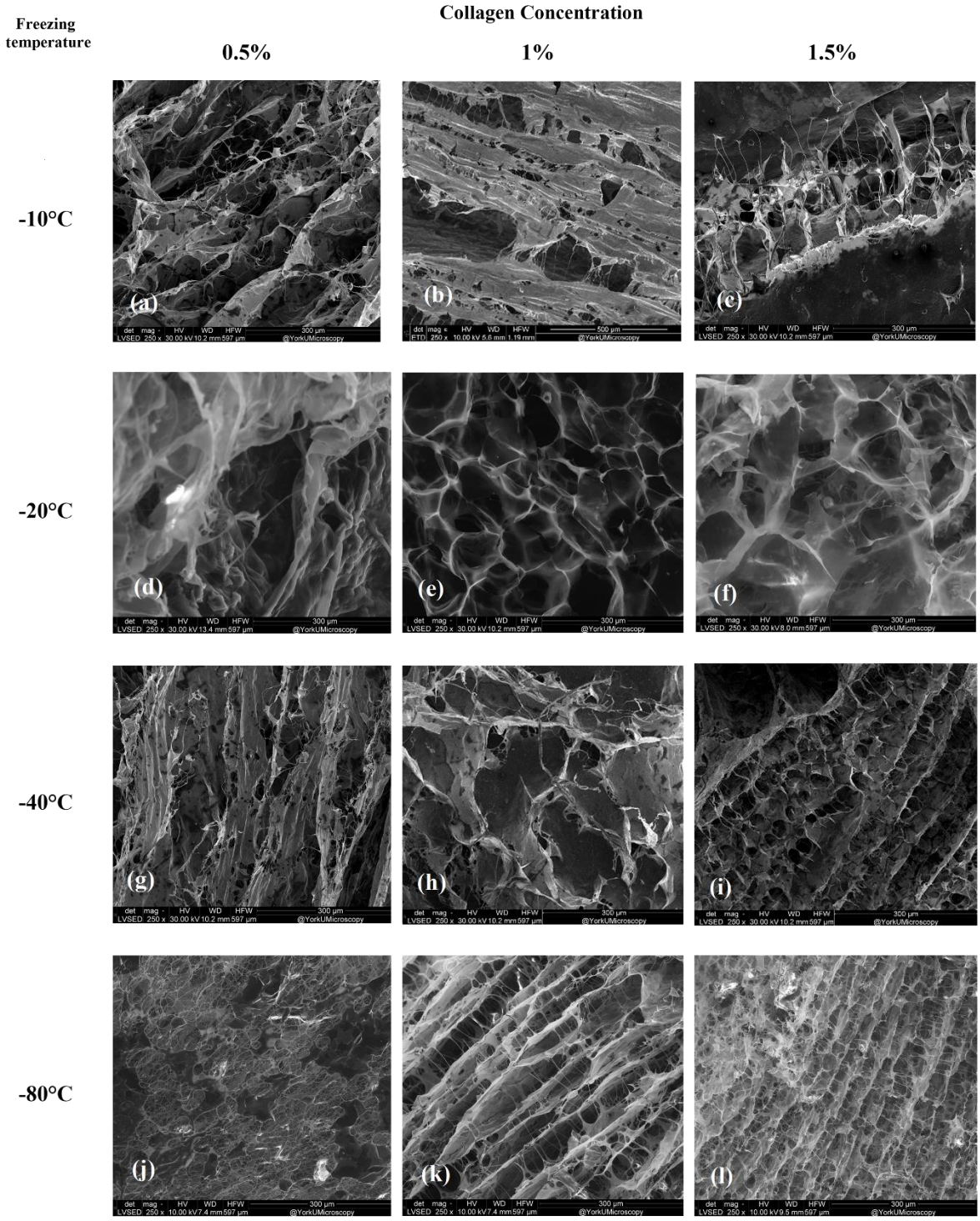


*Figure 3-6: A grid of SEM micrographs depicting the 3D sponge collagen at 250x magnification. The variations in collagen concentrations are represented in each row, while freezing temperatures variations are depicted in each column. Figures in panels d, e, f, j, k and l are from a collaborative work reprinted with permission of Joab Ogato.*

composition of layered collagen sheets, which appear separated and disrupted in certain regions, contributing to a coarse surface texture. As the concentration increases from left to right, the collagen sheets become thicker. However, areas such as pores are less discernible, and empty spaces observed more between the sheets. The connection bonds between the structural collagen sheets are weaker, resulting in an overall less robust structure. Visual examination of the surface of -10 °C samples also confirm a coarser structure compared to samples subjected to other temperatures.

As depicted in Figure 3-6(d-f), characteristic circular pores are evident in samples frozen at -20 °C. The equiaxed round-shaped pores are particularly uniform in the case of 1% collagen concentration and have an approximate mean size of 65 µm. Although round pores are observable in all tested concentrations, they are more prominent in 1% and 1.5% collagen concentrations, with corresponding mean size ranges of 52 and 65 µm, respectively. Higher collagen slurry concentrations result in thicker walls surrounding these round-shaped pores.

The presence of round-shaped pores, especially in 1% collagen slurry frozen at -20 °C, can possibly enhance the potential for media and cell transfer through the pores. Moreover, these structures exhibit increased flexibility, proving advantageous during the application or handling of scaffolds in various experimental scenarios. The most uniform pores are achieved with 1% collagen slurry frozen at -20 °C and freeze-dried subsequently, featuring coaxial pores of almost identical sizes (Figure 3-6(e)).

In the samples frozen at -40 °C, as illustrated in Figure 3-6(g-i), the presence of round-shaped structures diminishes. Instead, branched sheets of collagen interconnect in the middle, developing along the direction of heat transfer during freezing and solidification of the slurry. This branching pattern, also observed in the sample image of Figure 3-5(c) as well, contributes to the development

of significant crack-like solidification lines within the structure. These lines, visible to the naked eye, create cavities that break apart the structure in -40 °C samples. As mentioned before, a comparable disruption in the organization of the porous microstructure has also been documented at a freezing temperature of -40 °C in other studies [37].

With higher concentrations, the collagen sheets become thicker and more densely packed with increased interconnections. This results in smaller hollow space left and a stronger network in the overall structure. This has also reported elsewhere after the measurement of mechanical properties [3] [35].

The most robust and refined morphologies are observed in samples subjected to -80 °C, as depicted in Figure 3-6(j-l). The smallest and closely packed pores, ranging from 19 to 30 µm has been achieved. When collagen concentration increases, it contributes to a denser structure. The overall composition still comprises sheets of collagen that are uniformly aligned and bonded together, resulting in the formation of fine pores. This alignment and bonding enhance the stability of the scaffold, marking it as structurally strong.

Similarities are also discernible among samples with identical concentrations, as depicted in the columns of Figure 3-6. Analyzing the SEM micrograph of samples with a 0.5% collagen slurry in the left column (Figure3-6 (d, g, j)), it is evident that certain areas exhibit empty spaces where the structure has collapsed. This phenomenon is attributed to the thinner collagen slurry and is consistently observed across all freezing temperatures. Consequently, there are less collagen fibrils there and the overall network is weaker, resulting in lower strength when the scaffold is handled. Collagen concentrations lower than 0.5% were not explored in this study due to their insufficient strength for the intended purposes.

Typical circular pores are evident in the 1% collagen slurry, as depicted in Figure 3-6(e, h, k) (middle column). These pores are arranged in a comb-like structure. However, at lower concentrations like 0.5%, the structure appears weaker, and the constituents seem more detached, as anticipated and mentioned earlier, owing to the insufficient presence of collagen fibrils needed to strengthen the structure.

At the other side in the right column of the grid, samples with higher concentrations, as shown in Figure 3-6(f, i, l), exhibit a denser arrangement, characterized by thicker and dominant sheets of collagen. This is attributed to an excess of collagen fibrils facilitating the formation of a sheet-like network with increased interconnections, resulting in irregular pores with reduced volume. Consequently, this culminates in a finer and more robust structure, particularly contributing to enhanced strength and stability, especially under higher cooling rates at lower freezing temperatures.

***Pores size analysis of 3D collagen sponges***

To enhance our understanding of the microstructure of the 3D sponge scaffold, we conducted quantitative pore size analysis. As depicted in Figure 3-6, samples prepared at temperatures of -20°C and -80°C exhibit a typical porous structure characterized by round-shaped pores. However, samples frozen at temperatures of -10°C and -40°C display a somewhat different morphology. They resemble planar sheets of collagen connected by fewer fibers, with a less defined porous structure. In the case of samples frozen at -40°C, pores appear to be ruptured and spaced farther apart, potentially due to significant deformation during collagen formation. Additionally, samples with lower concentrations (e.g., 0.5% as shown in the left column of Figure 3-6) seldom exhibit a

distinct porous structure, and the network is disrupted in most areas. Consequently, accurate pore size measurements for above groups of samples were challenging to obtain.

In samples prepared at freezing temperatures of -20°C and -80°C, a distinctive porous structure is evident. Therefore, quantitative analysis was technically achievable for these samples. Porosity and pore size distribution are commonly reported to elucidate the behavior of porous scaffolds. As described in Chapter 2, an algorithm was employed to measure pore size distribution using SEM images via the "Particle Analysis" feature in ImageJ. This feature enables the measurement of scaffolds with pores of various shapes and sizes. It can detect the number of pores, each pore area, perimeter, and spatial disposition within the frame. Additionally, it provides statistical data such as average pore size and porosity. One notable advantage of this algorithm is its independency from the shape, size, and orientation of the pores. Furthermore, it enables the measurement of each individual pore's size, reducing errors compared to manual methods, particularly in analyzing finer microstructures and irregularly shaped pores. Moreover, the algorithm facilitates the estimation of scaffold porosity, defined as the ratio of pore area (black background) to the total area of the frame [95].

Diagrams in Figure 3-7 to Figure 3-10 illustrate the distribution of pores across different sizes. Histograms in part (a) of the figures represent the range of pore areas (sizes) versus the frequency of pores analyzed within each range. Meanwhile, pie chart diagrams in part (b) display the percentage of the scaffold's structure occupied by different pore size ranges, providing a comprehensive view of the pore distribution within the scaffold. In these diagrams, pore size is reported as "pore area", as it is independent of the shape, size, and orientation of the pores. Assuming circular pores, we can estimate pore diameter for better insight. Pores observed at -20°C tend to have nearly round shapes, whereas those at -80°C appear more like flat ellipses than circular

pores. Mean pore area is also derived from measurements obtained in ImageJ. By comparing observations from the figures with quantitative results, the effects of parameter variations on the microstructures are justified.

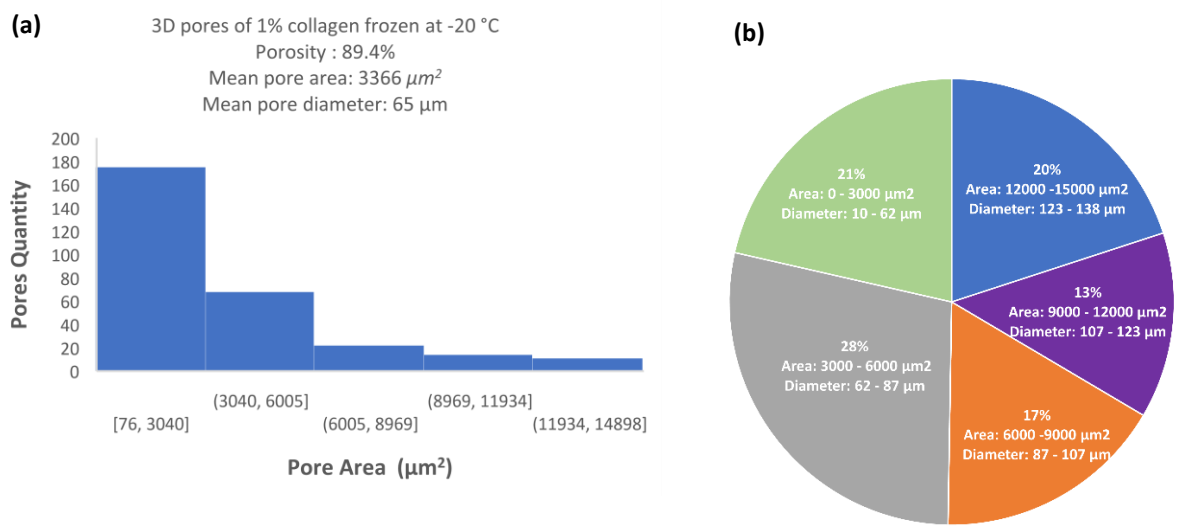


*Figure 3-7: Pore size distribution of 3D 1% sponge collagen frozen at -20 °C. (a) Frequency of pore area ranges and (b) Pie chart showing the shares of pores with different size ranges in the scaffold.*

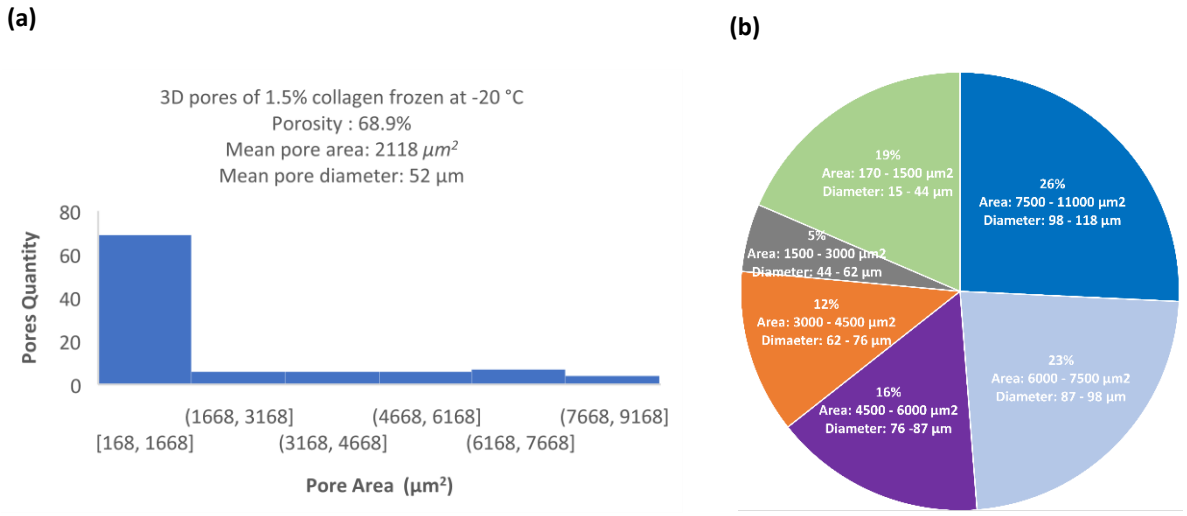


*Figure 3-8: Pore size distribution of 3D 1.5% sponge collagen frozen at -20 °C. (a) Frequency of pore area ranges and (b) Pie chart showing the shares of pores with different size ranges in the scaffold.*

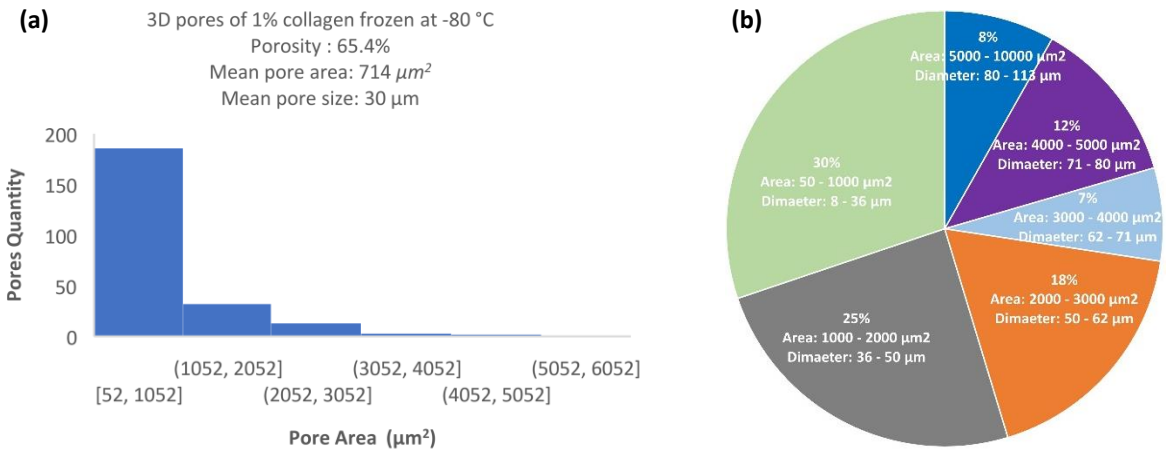


*Figure 3-9: Pore size distribution of 3D 1% sponge collagen frozen at -80 °C. (a) Frequency of pore area ranges and (b) Pie chart showing the shares of pores with different size ranges in the scaffold.*

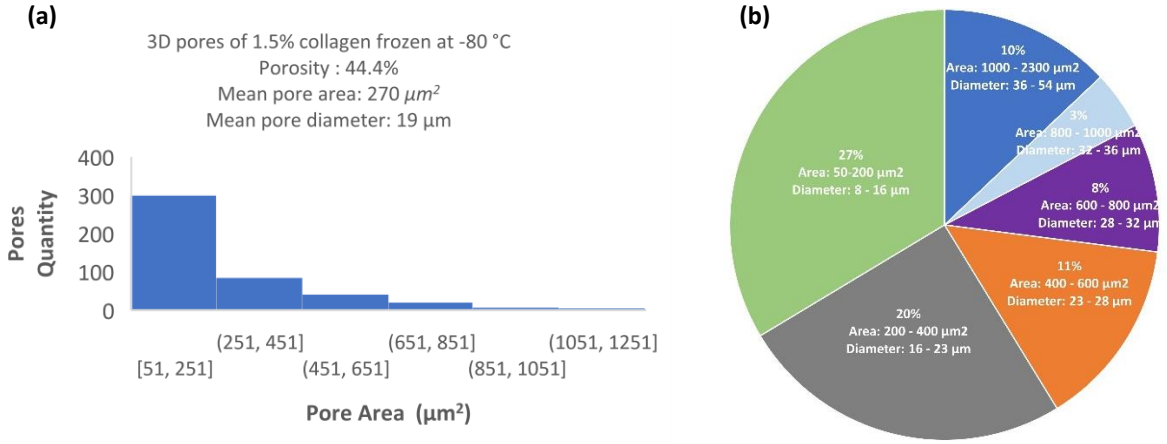


*Figure 3-10: Pore size distribution of 3D 1.5% sponge collagen frozen at -80 °C. (a) Frequency of pore area ranges and (b) Pie chart showing the shares of pores with different size ranges in scaffold.*

Porosity, or void fraction, quantifies the empty spaces within a material and is expressed as a fraction of the volume of voids over the total volume, typically ranging between 0 and 1 or as a percentage between 0% and 100%. In the context of this study, porosity can be estimated as the percentage of the area occupied by black pixels to the total area. Specifically, the porosity of the specimen, representing the ratio of empty spaces in pores to those captured by collagen fibrils, is determined based on the area of black pixels relative to the entire frame of the SEM image.

Table 3-2 provides a summary of pore analysis results. A closer examination of the diagrams confirms the visual inspections of the SEM samples. Higher porosity and larger pore size are achieved in samples prepared at -20°C with a 1% collagen concentration. Conversely, samples with higher collagen concentration and lower freezing temperatures exhibit lower porosity and smaller pore sizes as reported elsewhere [36] [45]. Although the mean pore size may not vary significantly among samples, the distribution of pore sizes reveals notable differences. For instance, in samples prepared at -20°C with a 1% collagen concentration, the mean pore size is 62 µm. However, 49% of pores are larger than 87 µm, and 25% of pores are larger than 100 µm and as shown, the mean pore size of the 80% of the structure is 114 µm.

*Table 3-2: The summary of pore analysis results for 1% and 1.5% 3D sponge collagen at -20 and -80 freezing temperatures*

| | **Freezing Temperature (°C)** | | | | | | | |
|---|---|---|---|---|---|---|---|---|
| | **-20 (°C)** | | | | **-80 (°C)** | | | |
| **Concentration** | **Porosity** | **Mean pore area** | **Mean pore Diameter** | **Min pore size of 80% of structure** | **Porosity** | **Mean pore area** | **Mean pore Diameter** | **Min pore size of 80% of structure** |
| (w/v) | % | ($\mu m^2$) | (µm) | (µm) | % | ($\mu m^2$) | (µm) | (µm) |
| **1%** | 89.4 | 3366 | 65 | 114 | 65.4 | 714 | 30 | 73 |
| **1.5%** | 68.9 | 2118 | 52 | 88 | 44.4 | 270 | 19 | 34 |

This algorithm enables detailed quantitative analysis of collagen scaffolds, facilitating the evaluation of scaffold suitability for specific applications. By assessing pore size distribution, measured using the algorithm, it becomes possible to identify optimal parameters for scaffold

manufacturing processes. This information may prove invaluable in understanding scaffold behavior when cultured with various cell types [37].

As discussed earlier, an increase in collagen concentration tends to result in finer pores. The increase in collagen concentration led to a rise in Young's modulus, likely due to the formation of a more compact collagen matrix [45]. Additionally, microstructure refinement is notable at lower freezing temperatures. Typically, a low temperature results in the rapid formation of dense, small ice crystals and a high temperature results in the slow formation of sparse, large ice crystals [38] [45] [54].

The irregular distribution of internal pores, characterized by varying sizes and directions of growth, arises from the formation of ice crystals during freezing due to heat transfer mechanisms within the dispersed material. As the ice front moves within the dispersion, it does not follow a linear path; instead, multiple ice fronts compete with each other, leading to the formation of pores in random and unpredictable directions. When ice crystal formation occurs at slower rates, typically at higher freezing temperatures, more collagen is forced into the interstices between the crystals, resulting in the formation of thicker walls [14].

The pore size of scaffolds is a critical factor in tissue engineering, influencing cell migration, nutrient diffusion, and waste removal. If pores are too small, cells may struggle to migrate towards the scaffold center, hindering vital processes [45] [54]. Conversely, overly large pores decrease the specific surface area available for cell attachment [54]. In previous research, collagen pore sizes have varied widely based on factors such as concentration, freezing temperature, and matrix materials. Reported values range from 44 to 135 μm [36], 94 to 114 μm [37] 50 to 150 μm [3]. Achieving consistent pore sizes across different studies and laboratories poses a challenge [45].

On the other hand, the relationship between pore size and cell activity is complex and influenced by various factors, including scaffold composition and manipulation conditions. The optimal pore size for tissue engineering remains elusive due to conflicting reports in the literature. Studies suggest a range of mean pore sizes, from 96 to 150 μm while others suggest 300 to 800 μm, for optimal attachment and bone growth in scaffolds [54]. Larger pore sizes, in the range of tens of microns, can accommodate larger cells but lack the precision required for organizing cells into highly aligned structures like blood vessels. Smaller pore sizes, possibly with microchannel assistance, may offer better control and alignment potential for tissue engineering applications [39] [91]. Consequently, careful selection and design of concentration and freezing temperature are crucial in achieving desired properties for the 3D sponge segment of the scaffolds.

### 3.2.2 Structural analysis of 2D collagen film

The other important component of the 2D-3D integrated scaffold is the 2D collagen film. This film may serve as an important biomimetic feature of the final scaffold in the future. Therefore, any manipulation of its properties such as thickness and porosity can have an impact on the final scaffold performance and applications. Accordingly, the results of the 2D collagen films characterization are presented below.

***Effect of casting volume and collagen concentration on the thickness of 2D collagen film***

As outlined in Chapter 2, one adjustable parameter affecting the properties of the final scaffold is the thickness of the 2D collagen film. Both the concentration of the collagen slurry and the volume used for casting the collagen film in the mold influence its final thickness. To investigate these effects, as described in section 2-3, 2D collagen films were fabricated by casting different

concentrations of collagen (0.5%-2%) onto a flat PDMS mold using varying volumes (0.5 – 2 mL) and allowing them to dry at room temperature. Subsequently, the cross-section of each collagen film was measured using optical microscopy.

The effect of these parameters on the collagen film thickness is depicted in the diagram presented in Figure 3-11. The diagram illustrates the measured thickness of the fabricated 2D collagen films using varying amounts and concentrations of collagen slurry per surface area of the PDMS mold. The Y-axis represents the measured thickness, while the X-axis denotes the mold surface-to-volume ratio. This ratio is defined as the surface of the PDMS to the volume of the casting slurry (which eventually evaporates and leaves a dried 2D collagen film on the surface). Utilizing this ratio enables the estimation of the final membrane thickness based on the dimensions of the PDMS mold. Given the mold's dimensions, the Surface-to-Volume ratio can be employed to estimate the casting volume necessary to achieve the desired thickness of the 2D collagen film.

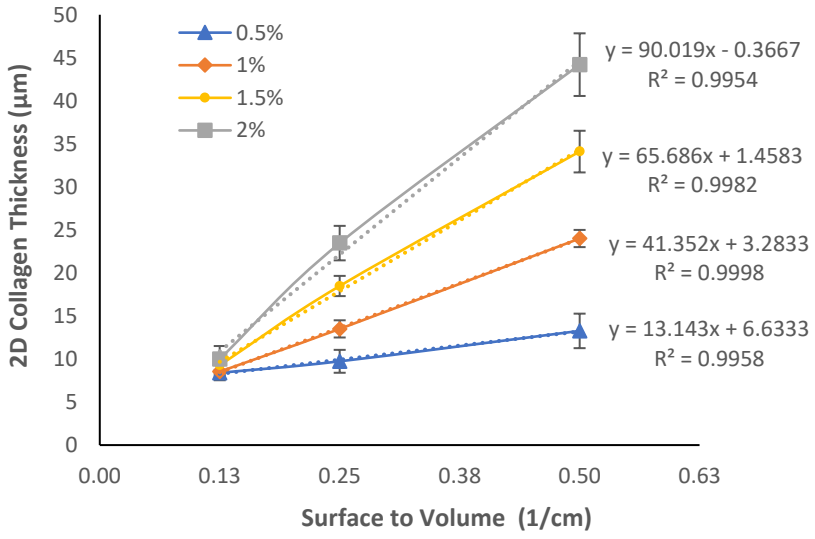


*Figure 3-11: Impact of 2D collagen film slurry volume on the thickness of the 2D collagen films for various collagen concentrations (legend: 0.5%, 1%, 1.5%, and 2%). Linear trendlines are fitted, and the line equations and $R^2$ values are presented, confirming good fits.*

As anticipated, the thickness of the measured specimens increases with the rise in the cast collagen slurry volume in each mold, as more collagen polymers remain on the PDMS mold surface. Likewise, a similar trend is observed with an increase in the concentration of collagen slurry. This is validated by the ascending lines in the diagram depicted in Figure 3-11. Furthermore, the lines representing higher concentrations are more sloped compared to those representing lower concentrations.

This diagram proves valuable in designing the thickness of the 2D collagen film by carefully choosing the collagen concentration and casting volume. The lower concentration, represented by the 0.5% slurry line, exhibits a relatively low slope, indicating a limited range of thickness control with minimal changes, approximately around 10 µm. Conversely, higher concentrations, such as 1%, present a wider range of changes, allowing for the fabrication of thicker 2D collagen films in the range of 9-26 µm. With higher concentrations of 1.5% and 2%, membranes within the range of 10 to 45 µm thickness can be successfully fabricated. Moreover, the relationship between the amount of collagen used per unit area and the resulting film thickness exhibits a linear dependency at all collagen concentrations. Linear trendlines are applied, and the corresponding line equations and $R^2$ values are provided, confirming good fits.

***Effect of freeze drying on 2D collagen film***

During the scaffold fabrication process, the room temperature dried 2D collagen film still undergoes freeze-drying while producing the 3D sponge part of the scaffold. To gain a deeper understanding of the formation of final scaffolds and to interpret the behavior of 2D collagen film during this process, the impact of freeze drying on the 2D collagen film was investigated. Individual 2D collagen samples (1% collagen slurry concentration and 0.25 surface-to-volume

ratio) were fabricated according to the procedure described in Chapter 2. Subsequently, they were freeze dried using the parameters outlined previously at -20°C. Surface morphology and weight variations of the films before and after freeze drying were compared for 3 different samples. Figure 3-12 presents the optical microscopy images of the 2D layer both before and after the freeze-drying process.

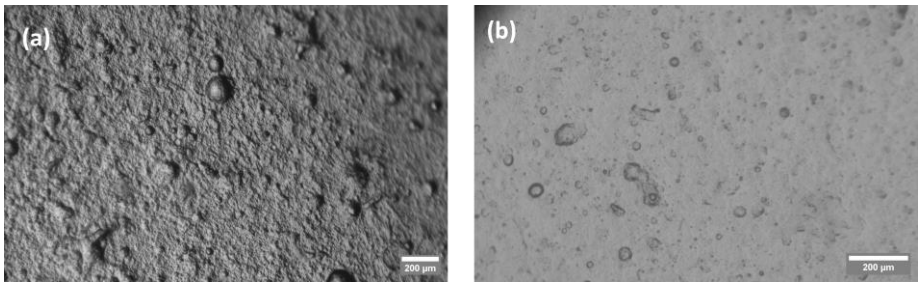


*Figure 3-12: Optical microscopy images of a 1% 2D collagen film layer (a) before and (b) after freeze drying at -20 C.*

As evident from the images in Figure 3-12, the surface of the collagen films becomes smoother after freeze-drying, and prominent points are flattened. As expected, freeze drying extracts the internal water content from the collagen 2D film. Moreover, weight measurements indicated that during freeze drying, the weight of the 2D collagen film decreased by 3% in average. This decrease is attributed to the removal of the remaining water inside the films after air-drying.

### 3.2.3 Structural analysis of 2D-3D integrated scaffolds

In this section, and after understanding the effects of various fabrication factors separately on the 2D collagen film and the 3D collagen sponge, we investigate the effects of these parameters on the integrated 2D-3D scaffolds that contained embedded microchannels. The interactions between

these layers that occur during fabrication process specially freeze drying may significantly influence the characteristics of the individual components.

***Surface morphology of collagen membrane on integrated 2D-3D scaffolds***

For the parametric study of influencing factors, three different thicknesses of collagen membranes were utilized in the fabrication of the integrated scaffold. All samples maintained a consistent 3D collagen slurry concentration of 1%, while the 2D collagen films were created with varying thicknesses of 13 μm, 22 μm, and 34 μm. These thicknesses were achieved by casting 1 mL, 2 mL, and 3 mL of collagen slurry respectively, which were fully dried before applying the 3D collagen slurry on top. Cylindrical plastic holder molds and flat PDMS layers were used.

During the fabrication of 2D-3D scaffolds, the 2D collagen and surrounding 3D sponge collagen undergo changes. These changes occur due to the dissolution of the 2D collagen film upon contact with the 3D sponge collagen slurry, releasing collagen fibrils. Consequently, the remaining portion of the 2D film and the adjacent area of the 3D sponge exhibit different structures. Therefore, we refer to this part as the "2D collagen membrane" hereinafter. Figure 3-13 presents SEM micrographs of the 2D collagen membrane in 2D-3D integrated scaffolds. Panels (a1), (b1) and (c1) show the top view of the surface of 2D-3D scaffolds with 13, 22 and 34 μm 2D collagen films, respectively; while panels (a2), (b2) and (c2) depict the cross section of the scaffolds. In these images, the transparent 2D collagen membrane is positioned in the front, while the 3D sponge is situated behind it. The white protruding boundaries visible on the surface are, in fact, the walls of the 3D sponge collagen that have extended beyond the surface of the 2D membrane. This phenomenon has resulted in the formation of a rough structure on the surface.

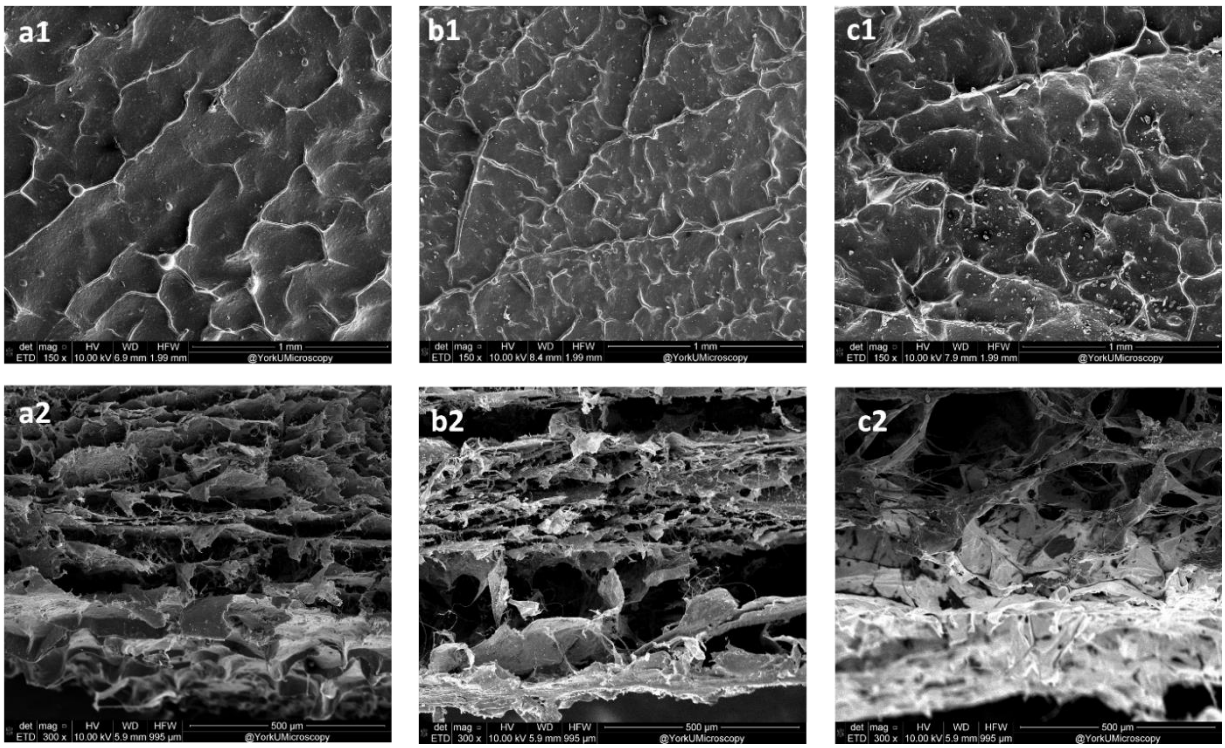


*Figure 3-13: SEM micrographs depicting the impact of 2D collagen film thickness on the morphology and structure of 2D membrane and neighbor sponge 3D in 2D-3D integrated collagen scaffolds. (a1) Surface view and (a2) cross-section view of 13 µm thick collagen 2D film, (b1) Surface view and (b2) cross-section view of 22 µm thick 2D film, and (c1) Surface view and (c2) cross-section view of 34 µm thick collagen 2D film. The 3D layer is visibly attached to the 2D layer, aligned and connected along most parts of the interface area. While some regions show slight separation with fewer bonding points, samples with 13 µm 2D collagen film exhibit notably better bonding.*

In Figure 3-13 (a2, b2, c2), the thickness of the 2D film increases from left to right. A comparison of different 2D film thicknesses reveals that the initial thickness of the membrane results in thicker and coarser walls protruding from the surface of the scaffold, and the density of these walls also increases. This phenomenon can be attributed to the partial dissolution of the air-dried 2D films when exposed to the 3D slurry during the fabrication process, leading to an increase in concentration in the affected area.

During the scaffold fabrication process, the cast 3D collagen slurry partially dissolves the 2D collagen membrane. A thicker initial 2D membrane results in a higher collagen concentration due

to the release of more collagen fibrils. Consequently, similar to the effect observed with a higher concentration of 3D slurry, as discussed earlier in Figure 3-6 regarding thicker collagen pore walls and finer pores, this leads to a greater density of 3D sponge typical branches protruding from the surface. The underlying reason for this phenomenon lies in the formation of a higher quantity of stronger collagen sheets at higher concentrations. These sheets, being both thicker and exerting more force to expand, are more capable of penetrating through the scaffold surface. As a result, they proceed to create more pronounced protrusions. This denser network of protrusion may affect the cells or tissue behavior that would be laid on them in future studies.

In Figure 3-13 (a2, b2, c2), cross sections of the samples are depicted at 300x magnification. The two different areas observed correspond to the 2D membrane and the 3D sponge. The 2D part appears brighter in color and is more compact, positioned lower in the frame. The 3D sponge layer is attached to this 2D layer, aligned with it, and connected in most parts along the interface area. However, in some regions, they are slightly separated, with fewer bonding points. The bonding is notably better in samples with 13 µm thick 2D film, as shown in Figure 3-13 (a2). The cross-section of the 2D part demonstrates consistency, although in some areas, it exhibits partial porosity. This well-established bonding is a result of carefully adjusted parameters, as discussed in Section 3-1.

Examining the protruded walls of 3D sponge from the surface in higher magnifications in Figure 3-14 reveals that the overall surface of the 2D-3D scaffold is uniform, with no visible pores or cracks in the boundaries. Consequently, the surface of the 2D-3D scaffold appears to act as a barrier, consistent with previous reports [82]. Nevertheless, additional investigations are warranted through further experiments to validate these findings for the existence of nano pores on the surface.

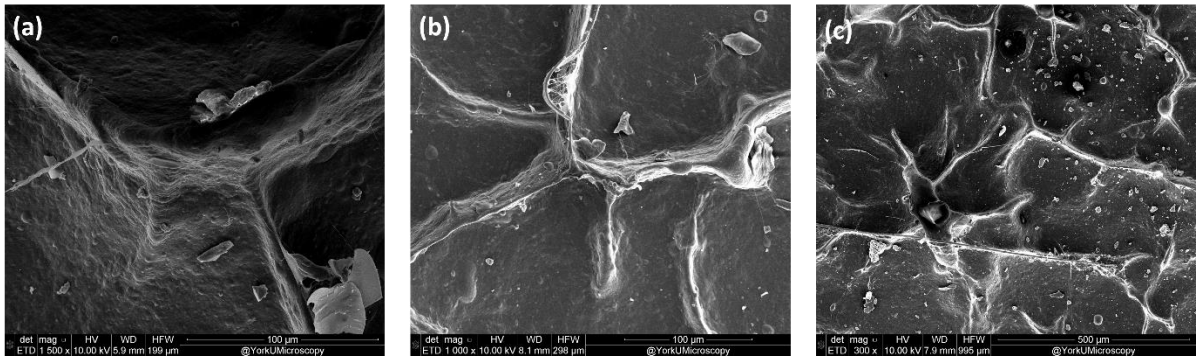


*Figure 3-14: High magnification SEM images depicting the interface of projected 3D sponge walls on 2D membrane surface on 2D-3D integrated scaffolds fabricated from fully dried collagen 2D films. (a) sample with 13 µm, (b) 22 µm, and (c) 34 µm collagen 2D films.*

***Influence of collagen 2D film drying time on 2D-3D scaffold properties***

Preliminary experiments conducted on samples revealed a significant impact of the wetness of the collagen 2D film on the ultimate surface morphology of 2D-3D scaffolds. The degree of wetness, determined by the amount of internal water remaining in the structure, is influenced by the drying time of the initial 2D film and the drying atmosphere. This factor plays a crucial role in shaping the final surface properties of the scaffold. We learned that if the drying time or drying atmosphere does not allow the 2D film to fully dry, the remaining water within the structure influences the freeze-drying process of the 3D sponge layer. Consequently, the exiting water during freeze drying may leave some pores inside the scaffold.

To investigate this effect, various samples of collagen scaffolds with 2D film consisting of 1 mL of 1% collagen were prepared with different drying times, namely 24, 36, and 48 hours. Subsequently, the 3D slurry was cast on top, and the samples were frozen at -20 °C and freeze dried later. The time intervals of 12 hours were chosen based on preliminary tests. All tests were conducted at room temperature. Figure 3-15 illustrates the SEM micrographs depicting the surface morphology and cross-section of 2D-3D integrated scaffolds dried at different temperatures. The

drying times decrease from left to right, with (a) 48 hours (fully dried), (b) 36 hours (partially wet), and (c) 24 hours (still wet).

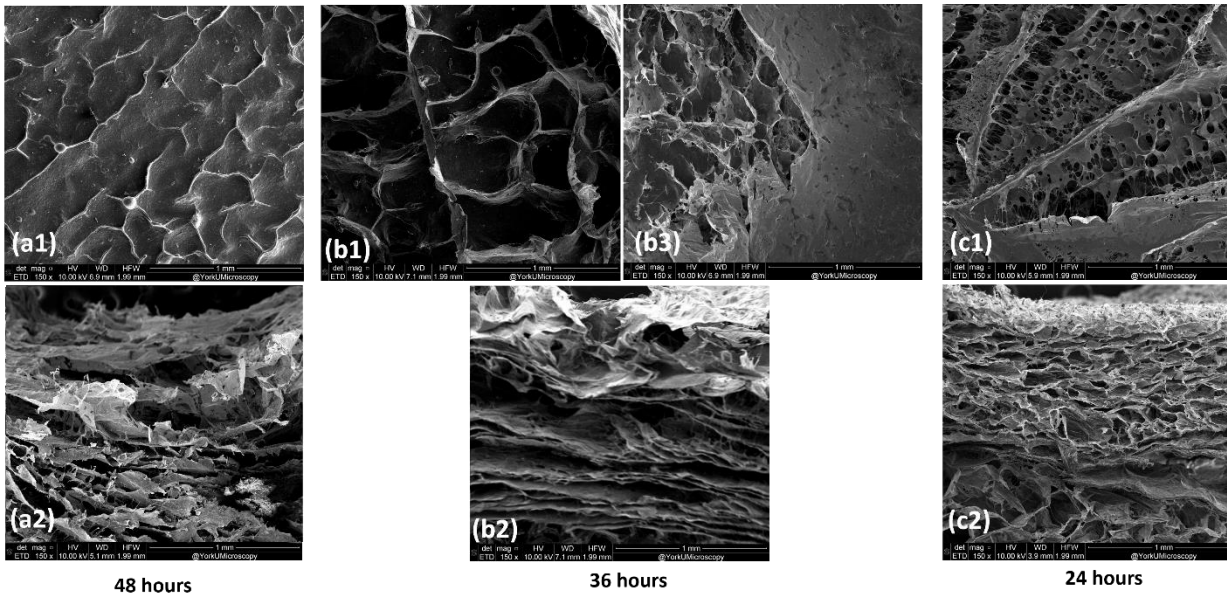


*Figure 3-15: Effect of 2D film drying time (wetness) on surface morphology and cross-section of 2D membrane and neighbor 3D sponge of 2D-3D integrated collagen scaffolds. (a1) Surface morphology and (a2) cross-section of a sample with 2D film dried for 48 hours, (b1) and (b3) surface morphology, and (b2) cross-section of a sample with 2D film dried for 36 hours, and (c1) surface morphology and (c2) cross-section of a sample with 2D film dried for 24 hours.*

In Figure 3-15 (a1), the 2D collagen film was fully dried after the longest drying time, in a way that it could be effortlessly peeled off from the top of the PDMS mold before casting the 3D slurry on top. The typical morphology, as discussed earlier, is evident on the surface, with a fully covered 2D membrane on the 3D sponge part. This aligns with observations reported before [82] and is depicted in Figures 3-13 and 3-14. However, in Fig 3-15 (b1, b2, and b3), a partially wet surface is evident. During SEM microscopy, two different areas spread in all around the sample surface were observed. In some areas, a porous structure similar to 3D sponge collagen discussed in Figure 3-6 is present, alongside the typical morphology of 2D membrane in previous sample fabricated with fully dried 2D film, with extended out wall boundaries from the background, as discussed

before in Figure 3-13. The areas that were dried completely formed the 2D layer covers. The areas that were still wet while casting 3D slurry on top were affected by excess water from the 3D slurry, merging and showcasing a structure similar to the bare 3D collagen sponge. This is why the structure was like 3D sponge's typical morphology, as described before. They also acted as a passage for transferring water out, which caused larger-than-expected pore sizes. Therefore, through controlled drying, it may be possible to manipulate and control the formation and shape of these islands, thus facilitating the realization of specific target designs as described later.

Figure 3-15 (c1, c2) reveals the surface morphology and cross section of 2D-3D integrated collagen scaffolds that underwent a 24-hour drying period. This sample retains a significant amount of water within its structure. During the freeze drying process, water found a pathway to exit, resulting in a 2D membrane with some porous features resembling the 3D sponge collagen. However, these pores appear to be much finer. In Figure 3-15 (c2), the color of the 2D membrane is lighter, and it has a completely porous structure. The pore size in this area is smaller. Moving away from the surface of the scaffold, the pore size in the interface and adjacent 3D sponge also increases. This can be attributed to the local concentration of collagen, which is higher and closer to the 2D membrane. As it gets farther away, the concentration decreases, resulting in larger pore sizes. This phenomenon closely resembles what was observed in the 3D sponge collagen discussed earlier in Figure 3-6. The pore size analysis result is provided in Figure 3-16.

Another noteworthy aspect is the uniform spread of the 2D membrane layer on the 3D sponge in still wet sample (Figure 3-15 (c)). This uniformity may be attributed to a consistent gradient concentration, ensuring a full and uniform bond between the 2D membrane and the 3D sponge.

The thickness of the 2D membrane, whether fully or partially dried in 2D-3D integrated scaffolds, exhibits non-uniformity across various regions. To enhance control over the structure and

thickness of the 2D collagen film, we recommend conducting experiments in a humidity-controlled environment at fixed temperatures. In our study, the drying process was conducted in our laboratory with an ambient temperature of ~21°C; however, the humidity levels must have varied to some extent, and we did not have consistent control over this parameter on a daily basis.

***Other observations and opportunities with 2D-3D integrated scaffolds***

***2D-3D Scaffolds with porous 2D membrane:*** Observations from samples with a reduced drying time of 2D collagen film revealed the potential to fabricate scaffolds with a porous 2D membrane. A collagen scaffold sample was prepared by applying a 2D film consisting of 1 mL of 1% collagen, which was then dried for 24 hours. Following this, a 1% collagen 3D slurry was cast on top of the dried film and subjected to freezing at -20°C and later freeze-dried. As explained earlier, when collagen films have higher water content, the removal of water during freeze-drying creates empty spaces, forming pores in the membrane. The integrated 2D-3D scaffold with a gradient structure is investigated more in detail in Figure 3-16, where the 2D membrane is distinct in the cross-section view (Figure 3-16(a)) as brighter collagen with smaller porous structures. The top view of the scaffold's surface is illustrated in Figure 3-16(b), showcasing evident pore sizes compared to fully dried samples described before in Figure 3-13.

The necessity of having specific pore sizes in the structures of scaffolds for some biological studies cannot be neglected. These pore sizes facilitate the nutrition reaching the surface of the 2D-3D scaffold, as discussed further in the next chapter. These scaffolds can be beneficial for accommodating certain tissues on the surface. A good idea can be adjusting the pore size and transferability of 2D membrane for further biological studies.

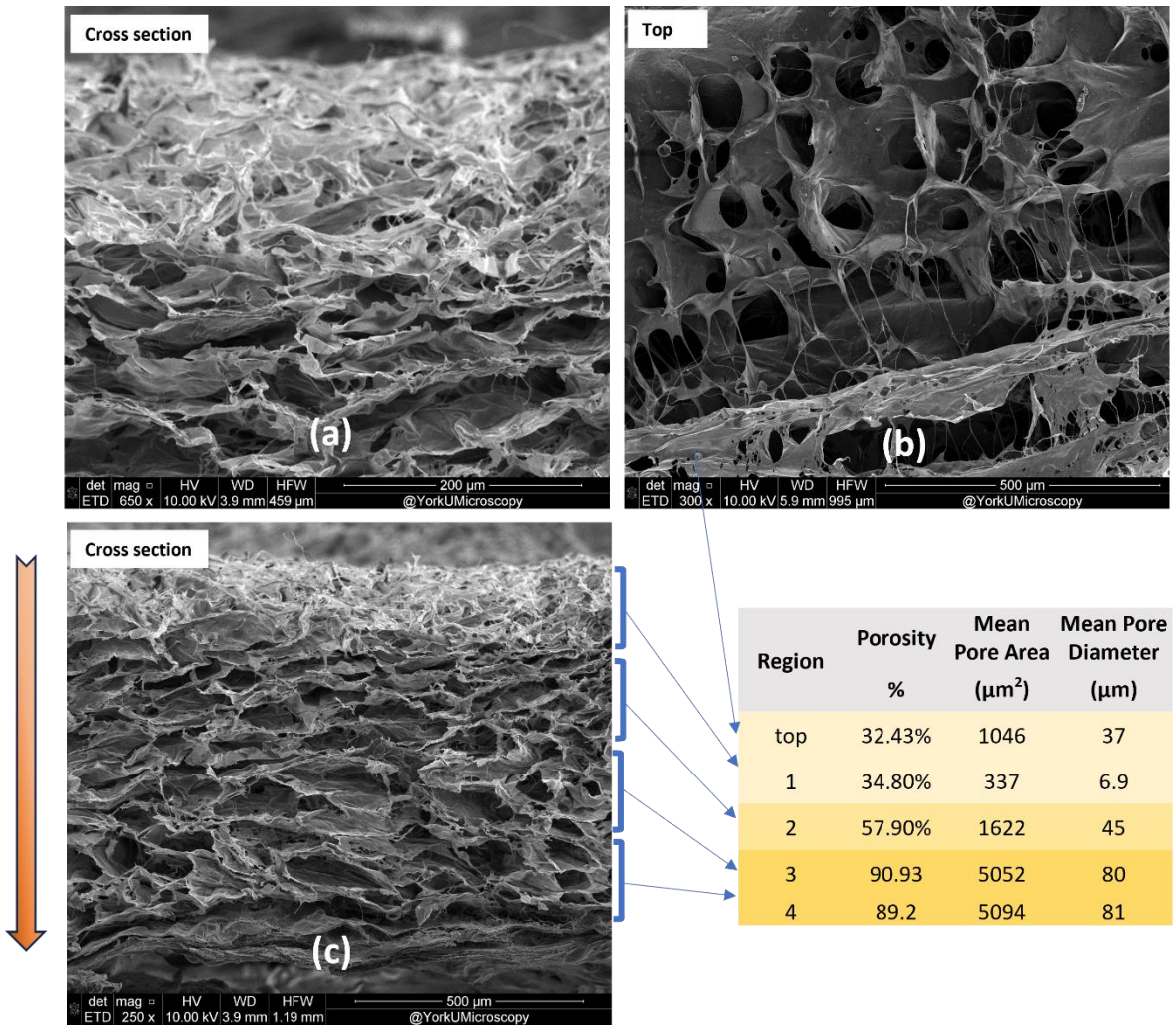


| Region | Porosity % | Mean Pore Area ($\mu m^2$) | Mean Pore Diameter ($\mu m$) |
|---|---|---|---|
| top | 32.43% | 1046 | 37 |
| 1 | 34.80% | 337 | 6.9 |
| 2 | 57.90% | 1622 | 45 |
| 3 | 90.93 | 5052 | 80 |
| 4 | 89.2 | 5094 | 81 |

*Figure 3-16: 2D-3D integrated scaffolds with porous 2D membrane. (a) scaffold cross section, (b) top view of porous 2D membrane and (c) gradient of porous structure in segmented area of scaffolds with smaller size pores on region 1 (2D membrane) to larger pores farther region 2 to 4. The porosity and pore size reported as mean pore area and mean diameter of pores (assuming a round shape pores) in the presented table.*

***2D-3D scaffolds with gradient of pores:*** As depicted more clearly in Figure 3-16(c), with moving away from the 2D-3D interface, the pore sizes increase due to the concentration gradient present during the fabrication process in the collagen slurry. The porosity and pore sizes, including both the area and diameter of pores (assuming a round shape pores), are provided in the table in Figure 3-16. These data were obtained using the technique described in Chapter 2 for pore size analysis.

The cross-section of the scaffold is segmented into different regions that are progressively farther from the surface. Finer pores are observed at the topmost segment, including the 2D membrane region (1), resulting in lower porosity. As one moves away from the surface, towards region (2) and (3), both pore size and porosity increase, eventually reaching a balanced size at region (4). This behavior can be attributed to the concentration gradient that arises in the 3D collagen slurry during fabrication, due to the partial dissolution of the 2D film. This leads to smaller pore sizes in areas with higher collagen slurry concentration and larger pore sizes in regions with lower collagen slurry concentration. This feature may become advantageous or disadvantageous, particularly when working with cells of varying sizes and aimed application of the scaffold. As previously mentioned, distinct cell types may exhibit preferences for different pore sizes, emphasizing the importance of optimizing these parameters for specific applications. Therefore, single scaffold with heterogenous pore size may have a probable application to be explored [36].

***Scaffold stability reinforcement:*** Another critical aspect specially for handling and functionality for cell culture studies is the stability of the scaffolds. Collagen scaffolds that solely consist of the sponge porous part (3D part) have been studied for cell culture applications, however, they exhibited mechanical weakness and instability, requiring reinforcement for successful cell culture studies [34]. One of the advantages of our fabrication approach is the enhancement of scaffold stability through the use of the integrated 2D-3D system. The strength of collagen 2D film is higher than that of 3D sponge collagen, making a composite integrated scaffold consisting of two suitable components for cell compatibility. This will be further discussed in section 4.3. Our design addresses the drawback of not having surface pores on the scaffold, which becomes particularly significant when scaffolds are exposed to culture media.

***Versatility in scaffold fabrication: Porous and nonporous zones on a scaffold through controlled drying:*** One advantageous aspect of this approach is the capability to create scaffolds with distinct regions featuring pores and others without on selected areas. By applying varying temperatures to different parts of the scaffold, specific zones can be dried earlier than others. For instance, heating a particular area accelerates drying, creating a gradient on the scaffold surface. Figure 3-17 illustrates a sample with a section dried while others remain wet. This results in a porous 2D membrane on the still wet area, while the dried portion remains nonporous, acting as a barrier.

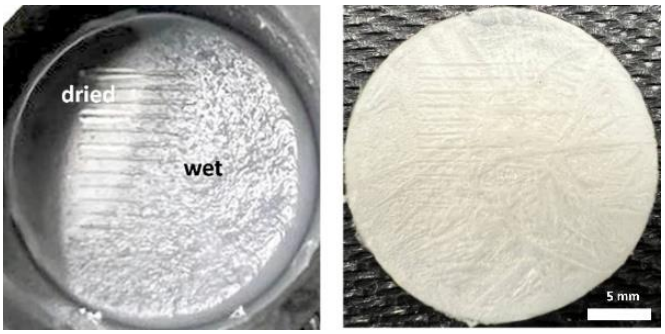


*Figure 3-17: Porous and nonporous zones through controlled drying on a sample with a part heated more on a hot plate.*

## 3.3 Replicating Microchannels in 2D-3D Scaffolds

As outlined in Chapter 1, microchannels play a crucial role in enhancing the functionality of scaffolds. They can facilitate the transfer of oxygen and nutrients while removing waste from the designated area. Additionally, microchannels can promote the controlled and aligned growth of cells, fostering a more organized and efficient cellular environment. Hence, our findings of the parametric study on influential factors on 2D-3D collagen scaffolds with embedded microchannels are detailed in this section. Various influential factors were introduced in Table 2-2 in Chapter 2.

The effects of factors such as 2D film slurry concentration, 2D film slurry casting volume, 3D slurry concentration, and freezing temperature on the microchannel dimensions (width and depth) of the integrated 2D-3D scaffolds were measured with optical microscopy and profilometry. The overall morphology and structure of the scaffolds was assessed via the microscopy or visual inspection. Each factor's impact on the scaffold was examined individually by maintaining all other variables constant while altering the target parameter. This approach allowed for an investigation into the effects of each changing parameter on the final characteristics of the scaffold. The results

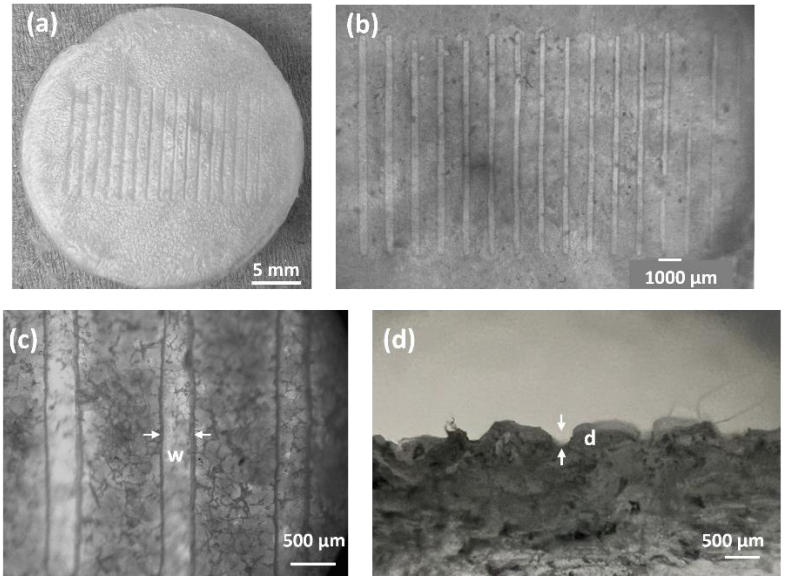


*Figure 3-18: Microchannels fabricated on a collagen scaffold produced with 1% 2D film and 3D sponge collagen slurry concentrations. (a) Disk-shaped integrated 2D-3D scaffold, (b) Optical microscopy image of the overall scaffold surface showing full integration of 2D film and 3D sponge components, (c) Top-view optical microscopy of microchannels (5x magnification) indicating the width (w) of a microchannel, and (d) Cross-section of a cut sample with wire saw marking the depth (d) of a microchannel. The cross section of the microchannels is curvy. It has been reported before that high curvature is favorable for formation of functional multicellular structures and aligned tissues [53]*

offer valuable insights for fabricating scaffolds with tailored microchannels. For instance, Figure 3-18 shows different images of the scaffold with neatly fabricated microchannels produced with 1% 2D film and 3D sponge concentrations freeze dried at -20 °C.

### 3.3.1 Effect of collagen 2D film concentration on microchannels

The effects of the concentration of the 2D collagen film on the microchannels were examined. Various concentrations of collagen slurries, namely 0.5%, 1%, and 1.5%, were used to cast 1 mL of 2D films prepared and dried completely in air. Then 2 mL of 3D collagen slurry was cast on top and then samples were subjected to freezing at -20 °C and further freeze drying. The results revealed that, in the case of low concentrations like 0.5%, the bonding between 2D membrane and 3D sponge is weak, resulting in a fragile physical attachment. During the removal of samples from the PDMS mold, some parts of the 2D membrane stick to the mold, leading to detachment between 2D membrane and 3D sponge. Consequently, the remaining 2D membrane on the scaffold is fragmented, resembling a loosely attached cover layer on the 3D sponge surface, as illustrated in Figure 3-19. This detachment issue persists across different casting volumes of 2D film (1 mL, 2 mL, and 3 mL), hence, microchannels are not integrated with 3D sponge. In essence, in lower concentrations like 0.5% of 2D collagen film slurry proves a weaker bonding between 2D film and 3D sponge, therefore facilitating detachment of the final scaffold from PDMS should be taken into account.

On the contrary, higher concentrations of 2D, such as 1% and above (1.5%, 2%), can form a robust 2D film that is well-bonded to the underlying 3D sponge as shown in Figure 3-18 for 1% 2D film. However, at a concentration higher than 1%, the jelly-like high viscosity of the slurry can result in uneven spreading during 2D film fabrication on the PDMS mold surface. Consequently, the final scaffold exhibits an uneven thickness and a brittle, nail-like layer that isolates the 3D sponge completely from the surroundings. This uneven layer can impact the overall properties of the 2D-3D scaffold. Therefore, the optimal concentration for 2D film, encompassing all desired characteristics, may be around 1% collagen slurry to obtain proper microchannels.

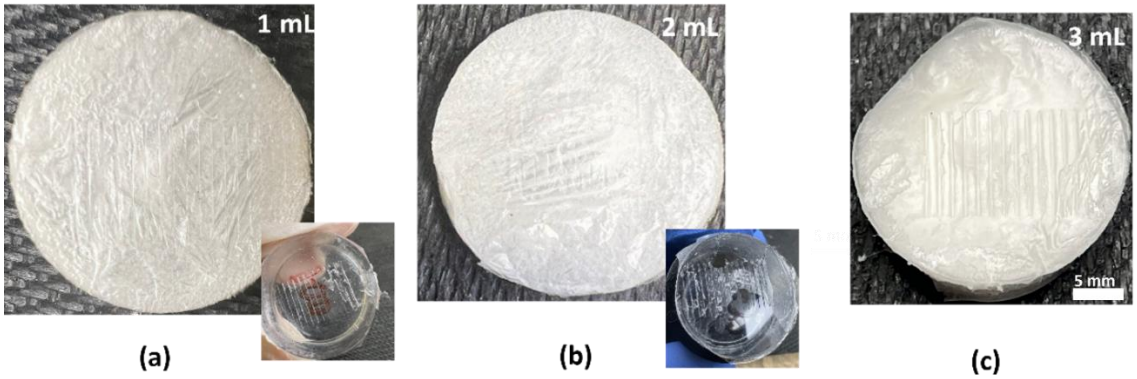


*Figure 3-19: Detached 2D membrane from the scaffold surface of 0.5% 2D film collagen slurry with casting volumes of (a) 1 mL, (b) 2 mL, and (c) 3 mL. The 2D membrane is detached from the 3D sponge in all casting volumes, indicating a weak bond between 2D membrane and 3D components at lower film concentrations.*

### 3.3.2 Effect of freezing temperature on microchannels

The influence of freezing temperature on the widths of microchannels in 2D-3D scaffolds with 10 µm, 19 µm, and 27 µm thick 2D collagen films is depicted in Figure 3-20. Both the 2D film and 3D sponge collagen concentrations were maintained at 1%, and samples were frozen at varying temperatures ranging -10 °C, -20 °C, -40 °C and -80 °C and freeze dried further. As described in Chapter 2, microchannels with widths ranging from 10 µm to 200 µm and a depth of 150 µm were designed, transferred to PDMS, and fabricated within the 2D-3D collagen scaffolds. The actual measured widths of the microchannels are plotted against the designed values to evaluate the precision of our fabrication process in achieving desired-width microchannels. Each measurement point is derived from the results of three distinct samples and various locations within the microchannel, as detailed in Chapter 2. Respective standard deviation of mean measured values for each channel at 3 different samples accompany each point, providing a comprehensive representation of the variability in the measurements.

As illustrated in Figure 3-20(a), freezing at -20 °C with 2D collagen film thickness of 13 µm, yielded the closest width to the design value. Specifically, for frozen samples at -10 °C and -80°C, the measured widths were comparable, while the microchannels frozen at -40 °C exhibited significantly larger widths. These variations can be attributed to the mechanisms of formation, deformation, and size changes in structures during fabrication. Understanding these measurements is crucial for informing the design and fabrication processes of microchannels for scaffolds. Lowering the freezing temperature resulted in decreased accuracy in fabricating the channels.

Analyzing Figure 3-15(b), which depicts the impact of freezing temperature on microchannel widths in 2D-3D scaffolds with a 22 µm thickness, reveals significant deviations in the alignment of designed and achieved channels. Specifically, the accuracy of microchannels frozen at -20 °C has decreased compared to what was achieved with scaffolds featuring 13 µm film thicknesses. Conversely, at other temperatures, the width has expanded.

The increased thickness of the 2D membrane resulted in a higher concentration of collagen slurry near it. Deformation during fabrication contributed to the irregularity or widening of the channels.

Achieving dimensions below 200 µm is not feasible; however, a consistent channel width in the range of 500 to 700 µm is typical. Importantly, this width range remained independent of the original microchannel design on PDMS molds.

This trend is similarly observed in scaffolds with a thickness of 34 µm, as depicted in Figure 3-20(c). The channels exhibit widening, and the fabrication of narrower channels is constrained.

(a) 2D Collagen Film Thickness: 13 µm

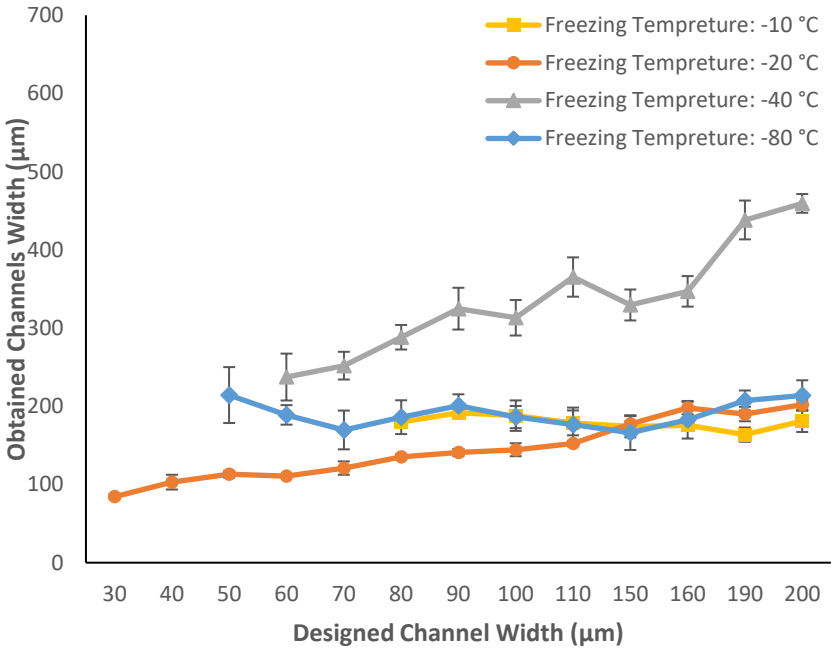


(b) 2D Collagen Film Thickness: 22 µm

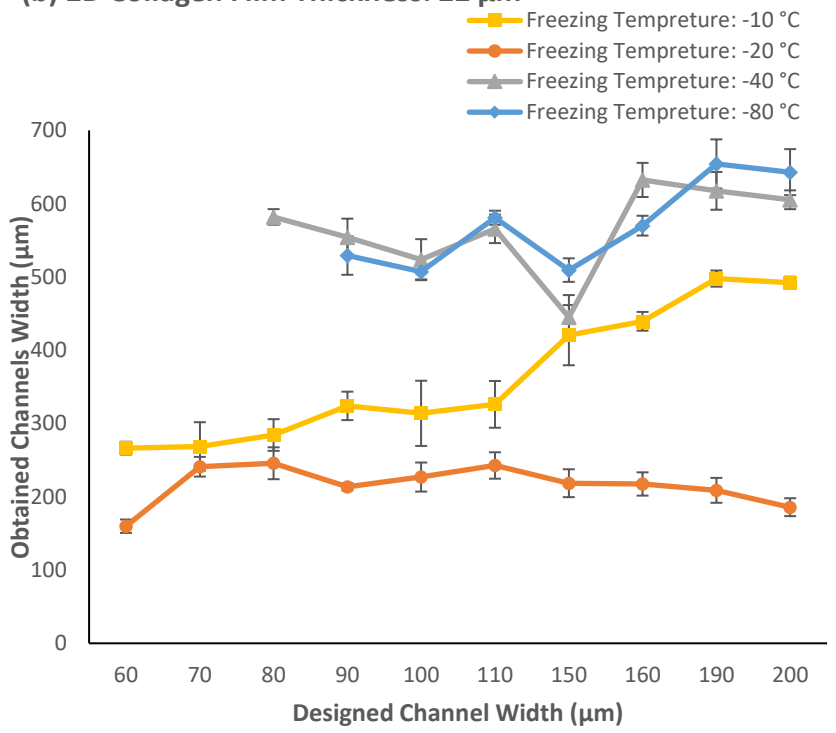

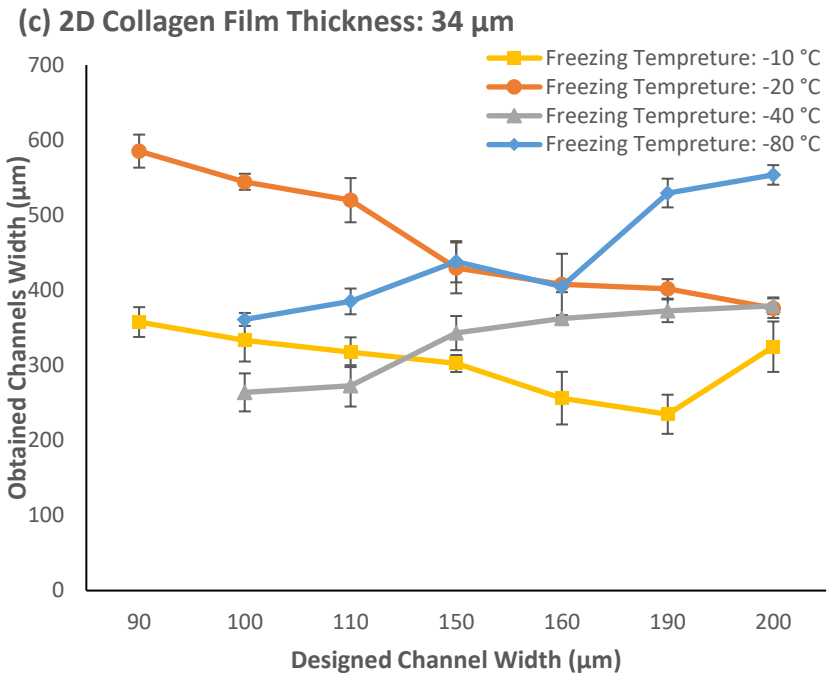


*Figure 3-20: Effect of freezing temperature on microchannels widths of 2D-3D scaffolds with (a) 13 µm, (b) 22 µm and (c) 34 µm thick 2D collagen films.*

This phenomenon is consistent, even in samples freeze dried at -20°C. Surprisingly, achieved channels in this temperature tend to broaden for smaller width channel designs. The elevated concentration of collagen slurry during fabrication is deemed responsible for this alteration. Further investigation into the mechanisms of formation is necessary to unveil the reasons behind these observations.

Upon comparing the results, it becomes evident that channels exhibit a tendency to open up at freezing temperatures, such as -10 °C and -40 °C. The values closest to the desired channels are achieved when employing a freezing temperature of -20 °C with a lower thickness of the collagen 2D film. It is worth to notice that not only the closest range of widths to the design was attained, but also the narrowest channels were fabricated. Therefore, this temperature, in conjunction with the specified initial 2D film thickness, is recommended for future microchannel designs.

These results can be elucidated by considering the influence of fabrication parameters on collagen pore sizes and the impact of local concentration near the interface of 2D film and 3D sponge. The thickness of the 2D film directly influences the density of released collagen fibrils resulting from its partial dissolution. Consequently, thicker 2D films harbor a greater abundance of collagen fibrils, thereby leading to a higher concentration. As previously discussed, this phenomenon significantly affects the formation of collagen sheets and pores, potentially resulting in rapid or more pronounced changes akin to those observed with higher concentrations. Further detailed investigations are warranted to elucidate these effects.

The observed additional deformation in microchannels of samples frozen at -40°C can be attributed to critical deformations resulting from the appearance of small crack-like solidification lines near the surface of the 2D-3D (similar to surface cracks depicted on Figure 3-4(b) and Figure 3-5(c). This arrangement of pores has been already reported while quenching [37]. This phenomenon is particularly noteworthy, given that the channel thickness falls within the range of 250 to 500 μm across all initial 2D film thicknesses (13, 22, and 34 μm).

Additionally, the impact of the collagen 2D film thickness and freezing temperature on microchannel depth in 2D-3D integrated scaffolds is illustrated in Figure 3-21. These results are derived from optical profilometry, as detailed in Chapter 2. It is evident that the channels achieve their closest design depth (150 μm) at -20 °C, whereas other freezing temperatures resulted in depths less than the designed values. Notably, scaffolds with thicker 2D collagen film exhibited shallower depths, with a discernible tendency for lower depth as the thickness of the initial 2D collagen film increases. This observation may be attributed to the thicker 2D collagen film occupying more space, thereby limiting the depth of the designed channels.

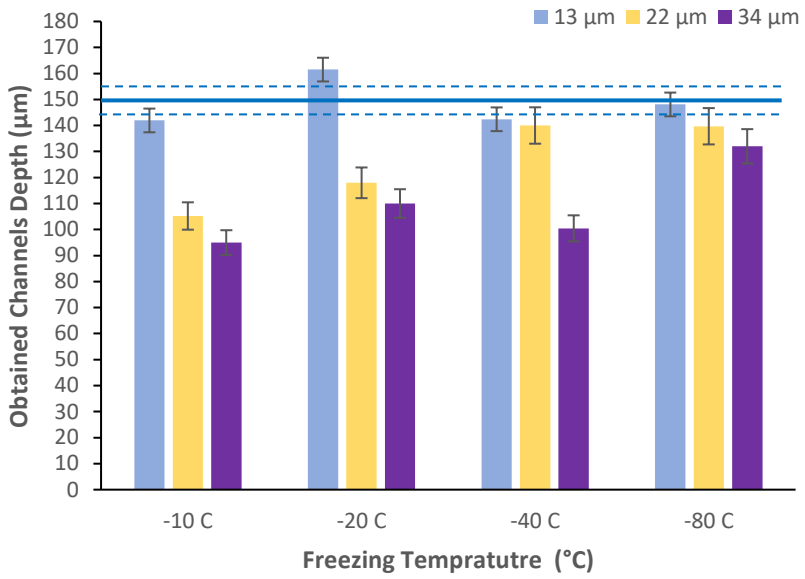


*Figure 3-21: Effect of collagen 2D film thickness (legend) and freezing temperature on microchannels depth of 2D-3D integrated scaffolds measured by optical profilometry. Blue lines show the molds depths (150 µm ± 5).*

Understanding the abovementioned properties can inform the design of various scaffolds for diverse applications. The investigation provides valuable insights for adjusting the range of achievable microchannels in the final scaffold.

### 3.3.3 Effect of 2D collagen film initial thickness on microchannels

The results of previous section can be examined from alternative perspectives. The impact of the thickness of the collagen 2D film on the final microchannel width can be evaluated for each freezing temperature independently. Figure 3-22 illustrates the effect of collagen 2D film thickness on microchannel widths in 2D-3D integrated scaffolds frozen at -10 °C, -20°C, -40 °C, and -80 °C freeze dried later. The fabrication procedure is the same as the previous section.

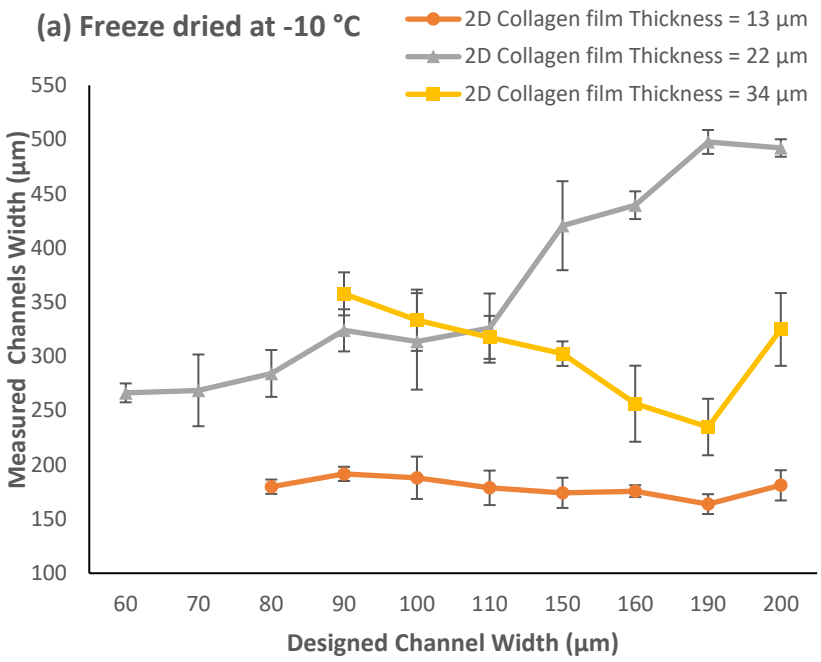
(a) Freeze dried at -10 °C
2D Collagen film Thickness = 13 µm
2D Collagen film Thickness = 22 µm
2D Collagen film Thickness = 34 µm
Measured Channels Width (µm)
550
500
450
400
350
300
250
200
150
100
60
70
80
90
100
110
150
160
190
200
Designed Channel Width (µm)

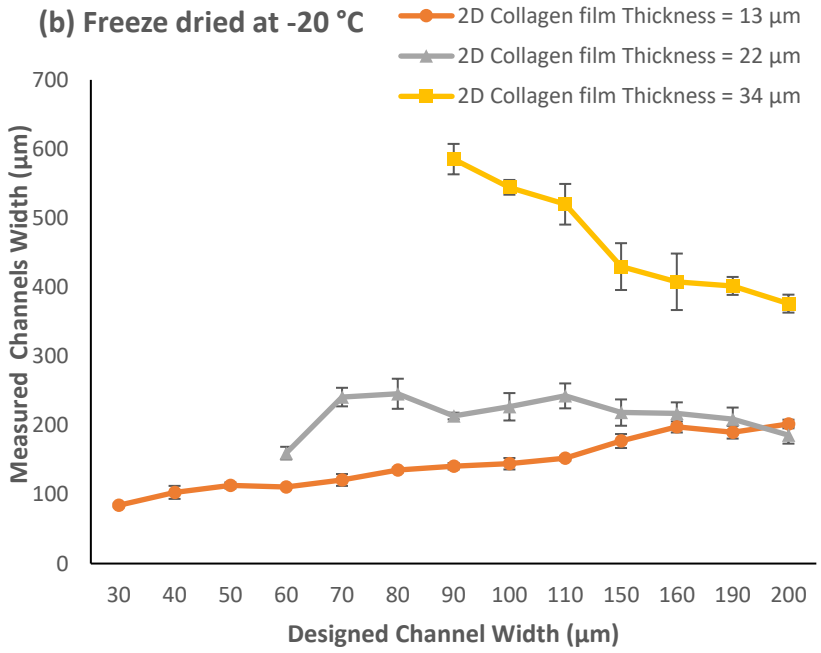
(b) Freeze dried at -20 °C
2D Collagen film Thickness = 13 µm
2D Collagen film Thickness = 22 µm
2D Collagen film Thickness = 34 µm
Measured Channels Width (µm)
700
600
500
400
300
200
100
0
30
40
50
60
70
80
90
100
110
150
160
190
200
Designed Channel Width (µm)

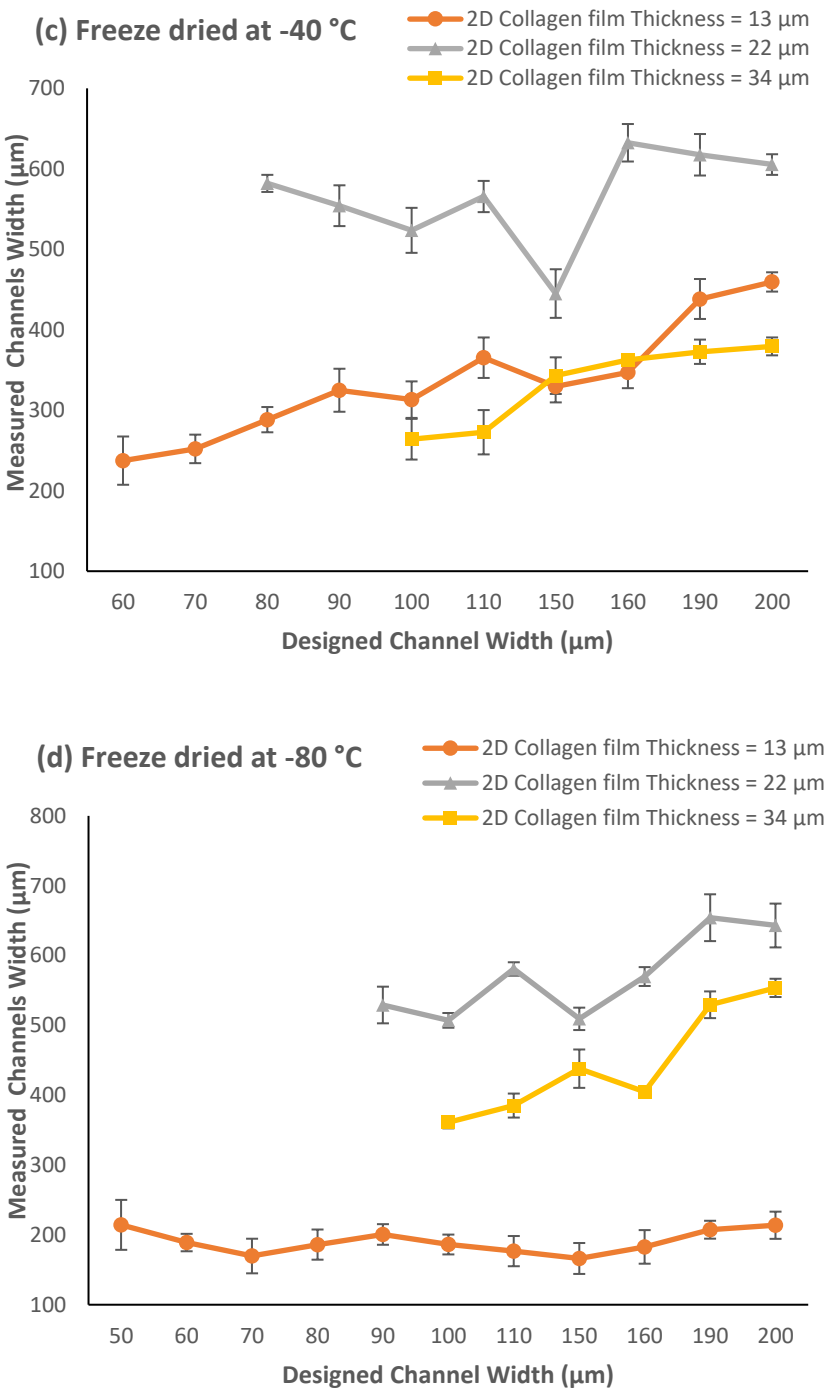


*Figure 3-22: Effect of collagen 2D film on 2D-3D integrated scaffolds at (a) -10 °C, (b) -20°C, (c) -40 °C and (d) -80°C freezing temperature.*

Upon comparing the results, it is apparent that microchannels tend to widen with thicker collagen 2D films, particularly accentuated at lower temperatures. In simpler terms, channels exhibit greater

width at lower freeze-drying temperatures. The closest match to the design value is achieved with narrower collagen 2D films.

These results can be explained with the effect of fabrication parameters on the pore sizes of the collagen and the effect of local concentration near the 2D-3D interface as discussed in the previous section. Those properties can be used in designing various scaffolds for different applications.

### 3.3.4 Effect of 3D collagen slurry concentration on the microchannels

The concentration of collagen in the 3D sponge also influences the properties of the final 2D-3D integrated scaffolds. To examine the impact of the 3D sponge collagen component, the thickness and concentration of the collagen 2D film was kept constant at 13 µm and 1% respectively across all samples, while varying concentrations of the 3D sponge collagen were introduced to assess the effect. The results of the visual assessment of the scaffolds are presented in Figure 3-23, where different concentrations of 0.5%, 1%, and 1.5% collagen slurry were employed in the fabrication of the 2D-3D scaffold at a freezing temperature of -20 °C.

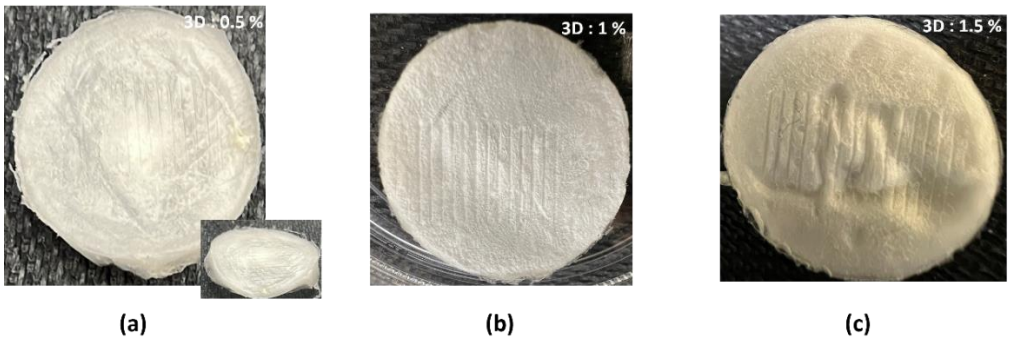


*Figure 3-23:Effect of different 3D collagen concentrations (a) 0.5%, (b) 1% and (c) 1.5 % on final integrated 2D-3D scaffold*

As discussed in Figure 3-6 and further illustrated in Figure 3-23(a), lower concentrations of the slurry (e.g., 0.5%) result in a weak network of collagen sponge. The structure appears lighter and

more delicate compared to other concentrations, leading to a deformed scaffold at this 3D slurry concentration.

In contrast, the structure of 2D-3D integrated scaffolds with 1% collagen slurry for the 3D sponge appears firm and robust. This concentration allows for the fabrication of flat and less deformed scaffolds. Opting for a higher concentration of collagen in the 3D sponge (1.5%) demonstrated increased scaffold strength. However, this concentration proved ineffective in achieving flat and undeformed microchannels, possibly attributed to the jelly-like structure of the 3D sponge component. Despite attempts to spread and gently press the jelly slurry during fabrication, using a 1.5% 3D collagen slurry, it remained challenging to obtain a flat and uniform scaffold. Therefore, the optimal concentration for achieving a flat scaffold appears to be 1% for the 3D collagen component.

## 3.4 Conclusion

In conclusion, this chapter presents a comprehensive analysis of various factors impacting the properties of engineered 2D-3D integrated scaffolds. Through examination of molds, casting methods, concentration selection, and freeze drying parameters, efforts were directed towards addressing the challenge of achieving flat scaffolds. Surprisingly, the primary cause of surface wrinkles was identified as the drying process of the 2D collagen film.

The effect of freezing temperature on 3D sponge collagen micropores demonstrated that lower temperatures resulted in finer pore sizes, contributing to denser scaffolds. Similarly, higher collagen concentrations led to thicker collagen sheets and denser structures, resulting in lower porosity and smaller pore sizes.

Furthermore, the unique morphology of 2D-3D scaffolds was observed, with the transparent 2D collagen membrane positioned in front and the 3D sponge behind it. The protruding boundaries visible on the surface were identified as walls of the 3D sponge collagen extending beyond the 2D membrane. Additionally, controlled drying time or atmosphere for the 2D film influenced the freeze-drying process of the 3D sponge layer, potentially leaving pores on the 2D membrane on the scaffold.

Investigation into replicating microchannels in 2D-3D scaffolds revealed the influence of collagen 2D film concentration and freezing temperature on microchannel formation. Higher thickness of 2D film and lower freezing temperatures resulted in less accuracy in channel fabrication. Notably, freezing at -20°C with a 2D collagen film thickness of 13 μm yielded the closest width to the design value. Microchannels tended to widen with thicker collagen 2D films, particularly at lower temperatures, emphasizing the importance of careful consideration of fabrication parameters.

In summary, thorough attention to fabrication parameters is crucial for achieving desired scaffold properties. These findings offer valuable insights for designing collagen scaffolds tailored to specific applications, highlighting the need for optimization in collagen scaffold fabrication processes.

# 4 Applications of 2D-3D Collagen Scaffolds with Embedded Microchannels

Supported by the qualitative and quantitative learnings of Chapter 3, we were able to fabricate different microchannels with desired designs on the surface of 2D-3D integrated collagen scaffolds. Figure 4-1 shows some examples of these devices which were developed with the optimum recipe of 48 hours air-dried 1% 2D collagen film with 13 µm thickness and 1% 3D collagen sponge frozen at -20 C and freeze dried later.

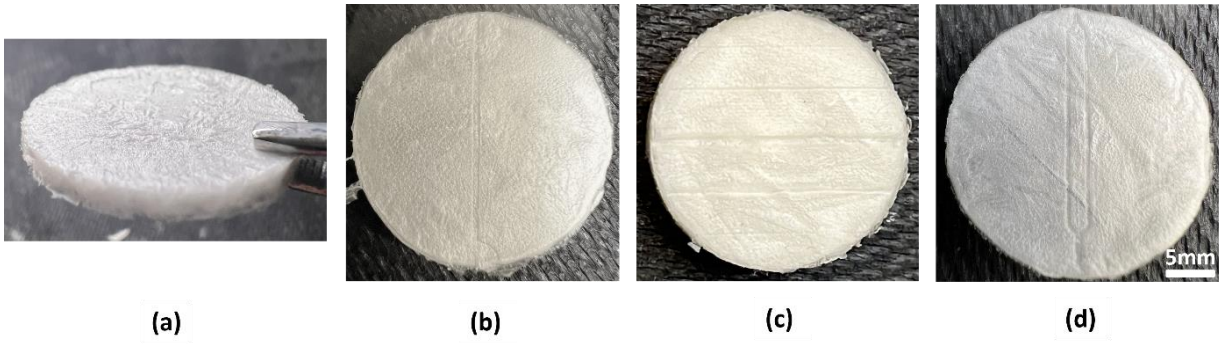


*Figure 4-1: Samples of 2D-3D integrated scaffolds with small features, developed using the optimal recipe of chapter 3 (48 hours air-dried 1% 2D collagen film with 13 µm thickness and 1% 3D collagen sponge frozen at -20 C and freeze dried later). (a) 2D-3D collagen integrated disk shape scaffold with a flat surface. (b) A disk scaffold featuring a single channel with a width of 150 µm on the surface, with an area functioning as a reservoir at one side. (c) Parallel channels with varying widths: 70 µm, 90 µm, 120 µm, 150 µm, and 200 µm. (d) Small-sized branch microchannels each with a width of 120 µm.*

Being able to fabricate the desired channels on the 2D-3D collagen layers supported us in terms of investigating the expansion of these scaffolds to branched channels and multi-layer devices as well as exploring their applications in biological areas as discussed in this chapter. These preliminary results are aligned with objective 1 of the thesis.

### 4.1.1 Integrated 2D-3D scaffolds with branched enclosed channels and flow studies

2D-3D scaffolds with branched enclosed microchannels were fabricated with the method elaborated in chapter 2 similar to a simple vein structure. Briefly, a SolidWorks model was created with a branched structure, featuring widths descending from 1000 µm to 500 µm and a depth of 750 µm (Figure 4-2(a)). This model was used to generate a 3D-printed negative mold, from which a positive PDMS replica was produced following established procedures. The fabrication process for 2D-3D scaffolds then commenced. Initially, 1 mL of 1% collagen slurry was used to cast a 2D collagen film, which was air-dried over the PDMS microchannels for 48 hours. Subsequently, a 3D sponge collagen layer was cast using 2 mL of 1% collagen slurry and applied on top of the 2D collagen film. The scaffold was then freeze dried at -20°C (Figure 4-2(b)). All the collagen fabrication parameters were informed by the research presented in Chapter 3.

Figure 4-2(a,b) depict the fabricated single layer scaffold alongside the SolidWorks design. Each part of the microchannel structure was marked with a letter and then dimensions of different areas were measured using optical microscopy and ImageJ. The measured values are summarized in the table in Figure 4-2(c). Discrepancies between the design widths of channels and those of the obtained scaffold were observed. Upon closer examination of the results, the most significant deviation was noted in the L-designated part. Overall, the scaffold exhibited a mean expansion of approximately ~17%. Consequently, it can be inferred that to achieve scaffold dimensions with the desired channel sizes, one should account for these expansions during fabrication and design the mold with sizes approximately 17% smaller than the expected final scaffold dimensions.

As detailed in Chapter 2, development of enclosed channels involved bonding the above layer consisting of a 2D-3D substrate with branched microchannels to another flat substrate (as

elaborated on Figure 2-8). Bonding was achieved using the contact printing method. The bonded layers were then placed within a PDMS holder and fitted with both an inlet and an outlet connected to tubes (Figure 2-10), facilitating the flow test procedure, described later.

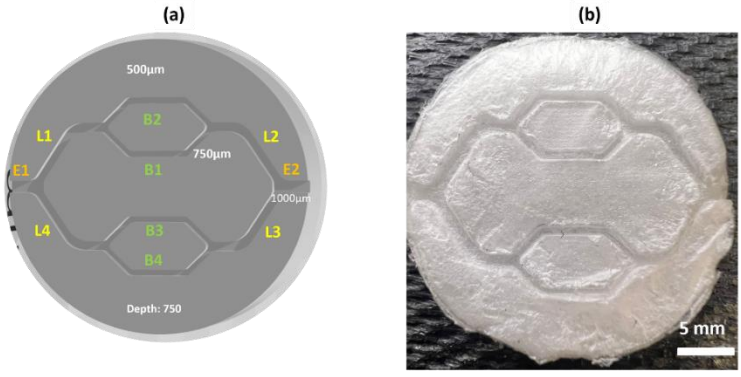


(c)

| Area | Design Width (µm) | Average Width (µm) | STD | % Deformation | Mean Deformation |
|---|---|---|---|---|---|
| E1 | 1000 | 965 | 16 | -3% | 11% |
| E2 | 1000 | 1256 | 26 | 26% | |
| L1 | 750 | 1023 | 63 | 36% | 28% |
| L2 | 750 | 934 | 53 | 24% | |
| L3 | 750 | 1004 | 48 | 34% | |
| L4 | 750 | 891 | 67 | 19% | |
| Br1 | 500 | 484 | 33 | -3% | 11% |
| Br2 | 500 | 653 | 21 | 31% | |
| Br3 | 500 | 502 | 22 | 0% | |
| Br4 | 500 | 572 | 11 | 14% | |

*Figure 4-2: 2D-3D integrated scaffold with a branch structure featuring widths descending from 1000 µm to 500 µm and a depth of 750 µm. (a) SolidWorks model displaying designated channels. (b) Fabricated scaffold obtained from the design. (c) Table summarizing measurements and percentage of deformation in each region.*

Figure 4-3 provides a detailed view of the two-layer scaffold with enclosed branch shape channels. In panel (a), the device with enclosed branch microchannels featuring an entrance and an exit connected to a tube is depicted, fitting snugly within a PDMS holder. Additionally, panel (b) displays cross-sectional images of the scaffold's middle portion, showcasing four microchannels highlighted by red arrows. For a closer examination, panel (c) presents two adjacent microchannels

with a designed width of 500 µm. Moving to panel (d), an image illustrates a microchannel post-transfer of red-colored water from its interior. Finally in panel (e), optical microscopy in the middle of the scaffold reveals the dimensions of the channels, measured as height: 538 ± 12 and width: 770 ± 23.

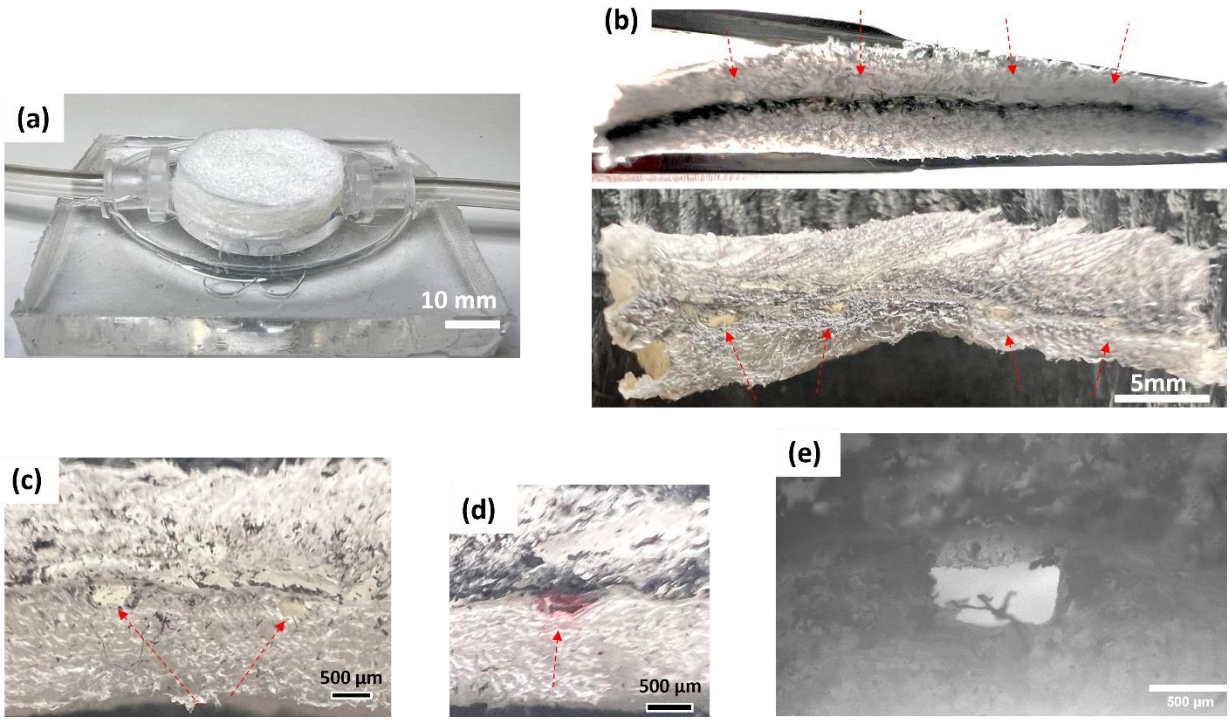


*Figure 4-3: Enclosed 2D-3D integrated scaffold with branch microchannels. (a) The enclosed device with interconnects. (b) A cross section image of the middle of the scaffold including 4 microchannels shown by red arrows* of 2 different samples. *(c) 2 neighbor microchannels with designed widths of 500 µm. (d) An image of a microchannel after the transfer of media. (e) Optical microscopy of microchannel in the middle of the scaffold (height:* 538 ± 12, *width: 770 ± 23)*

The results of the flow study of the above single-layer branched 2D-3D collagen scaffold are presented in this section. A flow test was performed to assess the performance of the collagen scaffold to withstand water flow in its channels. Enclosed scaffold prepared above included microchannels ranging from 1000 to 500 µm that were used to test the scaffold's ability to transfer media. The experiment utilized a dual syringe pump and a device set as a holder for media flow

through the scaffold (Figure 4-3(a)). Dyed water was passed through the microchannel at a flow rate of 50 µL/min for three different samples. The weight of the collected fluid was measured over time, and the volume and flow rate of water penetrating the scaffold was calculated based on the collected weight and density of the water. The volume passed through the scaffold versus time is depicted in Figure 4-4(a) for three different sample devices, and in Figure 4-4(b) as mean and SD of the three tests.

As demonstrated in Figure 4-4(a), the flow behavior of different collagen scaffolds with branched channel design is similar. This validates the viability of the fabrication method in consistently producing devices with comparable fluidic behaviors. Furthermore, the volumetric inflow and outflow rates correspond closely in value. For an inflow rate of 50 µl/min, the calculated averaged outflow rate was 48.8 ± 0.96 µl/min for tests conducted on the three specimens. This close correspondence is attributed to the presence of the less permeable 2D collagen membrane, though which minimal leakage may occur during the flow through the small-sized channels. Moreover, the flow of media through the branch channels with decreasing sizes can lead to enhanced hydraulic resistance and occasional leakage due to raised pressure in the channels. Lastly, fabrication defects like bonding issues and clogs in the channel may lead to flow resistances and leakage. These phenomena can potentially account for the fluctuations observed in the flow rates of different samples in Figure 4-4(a). For future assessments, more precise methods for quantifying flow rates should be employed to accurately determine penetration flow rates.

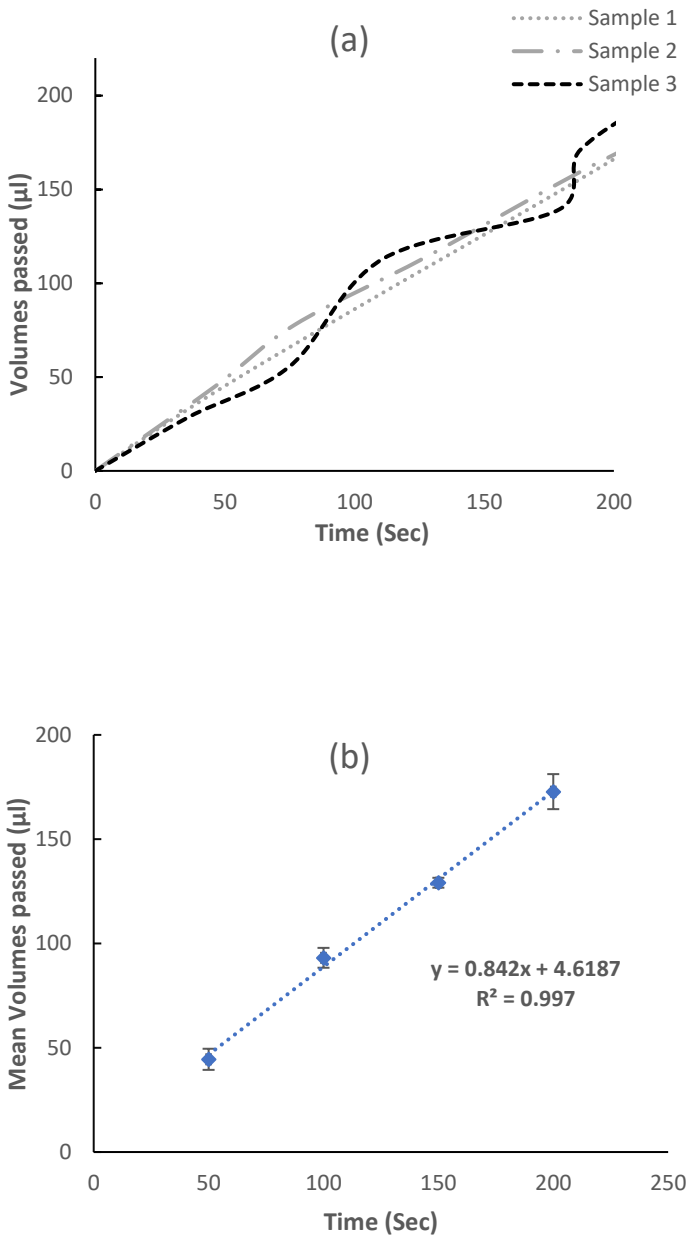


*Figure 4-4: Water volume passed through the branched channels of integrated 2D-3D scaffolds versus time for an inflow rate of 50 µl/min. (a) Three scaffolds tested separately. (b) Mean and SD data of the three scaffolds.*

## 4.2 Fabrication of Integrated 2D-3D Scaffolds with Microchannels in Different Layers

One notable benefit of our approach is its suitability for fabricating collagen scaffolds with multiple layers containing embedded channels at different layers. This may be useful in biological applications such as developing thick tissues with vesicles in the future. For the development of 2D-3D integrated scaffolds with two sets of microchannels at different layers, three distinct substrates were required as described before in section 2.9.2.

Figure 4-5 illustrates a schematic of a 2D-3D integrated scaffold featuring parallel microchannels at different layers. Three schematic models depicting potential applications of this scaffold design are presented. In model (a) on the left, a representation of a blood vessel is depicted, showcasing the distribution of blood through the scaffold across different layers. Here, the 2D membrane is nonporous, preventing the convective transfer of the medium to the 3D sponge parts. In the future, selective nanochannels can be integrated into the 2D membrane, promoting the exchange of specific chemicals between the channel and the 3D sponge region. In model (b) on the right, a model for co-culture studies of cells or for exposing cells to different mediums is showcased, potentially beneficial in cell and drug studies. Within this design, different mediums can flow through each channel, facilitated by the porous 2D membrane enabling media exchange to the 3D sponge structure. Additionally, the intermediate zone between two channels can be exposed to different mediums from the top and bottom directions. Different kind of cells can be cultured inside the channels as shown in panel (c).

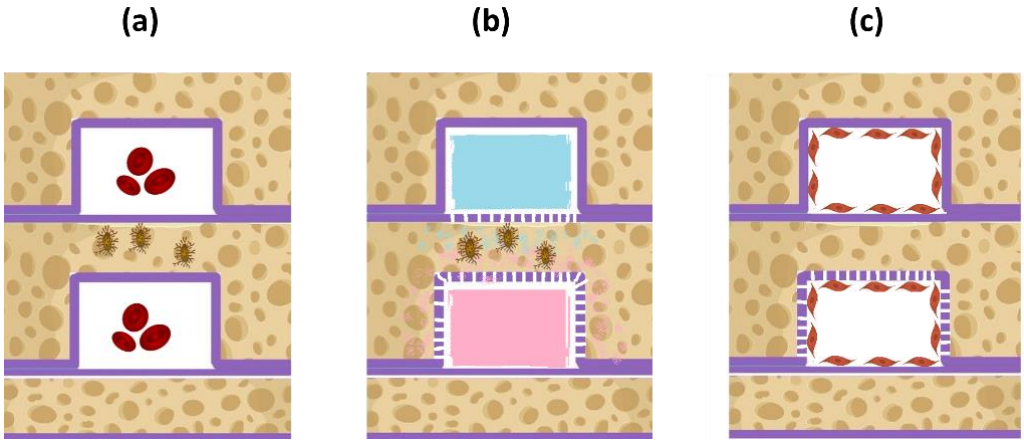


*Figure 4-5: 2D-3D integrated collagen scaffold schematics with parallel microchannels at different layers. (a) A representation of a blood vessel demonstrating the distribution of blood throughout the scaffold across various layers. The 2D membrane can be impermeable, preventing the convective transfer of medium to the 3D sponge sections. (b) A setup for co-culture studies of cells or for exposing cells to different media, potentially advantageous in cell and drug research. In this configuration, different media can flow through each channel, facilitated by the porous nature of the 2D membrane, enabling media exchange to occur within the 3D sponge structure. The intermediate zone between two channels can be exposed to different media from both the top and bottom directions. (c) Culturing cells inside the channels with porous and non-porous 2D membranes*

A real fabricated sample featuring two parallel microchannels at the center, spanning two different layers of the scaffold, has been successfully produced and is illustrated in Figure 4-6. The front view of the scaffold is shown in panel (b), where the two channels are distinct and separated by a layer of 2D-3D scaffold. A longitudinal cut along the channels was also conducted using a wire saw, and the cross-section encompassing the length of channel is depicted in Figure 4-6(c). As demonstrated, the channel maintains a well-defined shape and uniformity along the scaffold. The two different channels at the two layers are clearly distinguished and realized. A magnified view of the entrances of the channels is also provided in Figure 4-6(d-e). Although there is some deformation in the shape of the square channel the overall size remains relatively unchanged.

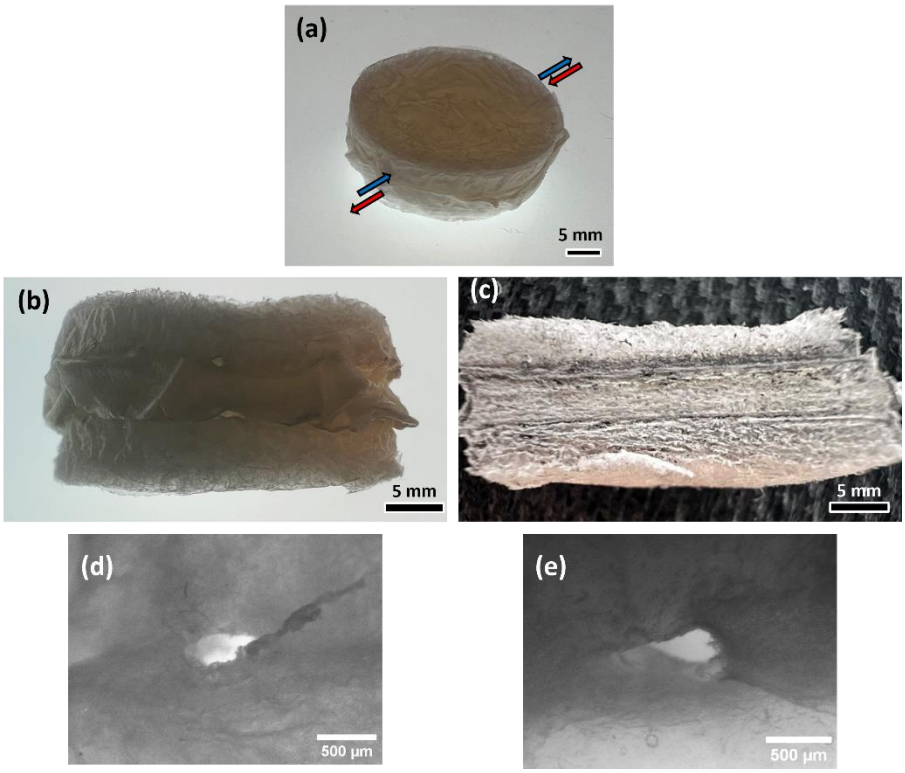


*Figure 4-6: Real fabricated sample showcasing two parallel microchannels at the center, situated across two different layers of the integrated multilayer 2D-3D scaffold. (a) General view of the scaffold. (b) Front view of the scaffold highlighting two distinct channels at separate layers. (c) Cross-sectional view depicting longitudinal view of the channels. (d and e) Optical microscopy images displaying the entrances of the channels.*

Flow tests, like those conducted in previous sections, can be performed to assess the functionality of this design. This feature opens doors for future applications, such as studying two different flows on a single scaffold.

## 4.3 Strengthening of Collagen Scaffold

As discussed in Chapter 1, type I collagen-based scaffolds have limitations, including rapid degradation rates and poor mechanical strength [34]. Figure 4-7 demonstrates the shrinkage of the scaffold following exposure to water-based cell culture media. The hydrophilicity and

permeability of the 3D sponge collagen allows the media to quickly permeate the scaffold, resulting in complete wetting due to pore interconnectivity, which leads to collapse. This rapid absorption causes noticeable shrinkage, with the hollow spaces within the pores filled by the media.

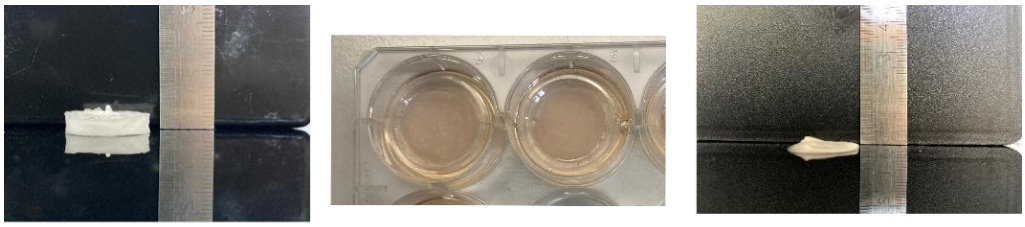


*Figure 4-7: Shrinkage of 3D sponge collagen after exposure to cell culture media. (a) 3D sponge sample before exposure and (b) during exposure to cell culture media and (c) after exposure.*

In this section, we aimed to analyze the effectiveness of two methods in addressing the issue of scaffold collapse and shrinkage to prepare for the next biological application. The first method involves the application of composite scaffolds, intended to overcome various limitations such as poor stability, high deformation of scaffold, and the loss of integrity of microchannels. The second method involves the use of cross-linking, which have been reported to enhance the structural integrity of collagen scaffolds, rendering them more stable and resistant to degradation. This increased stability is crucial for maintaining scaffold integrity during handling, implantation, and *in-vivo* use [34] .Various routes for cross-linking were previously discussed in Chapter 1.

In our preliminary experiments, we attempted physical cross-linking methods, including brief heating under denaturing collagen temperatures and exposure to UV radiation. However, these methods proved to be ineffective for our scaffolds. Consequently, we turned to chemical cross-linking as an alternative method. While various materials have been introduced for cross-linking and are widely regarded as effective such as Glutaraldehyde (GTA) [38] [53] [57], their use is often associated with some degree of toxicity to cells. Thus, we opted to employ ethanol as a safer

cross-linker known to cause less damage to the scaffolds [34]. To assess the behavior of our scaffold upon crosslinking, we employed a simple assessment technique to observe its response under exposure to water, the main component of water-based cell culture media.

We fabricated two sets of collagen scaffolds, i.e., first set comprised scaffolds solely made from 3D collagen sponges and the second group included the 2D-3D integrated scaffolds. Both sets of scaffolds were tested with and without ethanol crosslinking. For crosslinking, these samples were immersed in pure ethanol for approximately 1 hour, followed by sequential immersion in 70% (v/v) ethanol and then 50% ethanol, each for 30-minute intervals [18]. With the second group of samples, we aimed to investigate the composite effect of combining 2D film and 3D sponge collagen structures to enhance the mechanical properties of the scaffold in addition to the effect of the crosslinker.

All collagen samples were prepared using a 1% collagen slurry for the 3D sponge collagen parts. The 2D collagen film was also fabricated using the same 1% collagen slurry with a surface-to-ratio of 0.25. Freeze drying was carried out after freezing at -20°C, with detailed parameters outlined in Chapter 2. Each experimental group was replicated at least three times to ensure robust investigation of the effects.

Subsequently, the behavior of these scaffolds was monitored over the course of one week while exposed to water, representing the primary component of culturing media. Scaffold shrinkage percentage was measured as an approximate indicator of stability in the culturing media, with particular attention given to the integrity, stability, and perseverance of microchannels. The results are presented visually in Figure 4-8 and Figure 4-9, showcasing images of the fabricated scaffolds before and after exposure to water. Additionally, the shrinkage percentage of the scaffolds resulting from water exposure is graphically depicted in Figure 4-10.

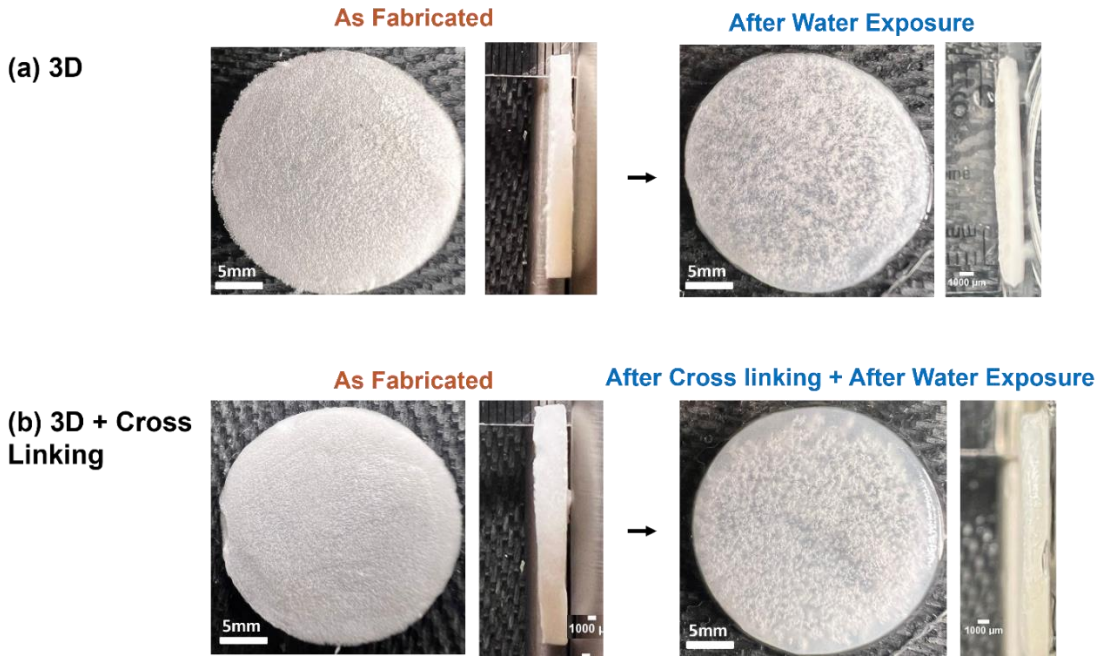


*Figure 4-8: Strengthening of 3D collagen sponges. (a) Normal 3D collagen sponge samples and (b) 3D collagen sponge samples followed by ethanol-based cross linking. The left panels display collagen scaffolds as fabricated, while the right panels show them after exposure to water.*

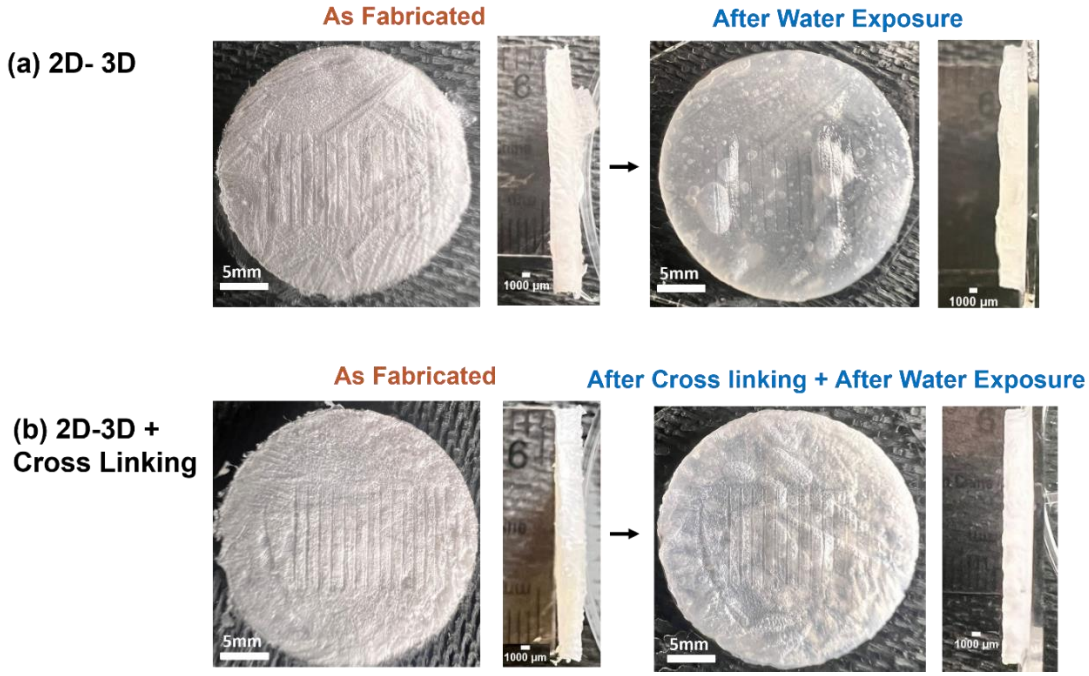


*Figure 4-9: Strengthening of 2D-3D collagen layers. (a) Normal 2D-3D collagen samples and (b) 2D-3D collagen samples followed by ethanol-based cross linking. The left panels display collagen scaffolds as fabricated, while the right panels show them after exposure to water.*

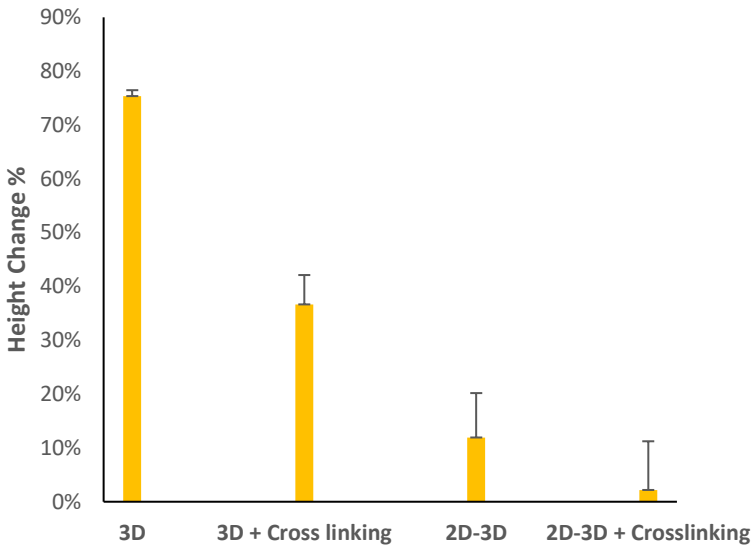


*Figure 4-10: The shrinkage percentage of various cross-linked and non-cross-linked scaffolds resulting after water exposure.*

In Figure 4-8(a), the first category of samples consisting of only 3D collagen sponges is depicted. In panel (a), the left picture displays a simple 3D sponge 'as fabricated', while the right picture shows it 'after exposure to water'. From the side view of the scaffold, it is evident that this scaffold has shrunk significantly, (akin to exposure to culture media in Figure 4-7(c)). This shrinkage occurred within minutes of exposure to water and remained unchanged thereafter. The permeability of 3D sponge collagen facilitated rapid water absorption, leading to complete wetting of the scaffolds due to pore interconnectivity and subsequent noticeable shrinkage. Such shrinkage may impose limitations on certain applications.

In Figure 4-8(b), the scaffold comprises 3D collagen sponges reinforced by the previously mentioned cross-linking cycle. As depicted in Figure 4-10, the shrinkage of the scaffold has significantly decreased from 75% to 37%, a clear improvement evidenced by the accompanying image. Nonetheless, notable contraction is still apparent. Upon physical examination, samples in this group exhibited increased hardness compared to their pre-treatment state, although they maintained a relatively soft and spongy texture. Notably, in samples featuring microchannels

(results not included), their visibility was greatly reduced after undergoing cross-linking and exposure to water.

The cross-linking process achieves this effect by altering the chemical bonds within the type I collagen molecule [34]. During cross linking with the method we used, ethanol led to dehydration [14] and it appears part of the initial 3D sponge collagen transforms into a material resembling the transparency and rigidity of 2D film collagen structures. This transformation enhances the overall integrity of the scaffold, resulting in a stronger, reinforced structure.

The second category of collagen scaffolds is depicted in Figure 4-9. In panel (a), the first group consists solely of 2D-3D scaffolds, exhibiting significantly improved stability after exposure to water for one week (less than 12%). These samples did not flatten as observed with previous 3D sponge collagen scaffolds during water exposure. This enhanced stability can be attributed to the composite effect of a robust and stable 2D film structure combined with a soft and spongy 3D collagen matrix. Notably, microchannels on the surface remained well-preserved and underwent minimal changes compared to samples from other groups.

The last group represents the combined effect of 2D-3D composition and cross-linking. As shown in Figure 4-9(b), these scaffolds experienced the least deformation after one week of water exposure, which is further confirmed by measurements presented in Figure 4-10. Despite cross-linking, porous structure in 3D sponge collagen were still evident in these samples, besides successful preservation of microchannels. This group demonstrated the most effective preservation of microchannels and exhibited the least shrinkage. The utilization of 2D-3D scaffolds allows for the preservation of microchannels on the scaffold surface, while cross-linking enhances stability and facilitates sterilization, addressing challenges often encountered in biological investigations such as cell culture.

Although the combination of cross-linking with the 2D-3D design provides optimal stability, it's worth noting that cross-linking can be omitted if the scaffold is only required to be kept in media. If microchannels are necessary, the utilization of 2D-3D scaffolds appears to be the most suitable option. However, it's important to acknowledge that cross-linking can also be utilized to modulate the degradation rate of collagen scaffolds, although this aspect was not investigated in this thesis.

## 4.4 Preliminary Biological Applications of Collagen Scaffolds

In some ongoing collaborations with the labs of Professors Andreas Vlachos and Mark Bayfield, we have started to test our scaffolds for some biological applications, i.e., co-culturing 3D sponges with brain slices as well as culturing HEp2D, HEp2, and HEK 293T cells cell lines on the 2D collagen films. All collagen related works were done by us while the biological assays were all performed by the collaborators.

### 4.4.1 Preliminary determination of collagen scaffold’s biocompatibility for organotypic brain tissue culturing

As a potential application area of our collagen scaffolds, we investigated the feasibility of culturing brain slices of mice, specifically hippocampal-entorhinal cortical slices, on these scaffolds. Our primary objective was to investigate the viability and hosting during tissue recovery and neuronal maturation of the mice brain slices on top of the 3D collagen sponges. For this, we collaborated with Prof. Andreas Vlachos lab at the University of Freiburg, Germany.

Hippocampo-entorhinal slice culturing is a method aimed at sustaining a viable brain structure, crucial for memory and learning, in an *ex-vivo* condition. The primary goal is to elucidate neuronal communication and synaptic plasticity mechanisms. In this process, slices are carefully placed on an insert filter, allowing the introduction of a specialized nutrient-rich medium optimized to replicate in vivo conditions. Through this method, researchers can investigate synaptic transmission, neuronal excitability, and long-term potentiation. This approach significantly enhances our understanding of neurodegenerative disorders and the processes involved in memory formation.

Four types of collagen 3D sponges, freeze dried at various temperatures (-10, -20, -40, and -80°C) were tested. A Culture Plate Insert (Millicell-CM, Ireland) was used to assemble collagen pieces and brain slices, with the collagen scaffolds sterilized using UV light at 254nm for 15 minutes. These scaffolds were placed atop the culture plate's PTFE filter, limiting the medium volume to 1 ml and directing its upward movement through the filter and scaffold (Figure 2-18(a)). Brain slice implantation involved placing small pieces of brain slices onto the scaffold surface right away (Figure 2-18(b)).

The samples were then incubated for 18 days under controlled conditions. Throughout the culture period, pH levels were monitored three times a week during medium changes, and adjustments were made as necessary to maintain a pH of exactly 7.30. Following the incubation period, DAPI and PI staining were conducted to evaluate the scaffold's impact on the brain slice.

After incubating the collagen scaffold with medium, we observed the scaffold absorb the media immediately after 10 minutes and became fully wet. Although the scaffold absorbed the medium and experienced some shrinkage, it maintained its overall disk-like shape, indicating its potential suitability for accommodating the brain slice. The reason we put the scaffolds on the PTFE filter

rather than media was to have a controlled exposure of media in contact with scaffold. Figure 4-11 shows the incubated samples carrying brain slices after 1 and 18 days of incubation. Sterilization with UV light proved effective, as no microbial contamination was observed.

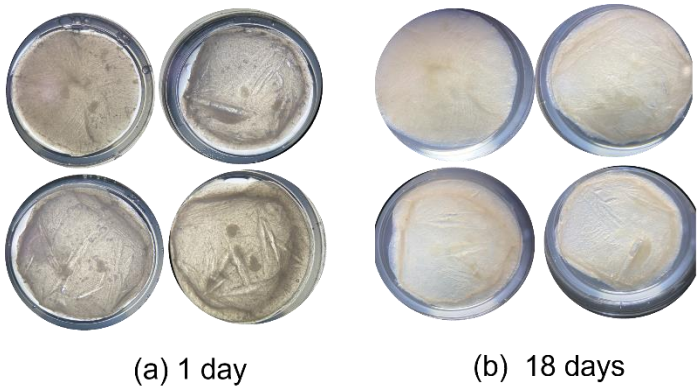


*Figure 4-11: Incubated samples carrying brain tissue after (a) 1 and (b) 18 days of incubation.*

Subsequently, we assessed the viability of brain slices on the four scaffolds post-sterilization, with results illustrated in Figure 4-12. It was revealed that after 18 days of incubation, the brain slices appeared unusually transparent, with visible liquid remnants indicating tissue liquefaction necrosis, suggesting tissue degeneration and poor survival. This was further confirmed by analysis of the PI and DAPI stained images. While both DAPI and PI are fluorescent DNA stains used in cell biology, DAPI primarily stains cell nuclei regardless of cell viability, while PI selectively stains dead cells with compromised plasma membranes. Comparative examination of PI and DAPI staining images of different samples against the reference sample (without a brain slice, Figure 4-12(e)) demonstrated extensive cell death across all samples as indicated by red color appearance, indicative of compromised tissue integrity. This outcome, commonly observed in neuronal tissue culture, may be attributed to the collapse and shrinkage of the scaffolds, hindering medium transfer

to the tissue and resulting in tissue necrosis. Such occurrences are typical in neuronal tissue culture due to the pivotal roles of oxygen and glucose deprivation in cell survival.

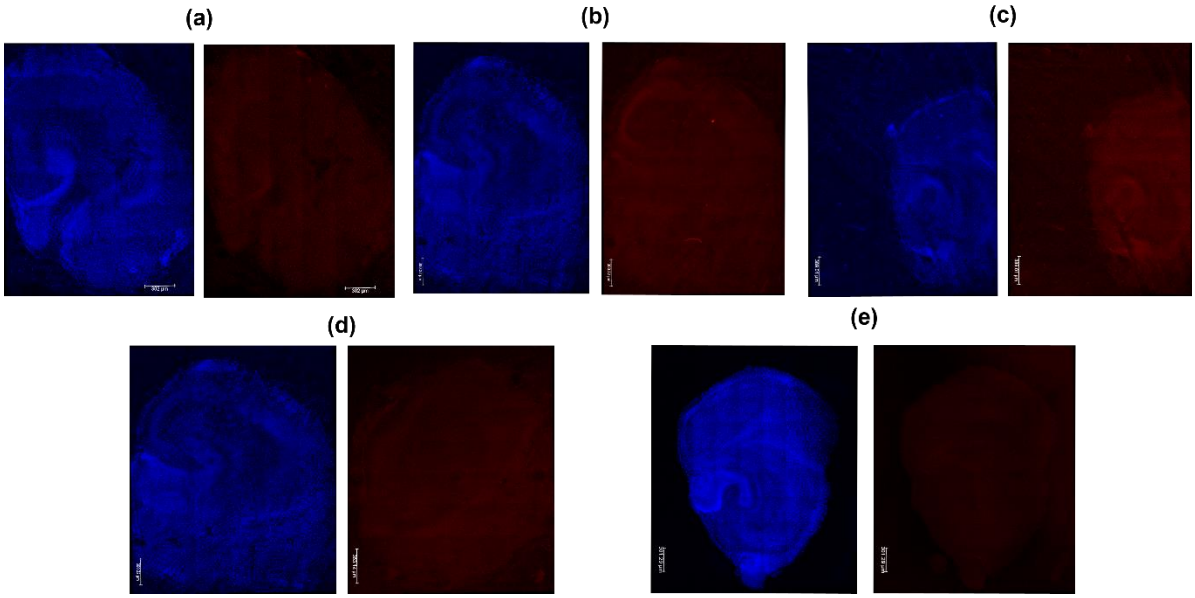


*Figure 4-12: Collagen 3D sponge samples freeze-dried at* (a) *-10, (b) -20, (c) -40, and (d) -80 °C. (e) Control sample. left images stained by DAPI and right images stained by PI*

Neuronal tissue, being highly sensitive to environmental factors such as pH, oxygen levels, and nutrient supply, exhibited no significant differences between samples frozen at different temperatures and with different microstructures. However, standardizing scaffold permeability and considering cross-linking methods may enhance scaffold stability and biocompatibility, although caution must be exercised to mitigate potential adverse effects. Further reinforcement of the scaffold and additional experimentation are necessary to obtain conclusive results.

### 4.4.2 Cell culture studies

Walls of cell culture well plates were lined with our 2D collagen films with casting of 1% collagen slurry with sufficient volume to maintain a surface to volume ratio of 0.25 and air-dried. The cell

lines employed in the study, included HEp2D cells engineered for inducible expression, HEp2 cells, and HEK 293T cells. For conducting cell culture study, cells were initially seeded at a density of $1.19 \times 10^5$ cells per well on Day 0, using DMEM supplemented with either 5% fetal bovine serum (FBS) for HEp2 cells or 10% FBS for HEK 293T cells. Media changes were performed every 2 days following seeding, with the addition of a 1X Penicillin/Streptomycin mix on Day 0 and at each subsequent media swap. Treatment and fixation steps were executed at Day 7 post-seeding according to the Immunofluorescence (IF) protocol, involving fixation with 4% Paraformaldehyde followed by permeabilization with 0.1% Triton in PBS. Subsequently, cells were counterstained with DAPI for 2-5 minutes after fixation and permeabilization, and imaging was conducted using an EVOS fluorescence microscope, utilizing GFP and RFP channels for monitoring components on the collagen membrane and Trans-Brightfield microscopy for imaging the membrane.

Figure 4-13 illustrates the outcomes observed for various cell types, including HEp2D, HEp2, and HEK 293T cells, upon interaction with the collagen membrane. Each cell type exhibited distinct behaviors, highlighting the heterogeneous responses that may arise within a seemingly uniform experimental setup. While HEp2 and HEK 293T cells demonstrated a diffuse distribution throughout the collagen scaffold (Figure 4-13(a,c)) the HEp2D cell line exhibited a propensity to aggregate into tumor-like structures (Figure 4-13(b)). Given DAPI is an intercalating agent that interacts with the minor-groove of double-stranded DNA, this channel enables to monitor the localization of nuclei throughout the collagen scaffold. In contrast, certain components of the collagen scaffold demonstrated a certain degree of fluorescence when excited, as observed in the GFP and RFP channels through monitoring the colocalization of what can best be described as background signal (Figure 4-13(b)). The observed differences in behavior suggest that seeding

density and genetic constitution may influence cell distribution within the scaffold. This variability underscores the intricate nature of cellular responses to the scaffold and emphasizes the necessity of considering cell type-specific characteristics during experimental design and interpretation. Despite these insights, the absence of a mock-seeding condition, where only media is introduced to the membrane without any mammalian cells, is noteworthy. Mock-seeding serves as a negative control to discern whether observed effects are attributable to cell presence or other factors. The omission of this control raises concerns regarding potential contamination, as indicated by the mention of yeast contamination despite the inclusion of antibiotics in the media. Consequently, future studies should incorporate appropriate controls to mitigate such concerns and ensure the reliability of experimental findings.

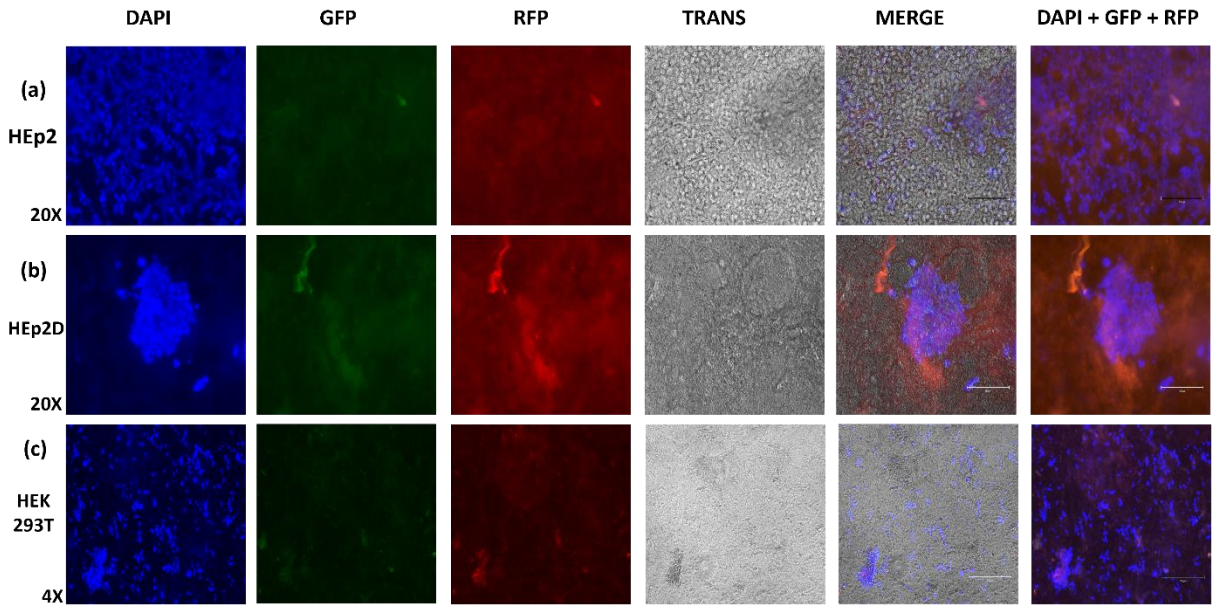


*Figure 4-13: Preliminary cell culture study results on flat 2D collagen membranes with different cells: (a) standard cell line Hep2, (b) genetically modified Hep2D, and (c) standard cell line HEK293T. The columns from left to right show the image type stained by DAPI, taken by GFP (Green Fluorescent Protein, RFP (Red Fluorescent Protein, TRANS (surface image from Trans-Brightfield microscopy), MERGE (merge of TRANS, DAPI, GFP and RFP) and the final column DAPI+GFP+RFP.*

## 4.5 Conclusion

With insights gained from the previous chapter, we successfully fabricated intricately designed microchannels on the flat surface of integrated 2D-3D collagen scaffolds, opening avenues for various biological applications aimed at organizing cell growth and proliferation through micropatterning.

Our exploration continued with the fabrication of 2D-3D collagen layers featuring enclosed branched channels. Microchannels of varying widths and depths, ranging from 1000 µm to 500 µm, were created by casting collagen layers over a PDMS replica generated from a 3D-printed negative mold. The fabrication steps, including freeze-drying and bonding, were employed to create these enclosed branched microchannels. The resulting scaffolds were validated for their ability to withstand water flow, attributed to the presence of a less permeable 2D collagen membrane within the channels. These findings affirm the method's consistency in producing devices with comparable fluidic behaviors, bolstering its applicability in biological contexts such as blood vessel models.

Another notable advantage of our approach lies in the creation of collagen scaffolds with embedded microchannels in multiple distinct layers, offering promise in tissue engineering. Models resembling blood vessels underscore the potential for distributing substances across different layers of the scaffold. Moreover, the scaffold serves as a model for co-culture studies and cell exposure to diverse mediums in each channel, opening avenues for cell and drug research. The versatility to culture different cell types within the channels further expands the potential applications, paving the way for future advancements in this field.

In addressing limitations of type I collagen-based scaffolds, our study evaluated composite structures and cross-linking methods to enhance stability and integrity. Results indicate that combining 2D-3D composition with cross-linking offers optimal preservation of microchannels and minimal deformation, rendering them ideal for cell culture studies.

Ongoing research explores the potential biological applications of collagen scaffolds, particularly in tissue culturing with brain slices of mice. Preliminary results reveal challenges related to tissue degeneration and poor survival, highlighting the need for scaffold permeability standardization and cross-linking methods to enhance stability and biocompatibility. Further experimentation is crucial to addressing these challenges and obtaining conclusive results. Furthermore, ongoing studies involving cell culture experiments with HEp2D, HEp2, and HEK 293T cells provide insights into distinct behaviors influenced by seeding density and genetic factors within the scaffold. Continued research in this area promises to uncover further insights into the biological implications of our scaffold design.

# 5 Summary and Future Work

## 5.1 Summary of The Thesis

Collagen, a major component of connective tissue, has long been utilized as a material in tissue engineering scaffolds due to its numerous advantages, including biocompatibility, biodegradability, and high bioactivity. Cells readily adhere to collagen's specific motifs, making it highly promising for tissue engineering applications. Its versatility is evident in the fabrication of scaffolds in various shapes and forms, making it a commonly employed biomaterial in tissue engineering.

The objective of this thesis was to fabricate and enhance the features and properties of an integrated 2D-3D collagen scaffold, mimicking key components found in living tissues. This included a noncellular extracellular matrix (ECM) consisting of a 3D porous interstitial matrix (IM) to support future cell growth, basement membrane (BM) linings on IMs, and microchannels acting as channels for nutrient exchange and waste removal, as well as aiding in cell growth and alignment.

The thesis outlined three main objectives. Firstly, to create 2D-3D integrated collagen scaffolds with minimal deformation, incorporating microchannels smaller than 200 μm, and studying the impact of fabrication factors through a parametric study. Secondly, to produce and analyze multi-layered 2D-3D integrated collagen scaffolds with enclosed microchannels in different layers. Lastly, to manufacture and analyze integrated 2D-3D collagen scaffolds with enclosed branch-shaped microchannels, ranging in size from 1000 to 500 μm, followed by conducting fluid tests on the scaffold. Preliminary biological studies on the application of the scaffolds were also conducted.

Chapter 2 explained the designs and experimental methodologies, covering various topics such as the design principles of collagen scaffolds, the use of different replication molds in scaffold fabrication, materials selection, scaffold fabrication processes, various types of fabricated scaffolds, test structures investigated, biological studies procedures and the characterization techniques utilized, such as image studies and flow tests.

Chapter 3 provided a thorough analysis of various factors that influenced the properties of engineered 2D-3D integrated scaffolds. The examination focused on molds, casting, concentration selection, and freeze-drying parameters, aimed at overcoming the challenge of producing flat scaffolds. It was found that the drying process of the 2D collagen film was the primary cause of surface wrinkles. The impact of freezing temperature on 3D sponge collagen micropores was investigated, revealing that lower temperatures resulted in finer pore sizes, leading to denser scaffolds. Similarly, higher collagen concentrations resulted in thicker collagen sheets and denser structures, leading to decreased porosity and smaller pore sizes. Moreover, the unique morphology of 2D-3D scaffolds was observed, with the transparent 2D collagen membrane positioned in front and the 3D sponge behind it, with protruding boundaries of the 3D sponge visible on the surface of the 2D membrane. Additionally, it was revealed that the drying time or atmosphere for the 2D film influenced the freeze-drying process of the 3D sponge layer, potentially leaving pores on the 2D membrane of the scaffold. Investigation into replicating microchannels in 2D-3D scaffolds showed that the concentration of collagen 2D film and freezing temperature influenced microchannel formation. Higher thickness of 2D film and lower freezing temperatures resulted in less accurate channel fabrication. Microchannels tended to widen with thicker collagen 2D films, particularly at lower temperatures.

Chapter 4 presented the successful fabrication of intricately designed microchannels on the flat surface of integrated 2D-3D collagen scaffolds. Additionally, the fabrication of 2D-3D collagen layers featuring enclosed branched channels was achieved. The resulting scaffolds were validated for their ability to withstand water flow, with potential applications in biological contexts such as blood vessel models. In addressing limitations of type I collagen-based scaffolds, composite structures and cross-linking methods were evaluated to enhance stability and integrity. Ongoing research explored potential biological applications of collagen scaffolds, particularly in tissue culturing with brain slices of mice, and provided insights into distinct behaviors influenced by seeding different kind of cells with various density and genetic factors within the scaffold. Continued research in this area promised to uncover further insights into the biological implications of the scaffold design.

In summary, meticulous attention to fabrication parameters was crucial for achieving desired scaffold properties. These findings provided valuable insights for designing tissue-engineered scaffolds tailored to specific applications, emphasizing the need for optimization in collagen scaffold fabrication processes.

## 5.2 Future Work

Future work for the thesis encompasses several areas of exploration and refinement. Firstly, the capability of the layer-by-layer fabrication approach to produce composite scaffolds with additional bioactive materials, such as laminin, VEGF (Vascular Endothelial Growth Factor), NGF (Nerve Growth Factor), and fibronectin, or combinations thereof, should be further investigated. This involves incorporating these substances into the aqueous collagen solution during scaffold fabrication. By integrating these substances into the scaffold, it is anticipated that the resulting

composite scaffolds would demonstrate enhanced properties or functionalities compared to scaffolds made solely from collagen.

Measurements of the mechanical properties of the scaffold after various cross-linking approaches may be necessary, depending on the intended application. Additionally, evaluating the degradation of these scaffolds with and without cross-linking may be required based on the application under consideration.

Moreover, to adjust the microstructure, exploring new methods to achieve larger pore sizes to accommodate the localization and transfer of larger cells, such as using ice progenitors or simplified routes targeting larger cell sizes, can be explored further. Furthermore, to achieve scaffolds with a more uniform distribution and equiaxed alignment of pores, preferential solidification methods and controlling the cooling rate can be investigated.

Fabrication of scaffolds in a controlled atmosphere to adjust the drying rate and water content in the 2D film could result in the production of integrated 2D-3D scaffolds with adjusted pore sizes on the surface. Additionally, further advancements in creating flat scaffolds with controlled moisture atmosphere and employing better bonding methods are necessary to fabricate enclosed scaffolds with smaller dimension microchannels and achieve uniform media distribution as needed on the scaffold.

Designing molds and utilizing soft photolithography can facilitate the creation of scaffold inlets and outlets entirely made of collagen. Additionally, precise flow studies can be conducted using advanced procedures such as line high precision flow sensor integration to obtain real-time flow rates in the scaffold can be conducted.

There are much more biological ideas out there that can be suggested further by its experts. In continuation of current brain tissue culture studies, standardizing scaffold permeability and considering cross-linking methods and improved sterilization procedures may enhance scaffold stability and biocompatibility. This can be performed alongside the assessment of 2D membrane pore size and adjustment of 3D sponge part pore size. Additionally, in culturing different types of cells on the scaffold surface, including experiments with 2D-3D integrated surfaces, can provide insights into cell behavior studies.

Exploring the development of a blood vessel models with porous and nonporous 2D membranes and integrating selective nanochannels into the 2D membrane for specific chemical exchange are potential avenues for future investigation. Co-culture models can be developed to study cell behavior and drug responses, with different mediums flowing through each channel, facilitating media exchange to the 3D sponge structure. Furthermore, pre-vascularizing tissues using endothelial cells along with proangiogenic growth factors like VEGF can be explored. For instance, seeding human umbilical vein endothelial cells (HUVECS) in scaffold microchannels and assessing their biocompatibility and growth facilitation within the scaffolds are areas for further investigation.

# References


[1] S. G.-Z.́nska, A. Sionkowska, Â. Carvalho and F. . J. Monteiro, "Biomaterials with Potential Use in Bone Tissue Regeneration—Collagen/Chitosan/Silk Fibroin Scaffolds Cross-Linked by EDC/NHS," *Materials* , 2021.

[2] Caldon J Esdaille1, enyatta S Washington and Cato T Laurencin, "Regenerative engineering: a review of recent advances and future directions," *Regenerative Medicine,* vol. 16, no. 5, pp. 495-512, 2021.

[3] C. Z. Liu,, Z. D. Xia, Z. W. Han and P. A. Hulley, "Novel 3D Collagen Scaffolds Fabricated by Indirect Printing Technique for Tissue Engineering," *Journal of Biomedical Materials Research - Part B Applied Biomaterials,* vol. 85, no. 2, pp. 519-528, 2008.

[4] Khademhosseini, A., A.; Vacanti and Langer, R., "Progress in tissue engineering," *Scientific American,* vol. 300, no. 5, pp. 64-71, 2009.

[5] S. Grabska-Zielińska, A. Sionkowska, Â. Carvalho and F. Monteiro, "Biomaterials with Potential Use in Bone Tissue regeneration—Collagen/Chitosan/Silk Fibroin Scaffolds Cross-Linked by EDC/NHS," *Materials,* vol. 14, p. 1105, 2021.

[6] A. D. Theocharis , S. S. Skandalis , C. Gialeli and N. K. Karamanos, "Extracellular matrix structure," *Advanced Drug Delivery Reviews,* vol. 97, pp. 4-27, 2016.

[7] "Wikimedia Commons,," 2007. [Online]. Available: https://commons.wikimedia.org/wiki/File:Extracellular_Matrix.png.

[8] J. Khoshnoodi, V. Pedchenko and B. G. Hudson, "Mammalian collagen IV," *Microscopy Research and Technique* , vol. 71, p. 357–370.

[9] B. S. Brooke, S. K. Karnik and D. Y. Li, "Extracellular matrix in vascular morphogenesis and disease: structure versus signal," *Trends in cell biology,* vol. 13, no. 1, pp. 51-56, 2003.

[10] R. Jayadev and D. R. Sherwood, "Basement membranes," *Current Biology,* vol. 27, no. 6, pp. 207-211, 2017.

[11] C. Leclech, C. F. Natale and A. I. Barakat, "The basement membrane as a structured surface–role in vascular health and disease," *Journal of Cell Science,* vol. 18, p. 133, 2020.

[12] N. E. V. ,. A. M. G. ,. P. Y. H. e. ,. G. B. M. Golestan Salimbeigi, "Basement membrane properties and their recapitulation in organ-on-chip applications," *Materials Today Bio,* vol. 15, p. 100301, 2022.

[13] D. Hutmacher , "Scaffold design and fabrication technologies for engineering tissues: state of the art and future perspectives," *Journal of Biomaterial Science Polymer edition,* 2001.

[14] E. Sachlos, N. Reis, C. Ainsley, B. Derby and J. Czernuszka, "Novel collagen scaffolds with predefined internal morphology madeby solid freeform fabrication," *Biomaterials ,* vol. 24, p. 487–1497, 2003.

[15] J. E. Iwen Wu, Natural and Synthetic Biomedical Polymers, Elsevier, 2014.

[16] J.-P. S.-P. Denis Fabricio Viera Rey, Handbook of Tissue Engineering Scaffolds: Volume One, Woodhead Publishing, 2019.

[17] S. MacNeil, "Progress and opportunities for tissue-engineered skin," *Nature,* Vols. 445,, p. 874–880, 2007.

[18] H. M. Aziz Mahmoudzadeh, "Tumor cell culture on collagenechitosan scaffolds as three-dimensional tumor model: A suitable model for tumor studies," *journal of food and drug analysis,* vol. 24, pp. 620-626, 2016.

[19] G. D. Pins, M. Toner and J. R. MORGAN, "Microfabrication of an analog of the basal lamina: biocompatible membranes with complex topographies," *FASEB J,* vol. 14, p. 593–602, 2000.

[20] S. A, K. H, K. T, K. Y, S. M, K. H, M. K, H. E, H. K, S. A, U. A, S. I, H. H, M. J and I. K, "Development of microstructured fish scale collagen scaffolds to manufacture a tissue-engineered oral mucosa equivalent," *Journal of Biomaterials Science, Polymer Edition,* vol. 31, no. 5, pp. 578-600, 2020.

[21] G. D. P. Katie A Bush, "Development of Microfabricated Dermal Epidermal Regenerative Matrices to Evaluate the Role of Cellular Microenvironments on Epidermal Morphogenesis," *TISSUE ENGINEERING: Part A,* vol. 18, no. 21, 2012.

[22] G. Li, X. Zhao, W. Zhao, L. Zhang, C. Wang, M. Jiang, X. Gu and Y. Yang, "Porous chitosan scaffolds with surface micropatterning and inner porosity and their effects on Schwann cells," *Biomaterials,* vol. 35, pp. 8503-8513, 2014.

[23] K.-Y. Shim, D. Lee, J. Han, N.-T. Nguyen, S. Par and J. H. Sung, "Microfluidic gut-on-a-chip with three-dimensional villi structure," *Biomed Microdevices,* pp. 19-37, 1 6 2017.

[24] G. D. Vatine, "Human iPSC-derived blood-brain barrier chips enable disease modeling and personalized medicine applications," *Cell Stem ,* vol. 24, p. 995–1005, 2019.

[25] T. Agency, "T2-Fgel Tight junction T2-fib-FCM T2-fib-TGF B Basement membrane," *Data research U.S.A,* vol. 2, 2014.

[26] J. Zeng, N. Sasaki, C. R. Correia, J. F. Mano and M. Matsusaki, "Fabrication of Artificial Nanobasement Membranes for Cell Compartmentalization in 3D Tissues," *Small,* vol. 16, no. 24, 2020.

[27] C. P. Tasiopoulos, L. Gustafsson, W. van der Wijngaart and M. Hedhammar, "Fibrillar Nanomembranes of Recombinant Spider Silk Protein Support Cell Co-culture in an In Vitro Blood Vessel Wall Model.," *ACS Biomater. Sci. Eng.,* vol. 7, p. 3332–3339, 2021.

[28] E. Dohle, "Human Co- and Triple-Culture Model of the Alveolar-Capillary Barrier on a Basement Membrane Mimic," *Tissue Engineering. Part C Methods,* vol. 24, p. 495–503, 2018.

[29] J. Zeng and M. Matsusaki, "Analysis of Thickness and Roughness Effects of Artificial Basement Membranes on Endothelial Cell Functions," *Anal. Sci,* vol. 37, p. 491–497, 2021.

[30] C. B. Weinberg and E. Bell, "A blood vessel model constructed from collagen and cultured vascular cells," *Science (80-. ).,* vol. 231, p. 397–400, 1986).

[31] P. H. C. I. D. A. Y. Y. Mona Sari, "Bioceramic hydroxyapatite-based scaffold with a porous structure using honeycomb as a natural polymeric Porogen for bone tissue engineering," *Biomaterials Research,* vol. 25, no. 2, 2021.

[32] S. P. D. S. Manju Rawat Singh, Nanobiomaterials in Soft Tissue Engineering, William Andrew Publishing, 2016.

[33] A. M. D. M. H. Lia Agustina, "Challenges and strategies for collagen delivery for tissue regeneration," *Journal of Public Health in Africa,* vol. 14, p. 2505, 2023.

[34] Y.-Y. L. T.-H. L. B.-Z. L. K. C. D. Z. T. L. Yu-Han Jiang, "Cross-linking methods of type I collagen-based scaffolds for cartilage tissue engineering," *American journal of translational research,* vol. 14, no. 2, pp. 1146-1159, 2022.

[35] D. A. W. ,. J. T. T. ,. J. T. C. Eleftherios Sachlos, "The impact of critical point drying with liquid carbon dioxide on collagen–hydroxyapatite composite scaffolds," *Acta Biomaterialia,* vol. 4, pp. 1322-1331, 2008.

[36] E. S. C. L. J. T. C. Denys A. Wahl, "Controlling the processing of collagen-hydroxyapatite scaffolds for bone tissue engineering," *Journal of Material Science: Material medicine,* vol. 18, pp. 201-209, 2007.

[37] L. Gibson, "Influence of freezing rate on pore structure in freeze-driedcollagen-GAG scaffolds," *Biomaterials,* 2003.

[38] K. Y. L. H. K. N. C. G. Oh H, H. Oh, Y. Ko, H. Lu, N. Kawazoe and G. Chen, "Preparation of Porous Collagen scaffolds with micropatterned structures," vol. 24, no. 31, pp. 4311-4316, 2012.

[39] S. Sarkar, G. Y. Lee, J. Y. Wong and T. A. Desai, "Development and characterization of a porous micro-patternedscaffold for vascular tissue engineering applications," *Biomaterials,* vol. 27, p. 4775–4782, 2006.

[40] K. S. K. E. C. S. L. J. Oh SH, "Fabrication and characterization of hydrophilic poly(lactic-co-glycolic acid)/poly(vinyl alcohol) blend cell scaffolds by melt-molding particulate leaching method," *Biomaterials,* vol. 24, no. 22, p. 4011–4021, 2003.

[41] G. D. F. J. Hou Q, "Porous polymeric structures for tissue engineering prepared by a coagulation, compression moulding and salt leaching technique," *Biomaterials,* vol. 24, no. 11, pp. 1937-1947, 2003.

[42] K. J. P. T. Yoon JJ, "Dexamethasone-releasing biodegradable polymer scaffolds fabricated by a gas-foaming/salt-leaching method.," *Biomaterials,* vol. 24, pp. 4011-21, 2003.

[43] F. C. R. R. W. X. Vaquette C, "An innovative method to obtain porous PLLA scaffolds with highly spherical and interconnected pores.," *Journal of Biomaterial Research applied bimaterial,* vol. 86, pp. 9-17, 2008.

[44] Choi SW, Xie JW and Xia YN, "Chitosan-based inverse opals: three-dimensional scaffolds with uniform pore structures for cell culture.," *Advance Material,* vol. 21, pp. 2997-3001, 2009.

[45] Zhang, Qin, Lu, Hongxu, Kawazoe, Naoki and Chen, Guoping, "Preparation of collagen scaffolds with controlled pore structures and improved mechanical property for cartilage tissue engineering," *Journal of Bioactive and Compatible Polymers,* vol. 28, no. 5, pp. 426-438, 2013.

[46] E. Rezvani Ghomi, N. Nourbakhsh, M. Akbari Kenari, M. Zare and S. R. Ramakrishna, "Collagen-based biomaterials for biomedical applications," *J Biomed Mater Res,* p. 1–14, 2021.

[47] J. &. K. A. Rouwkema, "Vascularization and angiogenesis in tissue engineering: beyond creating static networks," *Trends Biotechnology,* Vols. 34,, p. 733–745, 2016.

[48] W. K. L. PinFen Chua, "The strategic uses of collagen in adherent cell cultures," *Cell biology International,* vol. 47, pp. 367-373, 2023.

[49] M. R. S. ,. K. Arbind Prasad, "State of Art on Solvent Casting Particulate Leaching Method for Orthopedic Scaffolds Fabrication," in *5th International Conference of Materials Processing and Characterization (ICMPC 2016)*, 2017.

[50] L. L. L. A. S. Y. Y. R. I. Jia Xian Law, "Electrospun Collagen Nanofibers and Their Applications in Skin Tissue Engineering," *Tissue Eng Regen Med ,* vol. 14, no. 6, pp. 699-718, 2017.

[51] S. A. N. B. H. C. W. M. a. E. S. abor Forgacs, "Assembly of Collagen Matrices as a Phase Transition Revealed by Structural and Rheologic Studies," *Biophysical Journal,* vol. 84, p. 1272–1280, 2003.

[52] E. A. S. R. Z. J. W. R. Nima Saeidi, "Production of highly-aligned collagen lamellae by combining shear force and thin-film confinement," *Acta Biomaterials,* vol. 7, no. 6, pp. 2437-3447, 2011.

[53] S. C. N. K. G. C. Ying Chen, "Promoted Angiogenesis and Osteogenesis by Dexamethasone-loaded Calcium Phosphate Nanoparticles/Collagen Composite Scaffolds with Microgroove Networks," *Scientific Reports,* vol. 8, no. 1, 2018.

[54] M. G. Haugh, C. M. Murphy and F. J. O'Brien, "Novel freeze-drying methods to produce a range of collagen–glycosaminoglycan scaffolds with tailored mean pore sizes," *Tissue Engineering Part C: Methods,* vol. 16, no. 5, pp. 887-894, 2010.

[55] H. Wang, "A Review of the Effects of Collagen Treatment in Clinical Studies," *Polymers,* vol. 13, p. 3868, 2021.

[56] M. T. R. E. A. &. R. L. Yu Fu, "Exploration of collagen recovered from animal by-products as a precursor of bioactive peptides: Successes and challenges," in *Food scienece and nutrition*, 2018.

[57] V. G. a. J. A. M. R. Yong Y. Peng, "Stabilisation of Collagen Sponges by Glutaraldehyde Vapour Crosslinking," *International Journal of Biomaterials,* p. 8947823, 2017.

[58] S. Kew, T. Mead and N. Rushton, "Collagen gel for bonding porous collagen-based materials with non-porous collagen-based materials". Patent EP2542639A2, 2010.

[59] X. Zhang, M. Karim, M. M. Hasan, J. Hooper, R. Wahab, S. Roy and T. A. Al-Hilal, "Cancer-on-a-Chip: Models for Studying Metastasis," *Cancers,* vol. 14, no. 3, pp. 648-655, 2022.

[60] Y. heng, J. Chen, M. Craven, N. W. Choi, S. Totorica, A. Diaz-Santana, P. Kermani, B. Hempstead, C. Fischbach-Teschl and J. A. López, "In vitro microvessels for the study of angiogenesis and thrombosis," in *Proceedings of the national academy of sciences*, 2012.

[61] Y. Liu, S. Sun, S. Singha, M. R. Cho and R. J. Gordon, "3D femtosecond laser patterning of collagen for directed cell attachment," *Biomaterials,* vol. 26, no. 22, pp. 4597-4605, 2005.

[62] J. A. iménez-Torres, S. L. Peery, K. E. Sung and D. J. L. Beebe, "A practical method to pattern luminal structures in ECM gels," *Advanced healthcare materials,* vol. 5, no. 2, pp. 198-204, 2016.

[63] W. Y. Yeong, C. K. Chua, K. F. Leong, M. Chandrasekaran and M. W. Lee, "Comparison of drying methods in the fabrication of collagen scaffold via indirect rapid prototyping," *Journal of Biomedical Materials Research Part B: Applied Biomaterials,* vol. 82, no. 1, pp. 260-266, 2007.

[64] C. J. Bettinger, K. M. Cyr, A. Matsumoto, R. Langer, J. T. Borenstein and D. L. S. f. m. d. Kaplan, "Silk fibroin microfluidic devices," *Advanced Materials,* vol. 19, no. 19, pp. 2847-2850, 2007.

[65] S. Trevor, K. Nilabh, C. H. Huan, G. Linxia, A. Mohammad and K. Vipuil, "In vitro characterization of xeno-free clinically relevant human collagen and its applicability in cell-laden 3D bioprinting," *Journal of Biomaterials Applications,* vol. 35, no. 8, pp. 912-923, 2021.

[66] A. Wenz, K. Borchers, G. E. Tovar and P. J. Kluger, "Bone matrix production in hydroxyapatite-modified hydrogels suitable for bone bioprinting," *Biofabrication,* vol. 9, no. 4, 2017.

[67] R. G. H. F. H. N. F. L. D. &. L. S. Thakar, "Regulation of vascular smooth muscle cells by micropatterning," *Biochemical and Biophysical Research Communications,* vol. 307, pp. 833-890, 2003.

[68] H. T. Y. N. M. &. M. T. Kaji, "Pharmacological characterization of micropatterned cardiac myocytes," *Biomaterials,* vol. 24, pp. 4239-4244, 2003.

[69] L. S. W. T. J. &. B. R. Kam, "Axonal outgrowth of hippocampal neurons on micro-scale networks of polylysine- conjugated laminin," *Bimoaterials,* vol. 22, pp. 1049-1054, 2001.

[70] E. K. P. R. L. O. B. O. Jonelle Z. Yu, "Biomimetic scaffolds with three-dimensional undulated microtopographies," *Biomaterials,* vol. 128, pp. 109-120, 2017.

[71] X. Z. ,. W. Z. ,. L. Z. ,. C. W. ,. M. J. ,. X. G. ,. Y. Y. Guicai Li, "Porous chitosan scaffolds with surface micropatterning and inner porosity and their effects on Schwann cells," *Biomaterials,* vol. 35, no. 30, pp. 8503-8513, 2014.

[72] R. N. M. D. &. T. P. A. Biran, "Directed nerve outgrowth is enhanced by engineered glial substrates," *Experimental Neurology,* vol. 184, pp. 141-152, 2003.

[73] S.-Y. K. I.-C. R. W.-Y. C. R. L. K.-W. L. Suk-Won Lee, "Influence of microgroove dimension on cell behavior of human gingival fibroblasts cultured on titanium substrates," *Clinical Oral Implants Research,* vol. 20, no. 1, pp. 56-55, 2009.

[74] E. W. G. I. D. C. C. Ostuni, "Substrates, Using Self-Assembled Monolayers to Pattern ECM Proteins and Cells on," in *Even-Ram, S., Artym, V. (eds) Extracellular Matrix Protocols. Methods in Molecular Biology,* 2009.

[75] A. K. R. Gauvin, "Microscale technologies and modular approaches for tissue engineering: moving toward the fabrication of complex functional structures," *ACS NanoACS Nano,* vol. 5, pp. 4258-4264, 2011.

[76] G. R. M. H. R. Z. G. S. T. E. M. V. T. H. R. W. P. R. E. T. P. V. P. L. J. M. Z. J. S. R. B. W. F. D. T. H. Gerwen Lammers, "Construction of a Microstructured Collagen Membrane Mimicking the Papillary Dermis Architecture and Guiding Keratinocyte," *Macromolecular Bioscience,* vol. 12, no. 5, pp. 675-691, 2012.

[77] K. H. K. T. K. Y. S. M. K. H. M. K. H. E. H. K. S. A. U. A. S. I. H. H. M. J. I. K. Suzuki A, "Development of microstructured fish scale collagen scaffolds to manufacture a tissue-engineered oral mucosa equivalent," *Journal of Biomaterials Science, Polymer Edition,* vol. 31, no. 5, pp. 570-600, 2020.

[78] Y. M. S. T. Nobuhito Mori, "Skin integrated with perfusable vascular channels on a chip," *Biomaterials,* vol. 116, pp. 48-56, 2017.

[79] S. N. C. M. B. J. D. L. E. &. C. C. S. Raghavan, "Geometrically controlled endothelial tubulogenesis in micropatterned gels," *Tissue Engineering Part A* , vol. 16, pp. 2255-2263, 2010.

[80] N. K. G. C. Shangwu Chen, "Biomimetic Assembly of Vascular Endothelial Cells and Muscle Cells in Microgrooved Collagen Porous Scaffolds," *Tissue Engineering - Part C,* vol. 23, no. 6, pp. 367-376, 2017.

[81] W. C. C. L. K. C. M. a. L. M. Yeong, "Indirect fabrication of collagen scaffold based on inkjet printing technique," *Rapid Prototyping Journal,* vol. 12, no. 4, pp. 229-237, 2006.

[82] N. Fakhri, *INTEGRATED TWO-DIMENSIONAL/THREE-DIMENSIONAL COLLAGEN SCAFFOLDS WITH EMBEDDED CHANNELS,* Toronto: York University, 2023.

[83] P. Pagella, N. E., L. M. and T. Mitsiadis, "Investigation of orofacial stem cell niches and their innervation through microfluidic devices," *European Cells and Materials,* vol. 29, pp. 213-223, 2015 .

[84] N. R. Wevers, R. v. Vught, K. J. Wilschut, A. Nicolas, C. Chiang, H. L. Lanz, S. J. Trietsch, J. Joore and P. Vulto , "High-throughput compound evaluation on 3D networks of neurons and glia in a microfluidic platform," *Scientific Reports,* vol. 6, 2016.

[85] R. v. V. ,. K. J. W. A. N. C. C. ,. H. L. L. ,. S. J. T. ,. J. J. &. P. V. Nienke R. Wevers, "High-throughput compound evaluation on 3D networks of neurons and glia in a microfluidic platform," *Scientific reports,* vol. 6, no. 1, pp. 1-10, 2016.

[86] G. M. Price, K. K. Chu, J. G. Truslow, M. D. Tang-Schomer, A. P. Golden, J. Mertz and J. Tien, "Bonding of macromolecular hydrogels using perturbants," *Journal of the American Chemical Society,* vol. 130, no. 21, pp. 6664-6665, 2008.

[87] S. Dikici, F. Claeyssens and S. MacNeil, "Bioengineering vascular networks to study angiogenesis and vascularization of physiologically relevant tissue models in vitro," *ACS Biomaterials Science & Engineering,* vol. 6, no. 6, 2020.

[88] Y. Fang, T. Zhang, L. Zhang, W. Gong and W. Sun, "Biomimetic design and fabrication of scaffolds integrating oriented micro-pores with branched channel networks for myocardial tissue engineering," *Biofabrication,* vol. 11, no. 3, 2019.

[89] I. Miranda, A. Souza, P. Sousa, J. Ribeiro, E. Castanheira, R. Lima and G. Minas, "Properties and Applications of PDMS for Biomedical Engineering: A Review.," *Journal of Functional Biomaterials.* , vol. 13, no. 2, 2022.

[90] S. Kew, T. Mead and N. Rushton, "Collagen gel for bonding porous collagen-based materials with non-porous collagen-based materials.". Patent In Google Patents:, 2016.

[91] M. D. P. R. T. A. D. J. Y. W. Sumona Sarkar, "Vascular tissue engineering: microtextured scaffold templates to control organization of vascular smooth muscle cells and extracellular matrix," *Acta Biomaterialia,* vol. 1, pp. 93-100, 2005.

[92] J. W. L. ,. I. C. ,. Y.-C. K. J. B. L. ,. a. J. H. S. Si Hyeon Kim, "A Microfluidic Device with 3-D Hydrogel Villi Scaffold to Simulate Intestinal Absorption," *Acta Biomaterialia,* vol. 4, p. 1322–1331, 2008.

[93] B. Müller, S. Lang, M. Dominietto, M. Rudin, G. Schulz, H. Deyhle, M. Germann, F. Pfeiffer, C. David and T. Weitkamp, "High-resolution tomographic imaging of microvessels," in *Developments in X-Ray Tomography VI. Edited by Stock, Stuart R. Proceedings of the SPIE*, 2008.

[94] *Harvestright Scientific Freeze dryer Owners Manual - v 052022,* Harvestright.com.

[95] N. H. ·. P. G. ·. A. M. F. ·. L. Šiller, "Automatic pore size measurements from scanning electron microscopy images of porous scaffolds," *Journal of Porous Materials,* 2022.

[96] M. F. D. B. C. B. S. F. L. U. C. M. T. D. a. A. V. Christos Galanis, "Amyloid-Beta Mediates Homeostatic Synaptic Plasticity," *The Journal of Neuroscience,* vol. 41, pp. 5157-5172, 2021.

[97] C. G. D. K. M. F. T. D. A. V. Maximilian Lenza, "Denervated mouse dentate granule cells adjust their excitatory but not inhibitory synapses following in vitro entorhinal cortex lesion," *Experimental Neurology,* vol. 312, pp. 1-9, 2019.